A numerical and experimental analysis of a transcritical, CO_2 heat pump water heater

by

Kayla Lewry

A thesis submitted to the Faculty of Graduate and Postdoctoral Affairs in partial fulfillment of the requirements for the degree of

Master of Applied Science

in

Sustainable Energy Engineering and Policy

Carleton University

Ottawa Ontario

Abstract

Due to the environmental concerns regarding traditional refrigerants, carbon dioxide (CO_2) is being studied as an alternative refrigerant in HPWHs. In this study, a commercially available, transcritical CO_2 HPWH was numerically and experimentally assessed. This included developing a model of the CO_2 HPWH and calibrating it with experimental data. The model was theoretically verified and utilized to predict the cycle pressures and compressor isentropic efficiency. While the predicted discharge pressures were within the expected range, the significant biases indicate that further work is required to increase the model accuracy. Additionally, study of the control system indicated that the water outlet temperature controls the water pump, the ambient temperature controls the compressor and evaporator fan, and that the expansion valve controls the high side pressure. Lastly, the performance data shows that the HPWH achieves the best performance at ambient air temperatures above 0°C and at water inlet temperatures below 30°C.

Acknowledgements

I would like to thank my supervisors, Dr. Ian Beausoleil-Morrison and Dr. Cynthia Cruickshank, for their encouragement and support throughout this project. I am very grateful for the experience of researching this technology with your guidance, knowledge, and expertise. Working with you on this project has greatly deepened my understanding of engineering work, experimental work, and thermodynamics.

I would like to thank my colleagues in the Solar Energy Systems Laboratory and the Sustainable Building Energy Systems group for their friendship, encouragement, and discussion. This includes Brock Conley, Chris Baldwin, Calene Treichel, Curtis Meister, Rebecca Pinto, Sarah Brown, Lumi Dumitrascu, Chris Campbell, Jordan McNally, Ben Beauchamp, Belal Daouk, Peter Svidler, Liam Mann, and Tait Seguin.

I would like to thank Chris Weissflog for the encouragement and kindness he showed before, during and at a crucial moment of the project. I cannot thank you enough for the kind words you gave to me that day.

I would like to thank the team at CANMET Energy for collecting additional data, answering my many questions, and providing support throughout the project. This includes Jeremy Sager, JP Poirier, Amr Daouk and Lucio Mesquita.

I would like to thank Steve Davies and Scott Sterling of EcoLogix for their expertise, labour and time.

Lastly, I would like to thank my parents and my partner. Thank you, mom, for moving here and keeping me well fed and encouraged. Thank you, dad, for teaching me algebra and to always ask

questions, may you rest in peace. Thank you, Gurpreet, for your love and reassurance. I would not be who I am today without the three of you and your unceasing love and belief.

Table of contents

List of figures

List of tables

Abbreviations

ASHP	Air-source heat pump
COP	Coefficient of performance
DHW	Domestic hot water
EES	Engineering equation solver
EEV	Electronic expansion valve
GHGs	Greenhouse gas emissions ($kgCO_2e$)
GSHP	Ground-source heat pump
HPWH	Heat pump water heater
IHX	Internal heat exchanger
TCHP	Transcritical CO_2 heat pump

Nomenclature

A	Surface area (m^2)
$dh3$	Difference in two enthalpy predictions at state point 3 (kJ/kg)
dP	Pressure difference (kPa)
dQ	Difference between the derived from measurements and model calculated evaporator heat transfer rates (kW)
h_{3L}	Enthalpy of state point 3 calculated using a first law energy balance (kJ/kg)
h_{3P}	Enthalpy of state point 3 calculated assuming the gas cooler is isobaric (kJ/kg)
f	Frequency (Hz)
$\dot{m}$	Mass flow rate of refrigerant (kg/s)
$\dot{m}_{\text{water}}$	Mass flow rate of water (kg/s)
N	Compressor shaft speed (RPM)
η_s	Compressor isentropic efficiency
Pr	Prandtl number
$\dot{Q}_{in,f}$	Evaporator heat transfer rate calculated from a first law energy balance (kW)
$\dot{Q}_{in,m}$	Evaporator heat transfer rate calculated from refrigerant conditions (kW)
$\dot{Q}_{out}$	Gas cooler heat transfer rate (kW)
T_s	Surface temperature (°C)
u_∞	Velocity of air (m/s)
V	Swept volume of compressor (m^3)
v	Volumetric efficiency of compressor
$\dot{W}_{\text{comp}}$	Compressor work (kW)

1. Introduction

This chapter includes the motivation for this research, necessary background information, and objectives. The motivation involves the current situation of water and space heating in Canada, their associated environmental effects, and potential options for minimizing these effects. The background information consists of the basics for heat pump water heaters, using CO_2 as a refrigerant, and heat pump controls. Furthermore, a general outline of the thesis is covered.

1.1. Motivation

While the general population has been warned about climate change for decades, mitigating it is becoming one of this generation's greatest challenges due to the increasing severity and frequency of natural disasters. Therefore, it is of utmost importance that all greenhouse gas (GHG) emission reducing strategies are explored. However, the main sources of GHG emissions need to be identified before determining which GHG reducing strategies should be employed. To that effect, Canadians are not only some of the highest GHG emitters per capita in the world, they have also committed to the goal of reducing their emissions to 30% below 2005 levels by 2030 [1]. Consequently, the preceding reasons make Canada an ideal country to study. In Canada, space heating and domestic water heating account for 80% of GHG emissions from residential buildings [2]. The breakdown for Canadian residential energy use is illustrated in Figure 1 - 1.

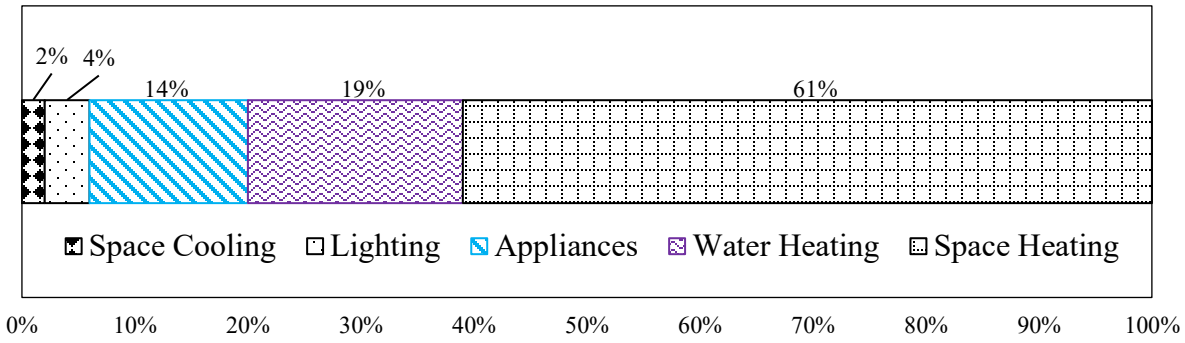

Figure 1 - 1: Canadian residential energy use, 2016

Space and water heating account for a significant percentage of GHG emissions because the traditional and common modes of space and water heating in Canada typically include electric heaters and burning natural gas [3]. One technology that can potentially reduce these emissions are heat pumps. A heat pump is capable of providing more energy (in the form of heat) than is used to power it. However, the use of heat pumps for space and water heating presents its own set of challenges: the most troublesome being refrigerant choice. Either through system leaks or from improper disposal of the system, inevitably a percentage (up to 30% in commercial systems) of the refrigerant will leak into the atmosphere and have negative environmental effects [4]. The negative environmental impacts of refrigerant leakage can be reduced by choosing a refrigerant that occurs in the natural environment, such as carbon dioxide (CO_2) [5].

1.2. Background

1.2.1. Heat pump water heaters

Heat pump water heaters utilize vapour compression refrigeration cycles to heat water for domestic use. Essentially, heat is absorbed into the refrigerant from a cold source and is rejected by the refrigerant into a hot sink. In the case of a HPWH, the “hot” sink is the water that is used for domestic hot water. A simple heat pump is made up of four basic components: compressor,

condenser, expansion valve, and evaporator. The components and processes of this heat pump are illustrated in Figure 1 - 2. In this configuration, the heat pump works as follows: the compressor compresses the fluid into a superheated vapour by exerting work on the fluid; thereby increasing the temperature and pressure (process 1-2). Next, the working fluid passes through the condenser and rejects heat to the "heat sink"; consequently, changing phase from a superheated vapour to a saturated liquid (process 2-3). The pressure and temperature are reduced through the process of expansion (process 3-4). Finally, the working fluid is heated by the "cold reservoir" and evaporated to either a saturated or superheated vapour before re-entering the compressor (process 4-1) [6].

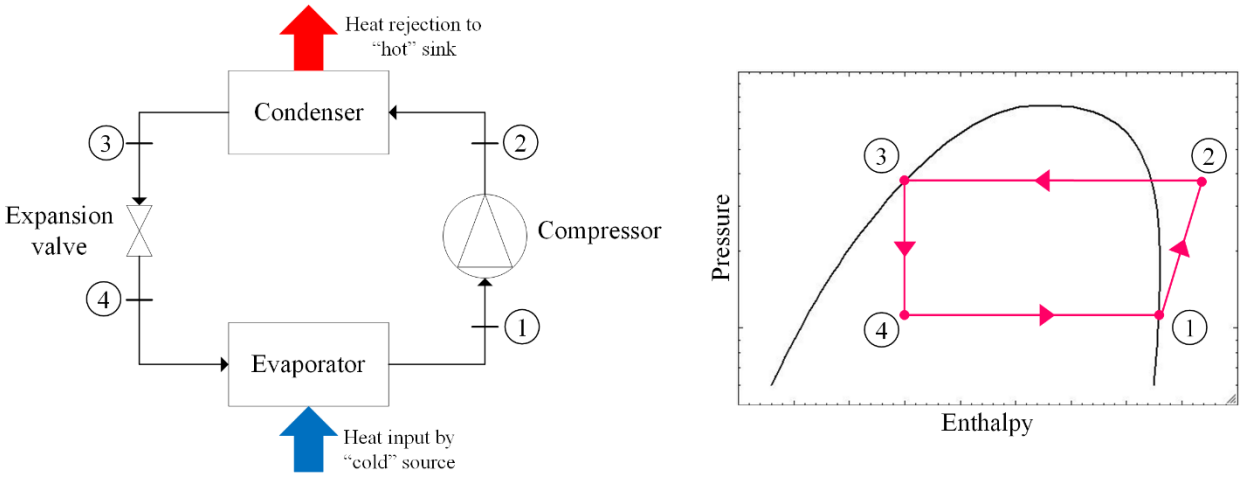

Figure 1 - 2: Basic heat pump cycle and corresponding pressure enthalpy chart

There are multiple sources that provide and remove heat to and from a heat pump, but the two that are described here are an air-source HPWH and a water-source HPWH. The differences between the two options lie on the source side, otherwise known as the evaporator side. For an air-source HPWH, the medium that provides heat is air, therefore a fan is required to move air over the coils of the evaporator. For a water source HPWH, water is the heat providing medium and thus a water pump is required for this design. For both options, the medium that is removing heat

from the heat pump is water. Therefore, the additional component of a water pump is required to move the water through the condenser for both options.

For this study, the coefficient of performance (COP) is the metric of choice for evaluating the efficiency of a HPWH. Generally, the COP is the measure of the heat output divided by the energy input used to provide that heat. The COP is typically calculated using the following equation:

$$COP = \frac{\dot{Q}_{\text{out}}}{\dot{W}_{\text{comp}}} \tag{1.1}$$

where $\dot{Q}_{\text{out}}$ is the heat rejected from the condenser to the water and $\dot{W}_{\text{comp}}$ is the power consumed by the compressor.

As was mentioned in Section 1.1, it is inevitable for refrigerant leaks to occur. Therefore, the refrigerant used is an important aspect to account for when considering HPWHs for an environmentally safe technology.

1.2.2. Refrigerant choice

There are two criteria that will be observed when comparing refrigerant choices: environmental effects and the critical point. The two measures that are commonly used to describe a refrigerant's environmental effect are the ozone depletion potential (ODP) and global warming potential (GWP). ODP expresses a substances ability to destroy ozone in the atmosphere by comparing the amount of ozone destroyed by said substance to the amount of ozone that would be destroyed by the same mass of CFC-11 [7]. GWP expresses how much heat one ton of a substance will absorb relative to how much heat one ton of CO_2 would absorb over 100 years [8]. A refrigerant will be environmentally benign relative to common refrigerants (chlorofluorocarbons

and hydrochlorofluorocarbons) if it has a low ODP and GWP. CO_2 is an ideal refrigerant choice for two reasons: it is naturally occurring in the environment and it has a low ODP and GWP. Choosing a refrigerant that already exists in the atmosphere reduces the risks of the unknown effects another refrigerant might have [9]. For example, the extensive use of chlorofluorocarbons (synthetic refrigerants that are not naturally occurring) eventually led to serious environmental consequences, even though they were thought to be safe and non-toxic [9]. The refrigerant related specifications of CO_2 are compared to other common refrigerants in Table 1 - 1.

Table 1 - 1: Common refrigerants specifications [5, 11]

Refrigerant	GWP	ODP	Natural Substance	Classification	Critical Temperature (°C)	Critical Pressure (MPa)
R744 (CO_2)	1	0	Yes	N/A	31	7.38
R404A	3700	0	No	HFC	72	3.72
R134a	1370	0	No	HFC	101	4.06
R22	1790	0.05	No	HCFC	96	4.99
R11	4000	1	No	CFC	198	4.11

The second criteria considered, the critical point, is an important parameter to consider because it greatly affects heat pump operation, design, and cost. The critical point describes the temperature and pressure at which the fluid no longer has separate liquid or gas phases [5]. CO_2 has the unique case of having a relatively low critical temperature (31°C) and high critical pressure (7.38 MPa absolute), which presents one of the key challenges in using CO_2 as a refrigerant [5]. This is because the critical temperature of 31°C is lower than the condenser temperature for applications such as domestic hot water and the critical pressure is relatively high compared to

common refrigerants. The condenser temperature is the saturation temperature that corresponds to the condenser pressure. For heat rejection to occur, the condenser temperature must be warmer than the temperature of the medium the heat is being transferred to. To prevent the formation of legionella bacteria in domestic hot water, the water is heated to at least 55℃ or 60℃ [10]. Therefore, the condenser temperature needs to be greater than 60℃, which is significantly greater than the critical temperature of 31℃. Consequently, when CO_2 is used as the working fluid in a HPWH, it will be in the supercritical phase on the high-pressure side of the HP. A fluid is in the supercritical phase when its temperature and pressure is above its critical point, which varies depending on the fluid. When a fluid is supercritical there is no distinct liquid or gas phase. Consequently, the components of a CO_2 HPWH need to withstand much higher pressures than traditional heat pumps. For example, the maximum high side pressure for the HPWH used in this study is 12 MPa while for a HPWH that uses R134a is 1.8 MPa [11]. Generally, this causes CO_2 HPWHs to be more expensive than traditional heat pumps of the same capacity. When a cycle is subcritical on the low-pressure side and supercritical on the high-pressure side, it is called a transcritical cycle. The specifics of the transcritical cycle are covered in the following section.

1.2.3. The transcritical cycle

The key difference between the transcritical cycle and the simple cycle described in Section 1.2.1 is that the compressor discharges the fluid in the supercritical region; thus the heat rejection process occurs in the supercritical region and not in the vapour dome region [5]. As a result, the heat rejection that occurs is in the form of sensible cooling instead of latent cooling; in other words, the temperature decrease followed by the isothermal condensing process is replaced with a large temperature change in the supercritical fluid [10]. Because the supercritical fluid remains in the gas phase during the heat rejection process, the condenser is replaced with a gas cooler [10]. This

important distinction is illustrated in Figure 1 - 3, where a simple heat pump cycle is shown with the solid line and the transcritical cycle is shown with the dotted line. This distinction is also depicted in Figure 1 - 4, where the condenser has been replaced with a gas cooler.

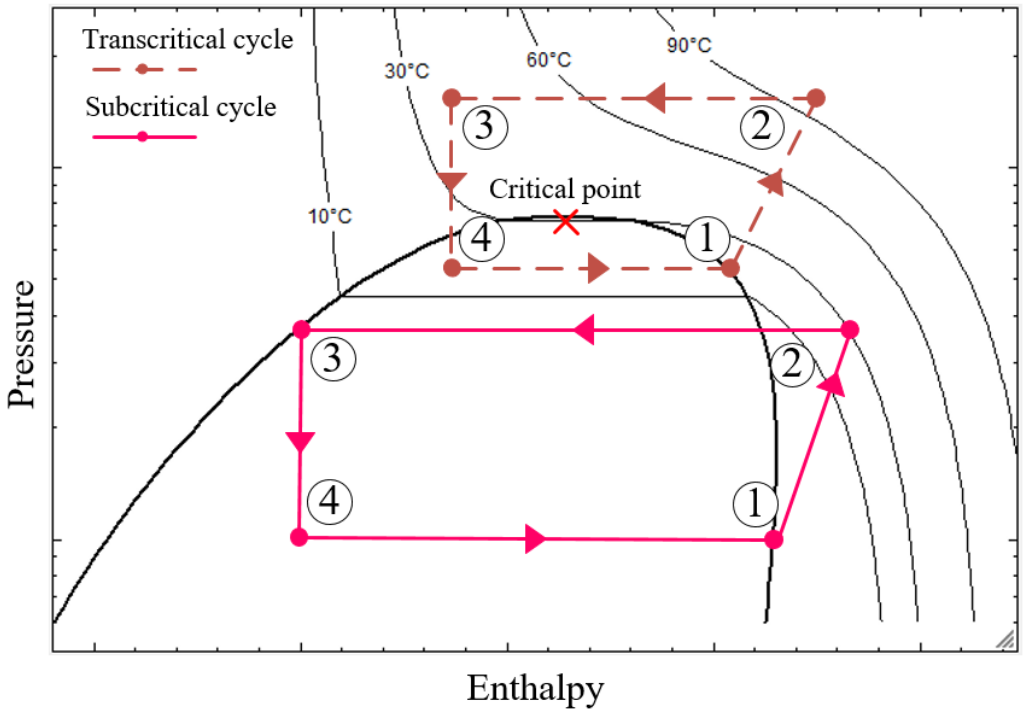

Figure 1 - 3: Pressure enthalpy chart for carbon dioxide illustrating the difference between a transcritical cycle and a subcritical cycle

Figure 1 - 3 depicts the difference between a subcritical and transcritical cycle as the fluid for the transcritical cycle surpasses the critical point and remains above it for the entirety of the heat rejection process.

The HPWH used in this study includes an additional component called an internal heat exchanger (IHX). This cycle is depicted in Figure 1 - 4. The IHX is located after the outlet of the gas cooler and on the suction line to the compressor. The function of the IHX is to transfer heat

from the high-pressure side to the refrigerant entering the compressor, and thereby reduce the work of the compressor and optimal discharge pressure [12]

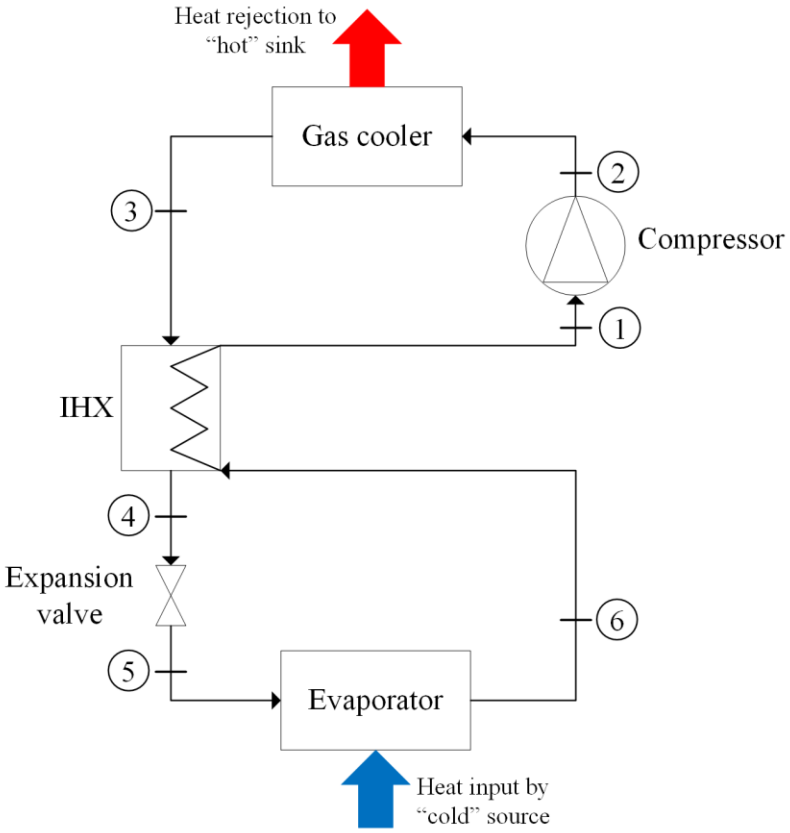

Figure 1 - 4: Basic transcritical cycle with internal heat exchanger

1.2.4. Heat pump control logic basics

In this section, the basics behind control logic for heat pumps (HPs) and its importance will be covered. Control logic refers to how and when the outputs of specific components of the heat pump are changed in response to varying conditions and measured variables.

Compressors, fans, and pumps are components whose rotational speed can be changed in response to varying conditions to adjust heat pump capacity or efficiency. In the past, only single-speed components were available for heat pumps. While the controls for these HPs have the advantage of being very simple, the disadvantage is that maximum efficiency is only attainable

when the HP capacity equals the demand. When the capacity is greater than the demand (which happens more often than not), energy is wasted and the performance of the HP suffers. This idea of the maximum performance occurring when the capacity equals demand is very important and led to the development of the capacity control method.

Capacity control refers to adapting the supply of heating to match the required load and thereby reduce energy waste. The two types of capacity control discussed here are intermittent control and variable-speed control. Intermittent control involves simply turning the heat pump on when the load requires it, operating at its designed speed (which is usually greater than the demand), then switching off once the predetermined setpoint has been reached [13]. For a HPWH, the predetermined setpoint is often defined for the temperature of the water in the water tank and is also referred to as the monitored temperature (MT). Likewise, a dead band (DB) is specified for intermittent control and it regulates the allowed difference in temperature between the actual and the setpoint [14]. Intermittent operation poses a problem for HPs because the HP will run at its maximum speed, which uses more energy than is often necessary. One way that has been used to increase the efficiency of intermittent control is to use a two-stage compressor and sequentially control their on/off cycles [15]. Visual representation of intermittent control involving single-stage and two-stage compressors is shown in Figure 1 - 5.

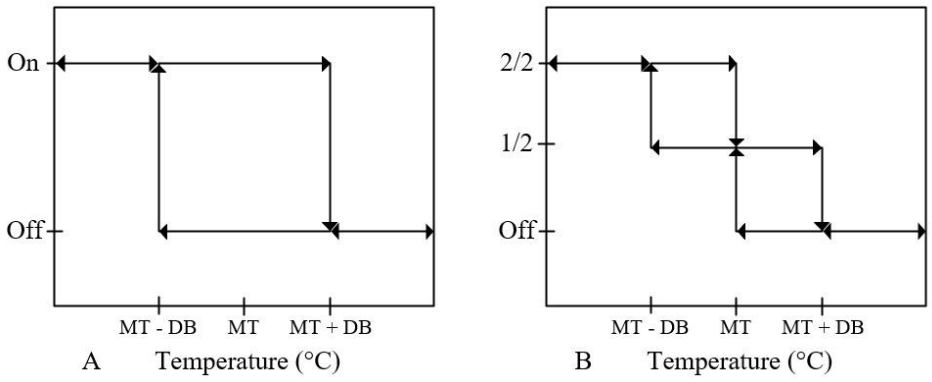

Figure 1 - 5: Intermittent controls for single-speed compressor (A) and two-stage compressor (B)

While intermittent control for two-stage compressors has its advantages, the dominating method of capacity control is achieved with variable-speed control [15]. Variable-speed control involves an inverter-driven motor coupled with the compressor (or pump or fan) that allows the motor to be controlled with a variety of frequencies resulting in a continuous range of speeds the compressor can be operated with [13, 15]. This allows the capacity of the HP to be matched with the demand most of the time.

1.3. Problem definition

Utilizing air-source (AS) HPWHs as outdoor units in Canada is not always feasible due to the wide range of temperatures experienced including the extreme lows that occur during the winter. As the source temperature for a HPWH decreases, so too does the energy transferred into the refrigerant from the air. Consequently, the compressor, fan and pump all require greater power input to ensure the refrigerant has sufficiently high enthalpy to heat the water to the required temperature. This drastically reduces the performance of the HPWH. Moreover, when the gas cooler is located outdoors and the ambient temperature is close to or below 0°C, the HPWH cycles on and off to prevent freezing of the water line which consumes additional power [17].

Ground temperatures do not experience as wide of a range as air temperatures do. Furthermore, during the extreme lows in winter the ground temperature is significantly warmer than the air temperature. Accordingly, utilizing the ground as the heat source for a HPWH eliminates the severely low source temperatures in the winter, the wasted energy spent on freeze prevention, and the resulting performance decrease. Therefore, ground-source (GS) HPWHs would achieve greater COPs and perform more reliably than AS HPWHs. Accordingly, the use of GS HPWHs could offer assurance and energy savings to residents that are not possible with AS HPWHs.

1.4. Research objectives

The overall goal driving this research is to assess the performance of a ground-source, transcritical CO_2 heat pump for domestic hot water and space heating for a multi-unit residential building. The scope of this thesis encompasses the first phase required to meet the overall goal and is comprised of the following research objectives:

- Acquire and modify a commercially available, air-source, transcritical CO_2 HPWH to a water-source configuration
- Develop and verify an empirical based numerical model of the heat pump in its original air-source configuration
- Approximate the cycle pressures and compressor isentropic efficiency by utilizing the numerical model
- Develop estimates for the error of the approximated cycle pressures and compressor isentropic efficiency

- Identify the control logic used in the heat pump's original configuration
- Create a performance map for the HPWH in its air-source configuration

Collaboration played an important role in meeting the objectives; the author collaborated with EcoLogix and with the Buildings and Renewables group from Natural Resources Canada (NRCan). The author chose a commercially available HPWH and developed an instrumentation plan for it while EcoLogix converted said HPWH to a water-source configuration and installed the instrumentation. NRCan implemented the author's instrumentation design on their air-source HPWH (same type as the one chosen for this research) and provided experimental data. This experimental data was used to verify the numerical model. Further work will include experimental testing of the HPWH in its water-source configuration as described in Chapter 6.

1.5. Thesis layout and methodology

This thesis includes six chapters to describe the completed research. These chapters are outlined below.

- Chapter 1 Introduction: includes motivation for research, relevant background information, and research objectives
- Chapter 2 Literature Review: presents a review of the literature on transcritical CO_2 HPWHs, including air-source configurations, ground-source configurations, which parameters are key to the HPWHs performance, and control strategies
- Chapter 3 Experimental Design: includes the configuration of the apparatus, specifications of the HPWH, data acquisition, experimental calculation methodology, and uncertainty analysis

- Chapter 4 Numerical Model: describes the methodology of the numerical model, the analysis of the HPWH, and any relevant approximations
- Chapter 5 Results and Discussion: presents the data obtained, the performance map, the model results and includes discussion on the implications of the results in the context of the control logic
- Chapter 6 Conclusions and Recommendations: restates the key findings of the research and reviews the next steps to continue this work

The approach that was followed during this study is illustrated in Figure 1 - 6.

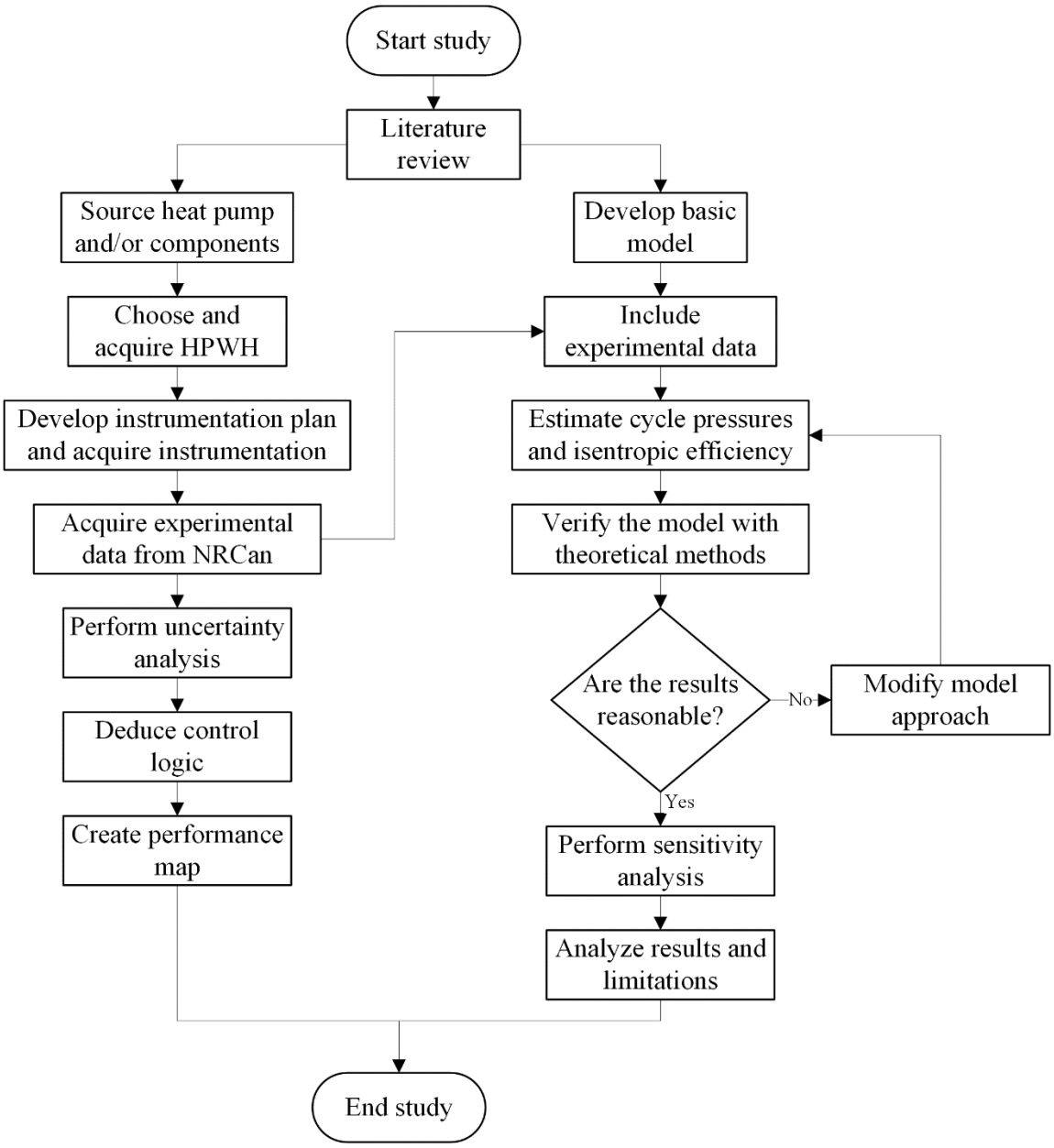

Figure 1 - 6: Project approach flow chart

2. Literature review

There has been extensive research done on CO_2 as a refrigerant to explore different configurations, applications, and its overall feasibility as a refrigerant. An overview of the research on transcritical CO_2 cycles, particularly in HPWHs, is covered in this section. This overview includes a heavy focus on cycle optimization and control strategies to reflect the objectives of this thesis.

2.1. Development of transcritical CO_2 systems

The idea of using CO_2 as a refrigerant is not a new idea, as the development of the systems now seen today began in the 19th century. In 1866, Thaddeus Lowe developed a compressor that was suitable for the use of CO_2 in a closed vapour compression cycle [18]. For a time, CO_2 was commonly used in cooling applications until it was replaced after the development of synthetic refrigerants [18]. CO_2 is now regaining popularity as new evidence showcased how detrimental synthetic refrigerants are to the environment [18], as described in Chapter 1.

2.1.1. Resurgence of popular use of CO_2 as a refrigerant

The resurgence of CO_2 began in 1993 when Lorentzen et al. [9] published a paper that claimed CO_2 as an acceptable alternative to synthetic refrigerants. The paper included validation of this claim through experimental analysis performed on a prototype of a transcritical CO_2 air conditioning system for cars [9]. The performance of the prototype was compared to reference data from a commercial CFC-12 air conditioning system over varying ambient temperatures. Lorentzen et al. [9] observed that the COP of the CO_2 system was at least comparable to the CFC-12 system and at higher ambient air temperatures it was better. This work may have been one of the first to compare CO_2 to traditional refrigerants, but it surely was not the last. Many have since proven CO_2 to be a competitive alternative to common refrigerants for different applications, such

as Tammaro et al. [19] and Nawaz et al. [20]. Shortly after Lorentzen et al.'s work, Neksa et al. [21] also compared the performance of CO_2 to other refrigerants but for the application of domestic water heating. It was postulated that the temperature change that occurs during the heat rejection of a transcritical CO_2 cycle is an idyllic match for water heating, because water heating requires the heat sink to be heated with a large temperature difference [21]. Based upon the theoretical and experimental analysis performed, Neksa et al. [21] concluded that CO_2 had the best thermodynamic properties for use in a HPWH. These initial works demonstrated that CO_2 had a promising future for the applications of air conditioning and HPWHs, thus creating the foundation for more research.

2.1.2. Optimization of transcritical CO_2 systems

After the initial phase of development for transcritical CO_2 HPWHs, the subsequent research became focused on optimization. Optimization of the transcritical cycle is complicated because there is not a linear relationship between the compressor work and the HPWH's heating capacity. As the compressor work is increased, the discharge pressure and the resulting heating capacity is also increased. However, the heating capacity does not increase proportionately with the compressor work increase. For example, White et al. [22] studied the effect of the discharge pressure on the system COP. It was found that by increasing the discharge pressure, the COP would increase until it reached an optimum and then any subsequent increases in discharge pressure would cause a decrease in COP. Therefore, an optimum discharge pressure exists at which the COP is at a maximum [21–24]. Accordingly, finding the variables that affect the optimum discharge pressure and calculating it for specific conditions and configurations of transcritical CO_2 HPs has been the subject of many studies, starting as early as 1999 with Kauf [23]. Within one year of each other, Kauf [23] and Liao [25] identified the gas cooler outlet temperature (the

temperature of the refrigerant leaving the gas cooler) and the ambient temperature as factors that significantly impact the optimum discharge pressure. In 2004, Sarkar et al. [26] validated that the gas cooler outlet and ambient temperatures had the greatest effects on the optimum discharge pressure and consequently the COP. Laipradit et al. [27], Cecchinato et al. [28], and Fernandez et al. [29] have since identified the water inlet temperature (the temperature of the water going into the gas cooler) as another important variable, especially since it directly affects the gas cooler outlet temperature. Additionally, they observed that decreasing water inlet temperatures increased the COP [10–12]. These observations were furthered by Fronk and Garimella's work. Fronk and Garimella [30] showed as the temperature difference between the refrigerant leaving and the water entering the gas cooler was reduced, so too was the optimum discharge pressure. Accordingly, the compressor work is decreased which increases the COP.

2.1.3. Transcritical CO_2 alternate configurations

There have been numerous configurations proposed and studied for transcritical CO_2 cycles, however, intercooling, simultaneous heating and cooling, ground source, and internal heat exchangers will be reviewed here.

Intercooling occurs when the refrigerant is cooled in between two stages of compression. The purpose of intercooling is to prevent overheating of the refrigerant and the consequent degradation of the lubricant and system components when compressing from a relatively low temperature to a supercritical temperature [5]. Additionally, through Cavallini et al.'s [31] experimental work, it was shown that intercooling with two-stage compression can improve the cycle's efficiency. Another energy efficient configuration that has been studied is simultaneous heating and cooling cycles. White et al. [22], Sarkar et al. [26], and Byrne et al. [32] have all contributed research for this configuration but with different heating and cooling applications. For example, Sarkar et al.

[26] studied the optimization of a system that provided heating of up to 140°C in a process plant and simultaneous refrigeration. In addition, Byrne et al. [32] compared the energy consumption of two individual heat pumps that performed the heating and cooling operations separately to a simultaneous heating and cooling system and found the latter system consumed 27% less energy than the former system.

As was mentioned in the introduction, ground-source heat pumps (GSHP) are a viable option in Canada due to the cold climate. In the winter, ground temperatures are generally warmer than air temperatures, therefore using the ground as an energy source instead of the air minimizes the energy penalties incurred from operating in very low temperatures. It is well documented in the literature that GSHPs achieve better performance than ASHPs by Bastani et al. [33], Nguyen et al. [34], and Atam et al. [35]. Therefore, the conversion of a commercially available CO_2 HPWH from an air-source configuration to a water-source configuration should result in better performance during the colder months. Furthermore, the use of a GSHP should significantly reduce the need for an auxiliary heater during the heating season. Recently, Badache et al. [36] used an experimentally validated model to perform a parametric study for a transcritical CO_2 GSHP. The majority of the parametric study focused on the specifics of the boreholes for the ground heat exchanger [36]. Nguyen et al. [34] expanded the same validated model used by Badache et al. to include an IHX and used it to observe different controls and ground conditions. The control methods observed involved varying the speed of the compressor and the valve opening to affect the refrigerant mass flow, discharge pressure and pinch point location in the evaporator [34]. While the above studies are focused on transcritical CO_2 GSHPs, the studies on transcritical CO_2 ground-source HPWHs are more limited. Bastani et al.'s [33] experimental work on a transcritical CO_2 ground-source HPWH shows that they could be especially well-suited for radiant floor space

heating because the best performance for the system was recorded at water inlet temperatures congruent with that application. Eslami-Nejad et al. [37] developed a theoretical model and a test apparatus to study a transcritical GSHPWH. The study showed that the degree of superheat at the compressor suction, the inlet water temperature, and gas cooler outlet temperature were important parameters to monitor regarding the performance of the system [37]. Furthermore, the study showed that improper control of some of those parameters decreased the performance of the unit by 25%. It was concluded that further work was necessary on this technology and that system controls were imperative to optimizing its performance [37].

A crucial configuration to cover in detail in this thesis is the basic transcritical CO_2 cycle with an IHX. An IHX is located after the outlet of the gas cooler and on the suction line to the compressor. Sometimes, the IHX is referred to as a suction line heat exchanger [38]. Lorentzen et al. [9] piloted the use of the IHX in transcritical CO_2 cycles and since then it has appeared in many cycles and studies [7, 9, 12, 15, 25–27]. With simulation, Robinson et al. [40] observed the COP of a basic transcritical cycle increase by 7% when an IHX was added. Shortly after Robinson et al.'s work, Chen and Gu [41] performed simulations that indicated an IHX can help stabilize the optimum discharge pressure, which can lead to higher COPs. More recently, Cao et al. [39] exclusively studied the effect of IHX length on transcritical CO_2 HPWHs. It was concluded that especially for water inlet temperatures above 40°C (which occurs frequently in domestic water heating), an IHX can increase the system COP by over 10% by reducing the discharge pressure [39]. The overall conclusion from these works is transcritical CO_2 cycles achieve greater performance with IHXs than without [7, 9, 12, 25–27].

2.1.4. Optimum discharge pressure correlations

An important portion of the optimization work that has been done involves correlations. Numerous correlations have been developed to calculate the optimum discharge pressure based upon different variables [3, 6, 8, 9, 27, 28]. Using a model, Liao et al. [25] developed a correlation for the optimum discharge pressure as a function of the evaporation and ambient temperatures. Using important conclusions from Liao et al's work, Chen [43] used pinch point analysis to create a correlation for the optimum discharge pressure. Chen's correlation had the important distinction of calculating the gas cooler outlet temperature. Most, if not all, of the previous correlations had fixed the gas cooler outlet temperature [43]. Chen determined that this assumption would underestimate the pressure and consequently overestimate the COP [43]. Ye et al.'s [44] correlation was the first to relate the ambient temperature, water inlet and outlet temperatures to the optimum discharge pressure. Before this, most correlations only used one or two of these important influencing factors [44].

There has been extensive work concerning the optimization of transcritical CO_2 cycles ranging from identifying key influencing variables, employing different configurations, and the development of correlations. A central theme that can be assumed from this review is the necessity for well-developed controls to ensure the system is operating at the optimum discharge pressure whenever possible [8, 22, 30].

2.2. Control methods for transcritical CO_2 systems

2.2.1. Control logic basics

In Chapter 1, the components for HPWHs and their functions were described. Now the components whose outputs can be changed to drive conditions of the refrigerant state points will be reviewed through the lens of control and operation in the heat pump. The first two components

are within the refrigerant loop and involve the compressor and the expansion valve. The compressor's role is to increase the enthalpy of the refrigerant; it does so by exerting work on the fluid and thereby increasing the temperature and pressure. The expansion valve is responsible for maintaining the pressure differential between the low-pressure side and the high-pressure side [10]. The other two important components are outside of the refrigerant loop and include the water pump and evaporator fan. The water pump and the evaporator fan are responsible for the rejection and addition of energy from/to the heat pump [15]. The water pump determines the mass flow rate of the water through the gas cooler, thereby influencing the rate of heat transfer from the refrigerant to the water. Similarly, the evaporator fan is a determining factor in the rate of heat addition to the refrigerant from the air by changing the mass flow rate of air over the evaporator coils.

Generally, all the aforementioned components could be single-speed components. Single-speed components have the advantage of being relatively simple to control, however, running at one speed severely limits the system efficiency. This is due to single-speed HPs only achieving maximum performance at the balance point temperature, the ambient temperature at which the output of the HP equals the demand [46]. Prior to the development of two-speed compressors in 1978, single-speed compressors were the only type of compressor available [47]. Single-speed and two-speed compressors used a form of capacity control called intermittent control. Further developments included compressors with more pre-set speeds and eventually the variable-speed compressor. With the development of the variable-speed compressor has come variable-speed control, which is also a form of capacity control. As heat pump technology has matured and developed over the past decades, it has become apparent that it is more economical to focus on increasing system efficiency through the use of controls instead of continuously improving the performance of compressors and heat exchangers [48]. Therefore, it is becoming more widespread

to use variable-speed components and more complex controls to increase the efficiency of HPs [15].

During the early development of variable-compressors, Tassou et al. [46] compared a variable-speed, capacity controlled HP (which also had a variable-speed evaporator fan) to a fixed-speed, intermittently controlled HP. Tassou et al's results were promising as the variable-speed HP boasted a seasonal efficiency 10% higher than the fixed-speed HP [46]. Notably, the variable-speed system had higher COPs for warmer ambient temperatures [46]. In 2007, Karlsson et al. [13] performed a comprehensive experiment on variable speed HPs. A vital conclusion to this work is that an optimal relationship exists between the refrigerant flow and heat transfer media flows and this relationship is of the utmost important to achieve maximum performance with variable-speed heat pumps [13]. Karlsson et al. is not the only one to have inferred this, Liu et al. [49] and Minetto [45] have also found the above statement to be true.

2.2.2. Control strategies

In 2004, Kim et al. [12] identified three different methods to control the optimum discharge pressure. These methods included: 1) controlling the refrigerant mass on the high pressure side, 2) controlling the volume inside the gas cooler, and 3) passively allowing pressure control through the refrigerant temperature. The first method described has been frequently used in the literature through varying the expansion valve opening and will be the focus of this section. A reduction in the valve opening causes refrigerant to accumulate on the high pressure side, resulting in an increased discharge pressure [12]. Ye et al.'s [44] work confirms that the discharge pressure can be increased or decreased by reducing or increasing the valve opening. Interestingly, it was Liao et al. in 2000 [25] that mentioned concurrent control of the valve opening and the compressor speed is a requirement for operating a CO_2 HPWH efficiently. As was mentioned before, Karlsson

et al. [50] and others have also attested that for efficient use of a variable-speed HP the heat transfer media flows must also be carefully regulated. The research that followed includes many combinations of varying the valve opening, compressor speed, pump speed, and fan speed as methods of control. Minetto's [45] control logic varied the valve opening and pump speed to control the discharge pressure and to maintain a constant outlet water temperature, respectively. Liu et al. [49] also studied the effects of varying water flow rates and valve openings on a CO_2 HPWH. They affirmed Minetto's conclusion that varying water flow rates is vital to achieve maximum performance. Conversely, Liu et al. [24] controlled a CO_2 HPWH with just the expansion valve and without the variable-speed pump. It was observed in this work that the heating capacity increased when the discharge pressure increased [24]. While the water flow rate is a commonly controlled variable, the source side flow rate is less so. In Baek et al.'s [51] study, the valve opening and evaporator fan speed were used to control the discharge pressure. It concluded that to maximize system efficiency, the optimum fan speed exists and should be utilized [51]. Carvahlo et al. [52] stress the importance of using continuous valve opening control for cycles that use both an IHX and a variable-speed compressor. This is recommended to prevent the significant decrease in COP that was observed at higher compressor speeds with a fixed valve opening [52]. Cecchinato et al. [53] determined a real-time algorithm that calculated the optimal discharge pressure for a CO_2 HPWH. The control logic includes varying the water flow rate, compressor speed, and the expansion valve. However, the expansion valve controls the discharge pressure according to a set point that is calculated by a self-learning supervisor [53]. Kim et al. [54] and Hu et al. [55] have also developed real-time algorithms but controlled fewer components. Kim et al. [54] only varied the valve opening and Hu et al. [55] varied the compressor speed with the objective of minimizing power consumption. Hu et al. [55] concluded that this form of control was

comparable to methods that focus on maximizing the COP but had the benefits of reduced number of measuring devices and its associated simplicity.

2.3. $SANCO_2$ studies

The commercially available HPWH that was studied in this research is called the $SANCO_2$. Existing studies and technical information on this HPWH will be reviewed in this section. Although cycle optimization has been reviewed previously, these studies and manuals outline the control methods and variables that have the greatest effect on performance.

In 2013, Larson et al. [56] evaluated the $SANCO_2$ for northern climates through a laboratory assessment. They observed the COP of the HPWH at the ambient temperatures of -1°C, 10°C, and 19°C and found that the system is controlled to maintain constant heat output [56]. Consequently, the compressor's speed and power draw increases as the ambient air temperature decreases, which causes a corresponding decrease in COP. However, ambient air temperature was not the only observed metric to alter performance. The results clearly indicated that the COP decreased as the water inlet temperature increased. Accordingly, a COP of 4.3 was observed when starting the heating cycle (the coldest water inlet temperature experienced) and it decreases to approximately 1.0 near the end of the heating cycle (the warmest water inlet temperature experienced) [56].

Four years later, Nawaz et al. [20] built upon the foundation that Larson et al. laid and conducted a more theoretical study on the Sanden HPWH. The study involved the creation of a numerical model for performance prediction and parametric analysis and used existing experimental data from Larson et al. to calibrate the model. Additionally, the performance of the Sanden HPWH was compared to a similar HPWH that used R-134a. The results confirmed that

the water inlet temperature significantly impacts the performance of the HPWH. Accordingly, a correlation was established for the optimum discharge pressure to be a function of water inlet temperature for each ambient temperature [20]. Moreover, it was determined that the SANCO$_2$ had equivalent performance to the R-134a unit [20].

2.4. Areas of limited research

Throughout the research on transcritical CO_2 HPWHs, there has been significant agreement amongst researchers that the ambient temperature and the water inlet temperature impact the optimum discharge pressure significantly. This is an important finding - especially for a water heater in Canada - because great variation exists in the ambient temperature. However, there is less consistency regarding the best method for control and optimization of transcritical CO_2 HPWHs. As illustrated in this review, there are many proven forms and methods to control the discharge pressure and optimize operation of a transcritical CO_2 cycle. The control method chosen should suit the application and the specific cycle employed. For HPWHs, it has been suggested by many that use of variable-speed components will assist in achieving maximum efficiency. Furthermore, it was concluded that efficient operation should include variable-speed heat transfer media flows [30, 36, 40]. Consequently, the research reviewed involves different combinations of variable-speed components. However, none of the reviewed literature combined variation of the compressor speed, valve opening, pump speed, and fan speed. Accordingly, the control method for the HPWH studied for this thesis combines variation in speed of the compressor, water pump, and evaporator fan and variation in the size of the opening of the electronic expansion valve.

Furthermore, there is limited research on the control methods concerning ground-source transcritical CO_2 HPWHs. There are sufficient studies concluding that GSHPs achieve greater performance than ASHPs, but there is little research concerning ground-source transcritical CO_2

HPWHs and their associated controls, as was concluded by Eslami-Nejad et al. [37]. The work that includes controls is focused on the evaporator and uses a variable-speed compressor and valve opening to control the discharge pressure [34]. To the author's knowledge, there are no studies that include a ground-source transcritical CO_2 HPWH that uses variable-speed pumps, compressor, and varying the valve opening.

Based upon the research objectives and literature gaps, this research looks at answering the following questions:

- What control methods are used for the air-source HPWH in this study to vary the compressor speed, water pump speed, evaporator fan speed and the electronic expansion valve opening?
- What control methods should be utilized if this commercially available air-source HPWH is converted to a ground-source HPWH?
- Does the HPWH perform as well for radiant floor heating as it would for its original application of DHW?
- Does the air-source HPWH perform better in an air-source or ground-source configuration?

While this research is motivated by the above questions, the scope of this thesis is limited to the air-source HPWH's control methods and determining if the HPWH performs better in an air-source or ground-source configuration.

3. Experimental design

The goal of the experimental apparatus was to calibrate a numerical model of a commercially available, transcritical CO_2 HPWH and to develop an understanding of the unit's control scheme. Accordingly, this chapter includes an overview of the experimental apparatus and details of its individual components. The instrumentation used, the corresponding data acquisition system and the uncertainty analysis are also described in this section.

3.1. Experimental apparatus overview

The apparatus used in this study was located at Canada Centre for Mineral and Energy Technology (CanmetENERGY) in Ottawa, Ontario. Accordingly, the apparatus was initially designed to suit the needs of CanmetENERGY - Ottawa; however, at the author's request additional instrumentation was installed and further testing was performed. The consequent setup will be described in three subsections: the HPWH, the cold water supply system, and the data acquisition system. The HPWH consists of the refrigerant loop and the water loop that connects the refrigerant loop to the hot water tank via the gas cooler. The HPWH was installed in a refrigerated container which was controlled to maintain steady temperatures. The hot water tank was installed in a shed that was maintained at 20°C for the duration of the tests. The cold water supply system consisted of a buffer tank and chiller, both of which were located in a separate conditioned building. CompactRIOs were used in conjunction with National Instrument (NI) modules, a router and a LabVIEW program to record data and control the setup. Figure 3 - 1 depicts the described system.

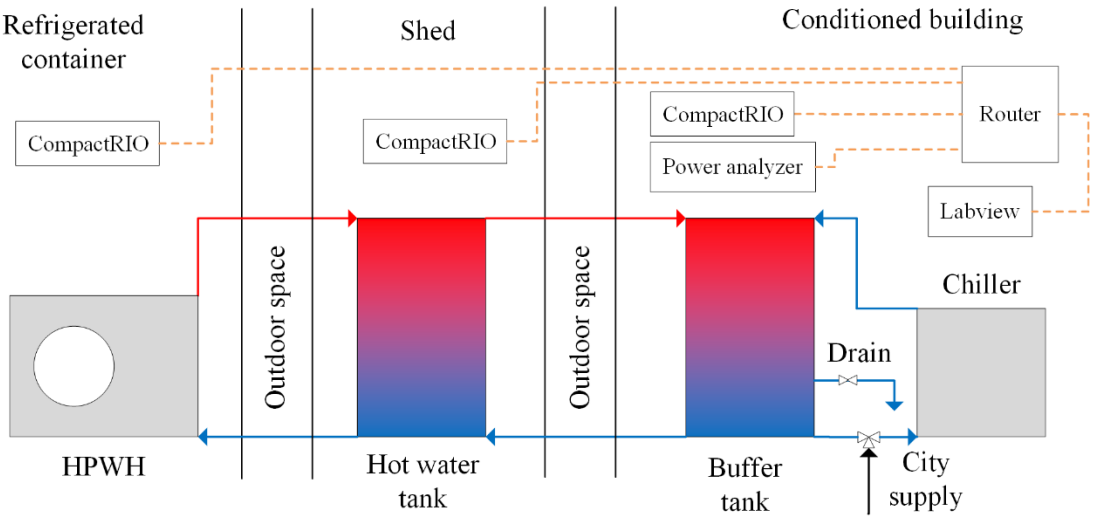

Figure 3 - 1: Overview of experimental apparatus

The objective of these experiments was to observe the performance of the HPWH and the state points as the conditions changed. As this research focuses exclusively on the HPWH's performance and response to increasing water inlet temperatures, no hot water draws were performed and no cold water was added to the hot water tank during the tests. The tests consisted of heating the water from a water inlet temperature of 12°C to 50°C (which is the temperature that triggers the HPWH to turn off). The system operated as follows: cold water from the cold water supply system was used to fill the hot water tank. After, the valves between the hot water tank and buffer tank were closed. Next, the HPWH would turn on and pump water from the bottom of the hot water tank through the HPWH. As the water passes through the HPWH, it is heated and then returned to the top of the hot water tank. The HPWH turns off once the water entering it reaches 50°C. For the duration of the tests, various temperatures, flow rates and power measurements were logged using a data acquisition system.

3.2. Heat pump water heater

The HPWH used in this study was the SANCO$_2$, model number GS3-45HPA-US. The HPWH consists of the refrigerant loop, the evaporator fan, water pump, compressor, expansion valve, control board and hot water tank. All these components, with the exception of the hot water tank, are contained within the HPWH cabinet. The evaporator fan, which moves ambient air over the evaporator coils, is in the center of the cabinet and the evaporator coils cover almost two full sides of the unit shell. The gas cooler is directly below the evaporator fan and is in an insulated box to minimize stray heat loss. The water pump that circulates water from the water tank to the gas cooler and back is housed on top of the gas cooler. The compressor is in a separate portion of the cabinet and is well insulated while the control board sits on top of the cabinet. These components are pictured below in Figure 3 - 2.

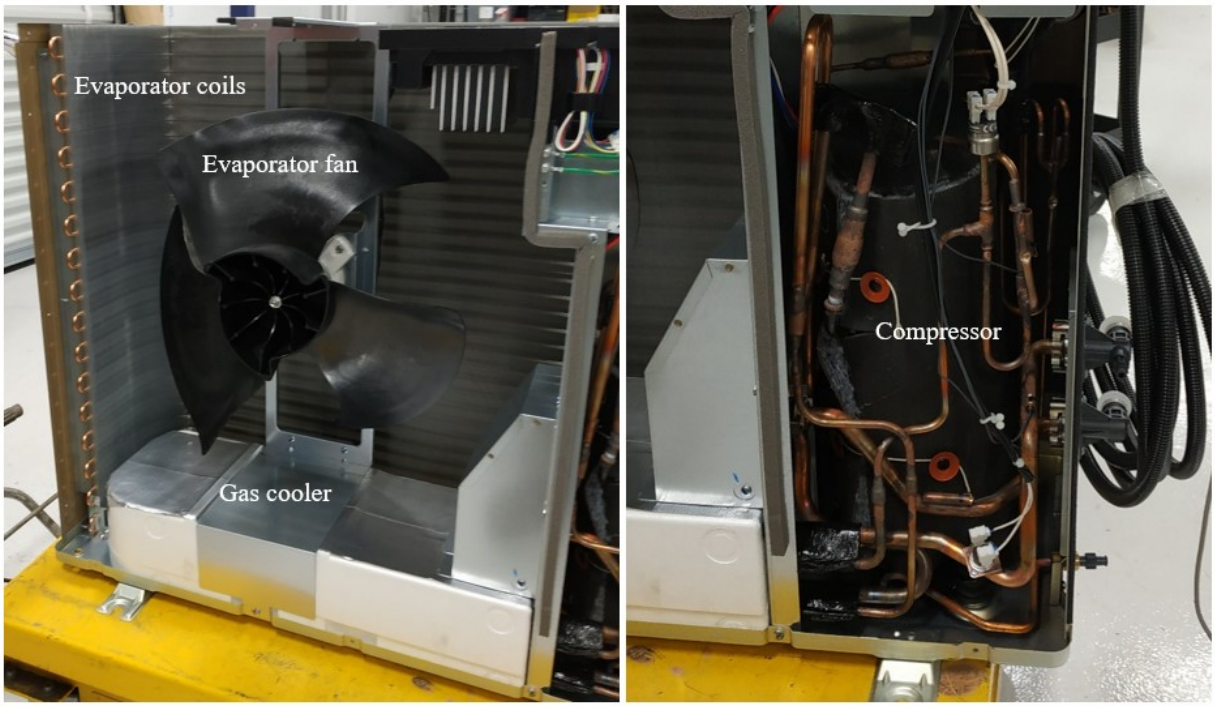

Figure 3 - 2: The components inside the HPWH

While some HPWHs are designed to be installed inside, the SANCO$_2$ was designed to operate outside. Thus, the HPWH cabinet and all the components contained would normally be installed outside and the hot water tank would be installed inside. To realistically mimic this design constraint, the HPWH was kept in a temperature controlled container that was separate from the hot water tank. Because the HPWH and water tank were housed in different buildings, they were connected by 5.5 m of insulated, ½" copper lines. The portion of the copper lines that were outside were installed with heat tape to ensure water did not freeze in the pipes. Details regarding the HPWH can be found in Table 3 - 1.

Table 3 - 1: Manufacturer's data for HPWH

HPWH Parameter		Value
Power	Gas cooler heating capacity (kW)	4.5
	System electrical consumption at max load (kW)	2
Refrigerant	Type	CO_2 (R744)
	Charge (g)	650
Water tank	Water tank capacity (L)	314
Temperature	Water supply temperature set points (°C)	55, 60, 65, 70, 75, 80
	Ambient temperature range (°C)	-29 to 35
Water pump specifications	Model #	PC28L15
	Power input (W)	30
Evaporator fan specifications	Power input (W)	70

In a transcritical CO_2 cycle, the compressor must be capable of achieving a higher discharge pressure than what is typically seen in HPWHs with common refrigerants [5]. Even though the discharge pressure is higher for transcritical cycles, the pressure ratio is usually smaller. Pressure ratios for typical cycles are as a great as eight while for transcritical cycles range from two to four [10]. Therefore, CO_2 HPWHs use specialized compressors to achieve these unique discharge pressures and pressure ratios. The SANCO$_2$ compressor details are listed in the table below.

Table 3 - 2: Compressor nameplate data

Compressor specification	**Value**
Type	Hermetic scroll
Range (RPM)	1800 to 5400
Motor	6 poles
Maximum discharge pressure (MPa)	12.0
Suction pressure range (MPa)	1.7 to 5.5
Maximum discharge temperature (°C)	120

Notably, the isentropic efficiency for the compressor was not available from the manufacturer. If either the suction or discharge pressure is known, the isentropic efficiency can be used to find the unknown pressure. This is achieved through relating the suction and discharge enthalpies to the compressor isentropic efficiency. Because enthalpy is a function of temperature and pressure, when the temperature and enthalpy is known they can be used to find the pressure. In this study, the suction and discharge pressures as well as the isentropic efficiency are all

unknown, therefore a numerical model is required to predict all three parameters. The numerical model and the method used to predict all three parameters is described in Chapter 4.

3.3. Cold water supply system

The water inlet temperature to the gas cooler is an important parameter to consider when studying the performance of a transcritical CO_2 HPWH. As such, it was desirable to test over a wide range of water inlet temperatures. The components mentioned in this section are the same components in Figure 3 - 1. While the water tank heats up, the water inlet temperature will slowly increase until it reaches 50°C, at which point the HPWH shuts off. Therefore, to maximize the range of water inlet temperatures, the water tank should start at as low of a temperature as possible. This was achieved by utilizing a buffer tank and a chiller. Water from the city supply was cooled by passing through the chiller and then deposited in the buffer tank. Once the buffer tank was filled, the water was circulated through the chiller until it reached the desired temperature. Then, the chilled water was used to fill the hot water tank.

3.4. Data acquisition and control program

The chiller and cold water supply system were controlled by the chiller's built-in controls. The chiller allows for a set point to be specified and uses its own temperature sensor to turn the compressor on and off. Once the set point has been defined and the chiller is turned on, it continues to run until the water reaches the setpoint temperature. The HPWH was also run with its built-in controls, which are described in Chapter 5.

The recorded data included the water flow rate that circulated through the gas cooler, the power of the compressor and pump, the motor frequency of the compressor, and a myriad of temperatures. Consequently, the setup was thoroughly instrumented and is illustrated in Figure 3 - 3.

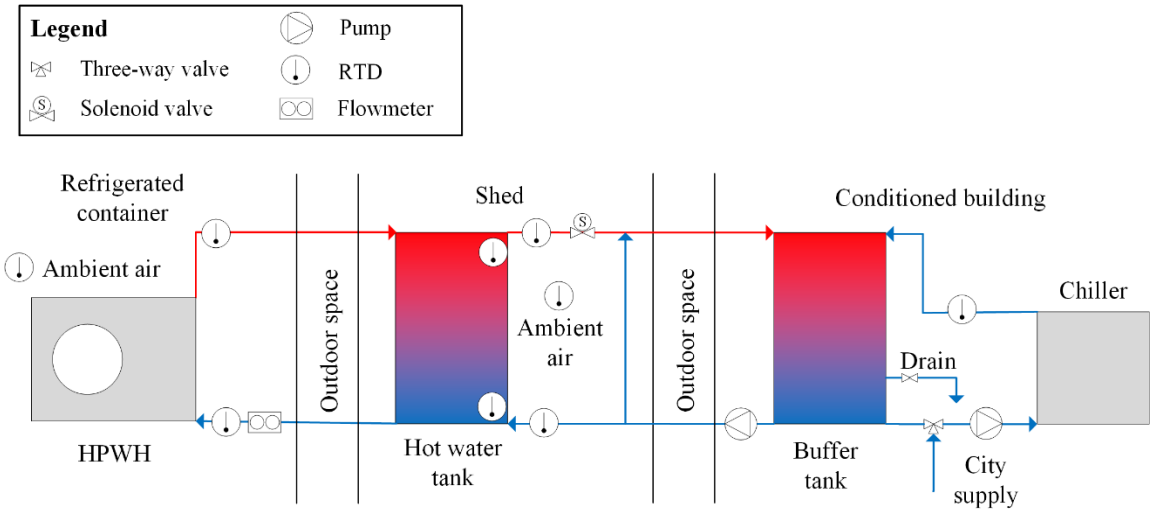

Figure 3 - 3: Location of instrumentation for hot water tank and cold water supply system

A flow meter measured the water flow rate through the gas cooler and two three-wire probe resistance temperature detectors (RTDs) measured the water inlet and outlet temperatures. The cold water supply system also used three-wire probe RTDs to ensure the desired temperature was achieved. An RTD is comprised of a thin wire wrapped around a non-conducting core. The RTD measures the change in resistance in the wire as it is heated or cooled. Based on known properties for the type of wire used, this resistance is converted to temperature.

The HPWH had temperature sensors built in for control purposes. These sensors measured the water inlet and outlet, ambient air, compressor discharge, and water tank temperatures. Additionally, six surface mounted RTDs were added onto the outside surface of the refrigerant lines. Figure 3 - 4 shows the instrumentation of the HPWH. A power analyzer measured the total system, compressor, and pump power as well as the compressor motor frequency. Details of the instrumentation used can be found in Table 3 - 3.

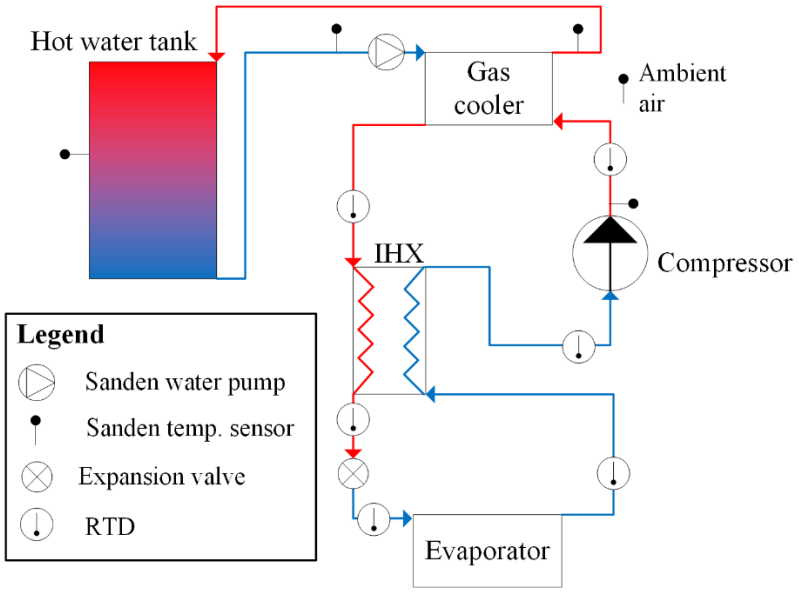

Figure 3 - 4: Instrumentation location for HPWH and refrigerant loop

Table 3 - 3: Experimental apparatus instrumentation specifications

System	Instrumentation type and model	Quantity
HPWH	RTD (SA1-RTD-4W-120)	6
	Power analyzer (Tektronix PA4000)	1
	Flow meter (MULTICAL 602)	1
	RTD (PR-20-2-100-3)	2
Cold water supply system	RTD (PR-20-2-100-3)	3

CompactRIOs were used with National Instrument (NI) modules to read and record data. CompactRIOs were especially convenient for this setup because they contain integrated controllers which allows them to run independently of the laptop. This was useful because the different components of the setup were housed in different buildings. Details regarding the NI modules that

were used can be found in Table 3 - 4. The power analyzer was connected to the laptop through a router and then the LabVIEW program retrieved the data through a hardware NI VISA.

Table 3 - 4: National Instruments card details

Card #	Type
NI 9216	RTD - input
NI 9482	Relay - output
NI 9403	Digital sink – pulse input (flow rate)

3.5. Experimental testing

The tests that were completed consisted of maintaining a steady ambient air temperature in the refrigerated container and allowing the water inlet temperature to vary from 12°C to 50°C. For all tests completed, the ambient air was held steady while the water inlet temperatures were transient. This process was repeated for all desired ambient air temperatures to ensure the performance could be calculated for a wide range of conditions. Temperatures, flow rate and power were measured and recorded every second. Some experimental data for the HPWH were available before additional instrumentation was added, consequently refrigerant temperatures, compressor and pump power, and compressor motor speed were not available for all ambient temperatures. Table 3 - 5 describes what data were collected for which ambient temperatures.

Table 3 - 5: Data collection map

Parameter	Ambient temperature (°C)								
	-29	-20	-15	-10	1	10	20	25	35
Water flow rate	●	●	●	●	●	●	●	●	●
Unit power	●	●	●	●	●	●	●	●	●
Compressor power		●		●		●		●	
Pump power		●		●		●		●	
Water temperatures	●	●	●	●	●	●	●	●	●
Refrigerant temperatures		●		●		●		●	
Compressor motor speed				●				●	

3.6. Calculation methodology

The two parameters that were calculated using only the experimental data and not the numerical model are the heat transferred to the water at the gas cooler, $\dot{Q}_{\text{out}}$, and the COP. The heat rejected at the gas cooler was calculated using the water flow rate and water inlet and outlet temperatures to the gas cooler. Several assumptions were made which allowed Equation 3.1 to be used. These assumptions included: the specific heat remained constant over the changing water temperatures, the heat rejection process was isobaric, and that kinetic energy, potential energy and stray heat loss were considered negligible.

$$\dot{Q}_{\text{out}} = c_{\text{p}} \dot{m}_{\text{water}} \left(T_{\text{w,in}} - T_{\text{w,out}} \right) \tag{3.1}$$

In Equation 3.1, c_{p} represents the specific heat of the water, $\dot{m}_{\text{water}}$ represents the mass flow rate of the water, $T_{\text{w,in}}$ represents the temperature of the water entering the gas cooler and $T_{\text{w,out}}$

represents the temperature of the water leaving the gas cooler. Typically, the COP is calculated using Equation 1.1 and uses only the compressor work ($\dot{W}_{\text{comp}}$) and gas cooler heat transfer rate ($\dot{Q}_{\text{out}}$) [1, 2]. In this study, COP calculations include the power consumed by the evaporator fan and the water pump, as these components are variable speed and therefore their power consumption is varied based on the conditions. Consequently, Equation 3.2 is used to calculate COP in this thesis.

$$COP = \frac{\dot{Q}_{\text{out}}}{\dot{W}_{\text{comp}} + \dot{W}_{\text{fan}} + \dot{W}_{\text{pump}}} \tag{3.2}$$

3.7. Uncertainty analysis

According to Moffat [57], the two main sources of error that should be accounted for in experimental data are bias uncertainty and precision uncertainty. Bias uncertainty is a result of the uncertainty of the equipment being used in the experimental set up while precision uncertainty accounts for scatter in measured data [57]. The uncertainty analysis in this section is theoretical because the uncertainty associated with precision is not included. Because this study's primary focus is on the performance of the heat pump and consequently the COP, this analysis will determine the bias for the heat rejected at the gas cooler ($\dot{Q}_{\text{out}}$) and for the work into the compressor, fan, and pump ($\dot{W}_{\text{in}}$).

$$COP = \frac{\dot{Q}_{\text{out}}}{\dot{W}_{\text{in}}} \tag{3.3}$$

Then, the biases will be combined to produce the total bias of the COP. The bias for $\dot{Q}_{\text{out}}$ will be covered first.

3.7.1. Uncertainty of heat rejection

The heat rejected at the gas cooler is calculated by the following equation:

$$\dot{Q}_{\text{out}} = \dot{m}_{\text{water}} C_{\text{p}} \Delta T \tag{3.4}$$

where the water flow rate ($\dot{m}_{\text{water}}$) is measured by a static flow sensor and the temperature differential (ΔT) is measured by two separate RTDs. To develop the total bias for the heat rejected, first the bias is determined for the mass flow rate and then for the temperature differential.

The flow meter used in this experiment uses bidirectional ultrasonic measuring techniques, meaning that one ultrasonic transducer sends the sound signal with the flow while the other transducer sends the signal against the flow. The time difference between the two signals is converted to a flow velocity and then a volume. The specific number of signals (or pulses) are proportional to a specific flow rate [58]. The uncertainty for the flow meter is comprised of three things: the bias associated with the pulse output, equipment bias and the bias related to the pulse counter. First, the reading bias ($B_{\dot{m},\text{k}}$) is formed from the relationship between the pulses and the flow rate and is determined as:

$$B_{\dot{m},\text{k}} = \frac{1}{kt} \tag{3.5}$$

where t is the sampling interval and k is a flow meter specification which is given on the physical flow meter. The parameter k represents how many pulses are generated for one gallon of fluid flowing through the meter. Second, the equipment bias ($B_{\dot{m},\text{e}}$) is determined by the manufacturer specifications, which provided an equation to calculate the bias based upon the flow rate and nominal flow rate. This source of bias ($B_{\dot{m},\text{e}}$) is approximately 1% of the measured value. Third, there is a bias related to the pulse counter to be quantified. This bias occurs because at the beginning of each measurement, a fraction of a pulse is counted as whole and at the end of each

measurement a fraction of a pulse is disregarded. To account for this bias, the equivalent bias of one pulse could be included in the total bias. However, for the flow rates used in this experiment, the equivalent bias of one pulse is negligible and is therefore not included. The root of the sum of squares method Equation 3.6 is used to calculate the total bias for the flow rate ($B_{\dot{m}}$).

$$B_{\dot{m}} = \sqrt{\left(B_{\dot{m},e}\right)^2 + \left(B_{\dot{m},k}\right)^2} \tag{3.6}$$

Next, the bias of the temperature difference will be calculated. The temperature difference is measured by two separate RTD readings; therefore, the bias for the temperature difference is the root of the sum of the squares of both temperature biases. Short probe RTDs were inserted into thermowells to measure the water inlet and outlet temperatures. The bias for each individual measurement includes the manufacturer's uncertainty and the uncertainty related to the position of the RTD. The RTD bias was provided by the manufacturer in the form of an equation that was based upon the temperature measured. Additionally, the RTDs used to measure the water inlet and outlet temperatures were 106 cm and 68 cm away from the points of interest (POI), respectively. Accordingly, the stray heat transfer from the water to the ambient air was estimated between the distance of the RTD and POI and then used to calculate the temperature difference between the two. Then, the temperature difference between the estimated and measured value was added to the bias for that reading. This temperature difference between the estimated and measured value is termed the location bias. More details regarding the calculation of the location bias can be found in Appendix A. An example of the bias for the water inlet temperature is found in Table 3 - 6.

Table 3 - 6: Temperature measurement bias example

Water inlet temperature (°C)	40
RTD bias (°C)	0.24
Location bias (°C)	0.16
Total bias (°C)	0.29

To describe the bias of the heat rejected at the gas cooler, the bias of the mass flow rate and the temperature differential must be propagated into bias in kW. To do this, Moffat's methods of sensitivity factors and the root sum of squares is used to give the equations below:

$$\theta_{\dot{m}} = \frac{\partial \dot{Q}_{\text{out}}}{\partial \dot{m}} = C_{\text{p}} \Delta T \tag{3.7}$$

$$\theta_{\Delta \text{T}} = \frac{\partial \dot{Q}_{\text{out}}}{\partial \Delta T} = \dot{m} C_{\text{p}} \tag{3.8}$$

$$B_{\dot{Q}_{\text{out}}} = \sqrt{(\theta_{\dot{m}} B_{\dot{m}})^2 + (\theta_{\Delta \text{T}} B_{\Delta \text{T}})^2} \tag{3.9}$$

where $\theta_{\dot{m}}$ is the sensitivity factor for the mass flow rate of water, $\theta_{\Delta \text{T}}$ is the sensitivity factor for the temperature differential across the gas cooler, and $B_{\dot{Q}_{\text{out}}}$ is the final bias for $\dot{Q}_{\text{out}}$.

3.7.2. Uncertainty of heat pump work

The other major component of the COP is the compressor, fan, and pump work, therefore the bias of the $\dot{W}_{\text{in}}$ will be covered in this section. The power consumed by the unit is measured by a power analyzer. The power analyzer measures the current, voltage, and phase angle and outputs pulses that are proportional to the power consumed. The bias for the work input is comprised of the bias of the power analyzer and the bias associated with counting pulses. The bias of the power analyzer involves the bias of the voltage (B_{V}) and current (B_{I}) reading. The

manufacturer's specifications stipulate the bias for both the voltage and current are 0.04% of the reading and 0.04% of the range. Therefore, the two main sources of bias for the work of the heat pump includes the power analyzer bias and the equivalent error of one pulse. Once again, the bias associated with one pulse is orders of magnitude smaller than the next smallest error, therefore it was omitted from the calculations. The same method used for the flow rate with sensitivity factors is applied here and the root sum of squares method is used to calculate the overall bias for the heat pump work measurements.

$$B_{\dot{W}_{in}} = \sqrt{(\theta_V B_V)^2 + (\theta_I B_I)^2} \tag{3.10}$$

In Equation 3.10, $B_{\dot{W}_{in}}$ represents the total bias for the power measurements, θ_V represents the sensitivity factor for the voltage, and θ_I represents the sensitivity factor for the current. Now the bias for the heat pump power and heat rejection must be propagated through to the COP. Again, this is done using sensitivity factors and the root sum of squares method.

$$B_{COP} = \sqrt{\left(\frac{\partial COP}{\partial \dot{W}_{in}} B_{\dot{W}_{in}}\right)^2 + \left(\frac{\partial COP}{\partial \dot{Q}_{out}} B_{\dot{Q}_{out}}\right)^2} \tag{3.11}$$

Table 3 - 7 shows some samples of the measured COP and the corresponding bias.

Table 3 - 7: Example of COP uncertainty

Ambient Temperature (°C)	COP	B_{COP}
25	4.5	0.71
10	3.7	0.54
-10	2.6	0.32
-20	2.0	0.23

Next, the error analysis for the refrigerant side will be included.

3.7.3. Uncertainty of refrigerant temperatures

The temperatures of the refrigerant state points were measured with surface mounted RTDs. Consequently, these measurements were prone to not only the manufacturer specified bias but also the bias introduced by measuring the pipe surface temperature instead of the fluid temperature. This is because when a surface mounted RTD is used, the temperature that is being measured is not the actual refrigerant temperature but is the temperature of the outer surface of the refrigerant tube. The temperature of the fluid inside the tube can differ greatly from the temperature of the outer surface of the tube. Gorman et al. [59] developed a relation to quantify this temperature difference. This relation was developed using numerical simulation which accounted for convective and conductive heat transfer and their effects on the pipe surface and fluid temperatures. The essential result from the numerical simulation, θ_{crit}, is described by Equation 3.12 [59]:

$$\theta_{\text{crit}} = \frac{T_{\text{surface}} - T_{\text{air,in}}}{T_{\text{fluid,in}} - T_{\text{air,in}}} \tag{3.12}$$

where T_{surface} represents the temperature of the pipe's surface, and $T_{\text{air,in}}$ and $T_{\text{fluid,in}}$ represent the temperatures of the air and fluid upstream of the measurement device. In Gorman et al. [59], values of θ_{crit} were tabulated for different combinations of the fluid's Reynolds number, the air's Reynolds number, and the Prandtl number for the fluid. θ_{crit} represents a ratio of the temperature differences between the measured and actual fluid temperature with the air and is used to estimate the actual fluid temperature. The fluid's Reynolds number and Prandtl number, along with the Reynolds number for air, were all estimated. Case 4 [59] most closely matched the estimated numbers for this research, therefore θ_{crit} was taken as 0.9280. Case 4 was described by a Reynolds

number of 30,000 for the ambient air, a Reynolds number of 150,000 for the refrigerant, and a Prandtl number of 1 for the refrigerant [59]. The actual fluid temperature is predicted by using the air (T_{air}) and measured (T_{meas}) temperature with θ_{crit} in Equation 3.13 [59]. The left-hand side of Equation 3.13 is calculated and added to the bias of each refrigerant temperature. Therefore, the bias for the six refrigerant temperatures is comprised of the error described in this section and the manufacturer's error.

$$B_{T_{location}} = T_{\text{fluid}} - T_{\text{meas}} = (T_{\text{meas}} - T_{\text{air}})\left(\frac{1-\theta_{\text{crit}}}{\theta_{\text{crit}}}\right) \quad 3.13$$

3.8. Limitations

Natural Resources Canada, CanmetENERGY – Ottawa recently instrumented and commissioned a $SANCO_2$ HPWH. Access to this apparatus was allowed by CanmetENERGY through a collaborative effort, therefore it was not built by the author. Due to restrictions imposed by CanmetENERGY, several desirable parameters were not measured. Consequently, a key limitation is the data of the state points included only the temperature and excluded the pressure. In addition, for the same reason previously mentioned, the mass flow rate of the refrigerant was not measured. Moreover, because this was an air to water heat pump, the heat transferred into the evaporator was not measured. Without pressures to fix the state and without mass flow rate, the heat transferred into the evaporator could only be estimated with the help of some assumptions. Consequently, without pressure measurements, the mass flow rate, or adequate manufacturer's data, the isentropic efficiency of the compressor could only be approximated.

3.9. Summary

Using the experimental setup and calculation procedure described in this chapter, it was possible to calibrate a numerical model, to study the control scheme, and to create a performance

map of the HPWH. The details concerning the experimental apparatus, including the equipment used, test conditions, instrumentation, and calculations were described in this section. Measurement error and the final error for the COP of the HPWH was also presented in this section. Furthermore, the limitations of the apparatus were outlined. The numerical model that was developed using the experimental data is reviewed in the following chapter.

4. Numerical model

A steady state numerical model of the CO_2 HPWH was created to predict the state points of the cycle and to estimate the compressor's isentropic efficiency. This chapter covers the modelling approach, the model logic, the verification of the model and the associated limitations and assumptions.

4.1. Numerical model overview

The numerical model was created in Engineering Equation Solver (EES). EES is an iterative equation solver that has a library of thermophysical properties for a range of engineering fluids, including CO_2 [10]. As discussed in the previous sections, the pressures of the cycle were not measured during the experimental evaluation of the HPWH, and therefore the isentropic efficiency of the compressor could not be experimentally determined. Additionally, the isentropic efficiency of the compressor was not available from the manufacturer. Typically, either the pressures or the isentropic efficiency is known and then the unknown parameter(s) can be calculated [1–5]. As a result, the purpose of the model developed in this study was to predict the high side pressure, the low side pressure, the enthalpy of the six refrigerant state points, and the isentropic efficiency of the compressor. These six state points refer to state points 1 through 6 from the system schematic in Figure 4 - 1. Furthermore, the model used experimentally measured data and thermodynamic analysis to approximate the desired parameters. The measured data used in the model and the model calculated parameters are illustrated in Figure 4 - 1. Each component of the system has its own submodel and is assumed to be at steady state. The assumption that each component is at steady state is a common one, as evidenced by Murray et al. [10], Cuevas et al.

[16], Liao et al. [25], and Yang et al. [60]. In the following section, each component will be covered in detail, beginning with the compressor and gas cooler.

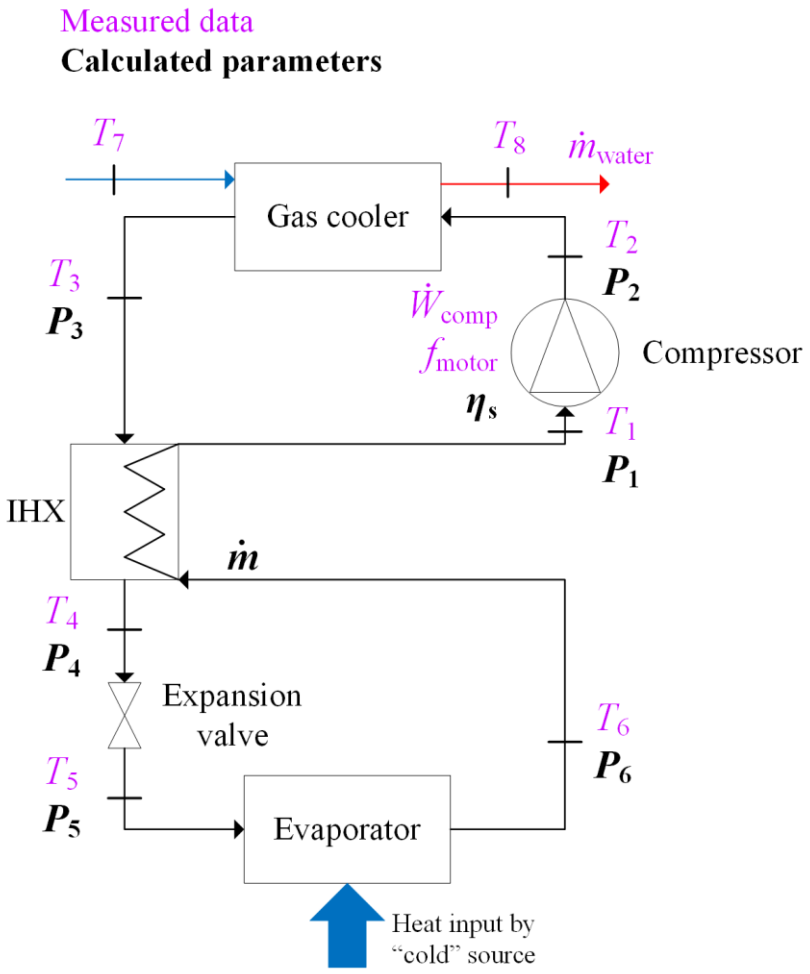

Figure 4 - 1: Sanden cycle schematic labelled with measured and calculated parameters

4.2. Compressor and gas cooler

The key components to observe when predicting the discharge pressure and isentropic efficiency are the compressor and gas cooler. This is due to the influence that the gas cooler outlet temperature (T_3) has on the discharge pressure (P_2) [6–8]; effectually, a change in the gas cooler outlet temperature results in a change in discharge pressure. In turn, the discharge pressure influences the discharge enthalpy because enthalpy is a function of temperature and pressure.

Furthermore, the isentropic efficiency is a function of discharge enthalpy, thus, isentropic efficiency is influenced by the discharge pressure. Additionally, the discharge pressure's influence on the isentropic efficiency is reflected in the literature by the numerous correlations that have been developed for the efficiency as a function of pressure ratio, which involves both the discharge and suction pressure [4, 5, 9, 10]. Thus, the gas cooler and compressor are modeled together because the conditions at the gas cooler affect the performance of the compressor. Both the compressor and gas cooler can be represented by a series of governing equations which are described in detail in the proceeding section.

4.2.1. Compressor and gas cooler equations

A first law energy balance was used to analyze the compressor and its reduced form is shown by Equation 4.1. To reduce the energy balance, several assumptions were made. These assumptions include that kinetic and potential energy effects are negligible and that the compressor is adiabatic. The compressor is assumed to be adiabatic because it is well insulated and the estimated heat loss from the compressor to the surroundings is minimal compared to the estimated heat loss from the gas cooler to the surroundings.

$$\dot{W}_{\text{comp}} = \dot{m}(h_2 - h_1) \tag{4.1}$$

$\dot{W}_{\text{comp}}$ is the experimentally measured compressor work, $\dot{m}$ is the refrigerant mass flow rate, h_2 is the compressor outlet (discharge) enthalpy, and h_1 is the compressor inlet (suction) enthalpy. Similar to the compressor, the gas cooler was analyzed with a first law energy balance and the assumptions that kinetic and potential energy effects are negligible. Unlike the compressor, the gas cooler was not adiabatic. The passive heat losses from the gas cooler to the surroundings

were estimated and termed $\dot{Q}_{\text{losses}}$. The estimation of $\dot{Q}_{\text{losses}}$ is outlined in Section 4.2.2. The reduced first law energy balance for the gas cooler becomes:

$$\dot{Q}_{\text{out}} + \dot{Q}_{\text{losses}} = \dot{m}(h_2 - h_3) \tag{4.2}$$

where $\dot{Q}_{\text{out}}$ is the derived from measurements heat transfer rate into the water and h_3 is the enthalpy of the gas cooler outlet. It has been previously mentioned that refrigerant mass flow rate measurements were not taken. Consequently, the mass flow rate was estimated using the compressor's motor frequency. First, the motor frequency was converted to compressor shaft speed using:

$$N = \frac{f \times 120}{\#\ of\ poles} \tag{4.3}$$

where f is the motor frequency in Hz, N is the compressor shaft speed in RPM, and the $\#\ of\ poles$ is given by the manufacturer. The compressor shaft speed is used to approximate the mass flow rate of the refrigerant with the following relation:

$$\dot{m} = \frac{\rho_1 N V v}{60} \tag{4.4}$$

where ρ_1 is the density of the refrigerant at the compressor inlet, V is the swept volume of the compressor, and v is the volumetric efficiency of the compressor. The above relation has been used by Wang et al. [64], Diaby et al. [62], and Yang et al. [60].

Finally, the isentropic efficiency of the compressor is defined as the isentropic compressor work divided by the actual compressor work and is expressed as:

$$\eta_s = \frac{(h_{2s} - h_1)}{(h_2 - h_1)} \tag{4.5}$$

where η_s is the isentropic efficiency and h_{2s} is the isentropic compressor outlet enthalpy. Now that the governing equations for the compressor and gas cooler have been covered, the approximations that were necessary to use the equations will be described.

4.2.2. Compressor and gas cooler approximations

To effectively employ the outlined model, several approximations were made concerning the specifications of the compressor and gas cooler. These approximations include the volumetric efficiency of the compressor, the passive heat losses from the gas cooler, and the gas cooler pressure drop.

The volumetric efficiency of the compressor is utilized to estimate the mass flow rate in Equation 4.4. An initial assumption of 90% for the volumetric efficiency was used based on the literature [64], and compared to the experimental data which produced results that were not physically possible. The volumetric efficiency of the compressor was then iterated with the experimental data to find the best fit, which was determined to be 80%. It was assumed that the best fit had been found when the predicted enthalpy for the compressor discharge (h_2) and the gas cooler outlet (h_3) was within the range of possible enthalpies for the measured temperature.

The gas cooler is a relatively large component in the HPWH and is positioned directly below the evaporator fan, thereby exposing it to forced airflow. Furthermore, the temperature of the working fluid is at least 55°C warmer than its surroundings. Although the gas cooler is insulated, the heat loss from the gas cooler was approximated and was found to be significant. The passive heat loss from the gas cooler was estimated through consideration of convective and radiative heat transfer. For both modes of heat transfer, the gas cooler was treated as a rectangular box with a uniform surface temperature of 50°C. To consider the convective heat loss, the air

velocity was assumed to be 2.1 m/s for all temperatures, which was calculated from an average airflow rate from the manufacturer. The Reynolds number was calculated with this air velocity and was found to be ~19,000, which is in the laminar range. Therefore, the following equation from Bergman et al. [65] was used to approximate the average Nusselt number for laminar flow over a flat plate.

$$\overline{Nu} = 0.664 Re^{1/2} Pr^{1/3} \tag{4.6}$$

In Equation 4.6, $\overline{Nu}$ represents the average Nusselt number, Re represents the Reynolds number, and Pr represents the Prandtl number. Next, the Nusselt number was utilized in conjunction with the length of the gas cooler "box" and the thermal conductivity of air to estimate the average convection coefficient. The thermal conductivity of air was evaluated by using the average of the ambient air temperature and the gas cooler surface temperature [65]. The resulting convection coefficient was used in Newton's Law of Cooling to approximate the convective heat losses, which are displayed in Table 4 - 1. Once the convective heat loss was determined, the radiative heat loss was calculated using the enclosure analysis approach, which is described by Equation 4.7 [65].

$$\dot{Q}_{\mathrm{rad}} = \sigma A_{\mathrm{gc}} \varepsilon_{\mathrm{gc}} (T_{\mathrm{gc}}^4 - T_{surr}^4) \tag{4.7}$$

In Equation 4.7, $\dot{Q}_{\mathrm{rad}}$ represents the heat loss from the gas cooler through radiation, σ represents the Stefan-Boltzmann constant, A_{gc} represents the area of the gas cooler, ε_{gc} represents the emissivity of the surface of the gas cooler, T_{gc} represents the temperature of the gas cooler surface, and T_{surr} represents the temperature of the surroundings. The surface of the gas cooler was assumed to have an emissivity of 0.9, which was chosen as an average value across materials that were similar in appearance and texture to the gas cooler insulation from Bergman [65]. The

approximated convective and radiative heat losses were combined and termed $\dot{Q}_{\text{losses}}$, which are presented in Table 4 - 1. To estimate the uncertainty of $\dot{Q}_{\text{losses}}$, a sensitivity analysis was performed by varying the assumptions made during the calculation process. Some of the assumptions that were varied include the gas cooler surface temperature, the convection coefficient, the air velocity, and the emissivity. The calculated differences from the sensitivity analysis were combined using the root sum of squares method and were used as the bias for $\dot{Q}_{\text{losses}}$. More details regarding the estimation of $\dot{Q}_{\text{losses}}$ and the associated bias can be found in Appendix B.

Table 4 - 1: Estimated gas cooler passive heat losses and associated error

Ambient Temperature (°C)	**Convection coefficient (W/m^{2}K)**	**Convective heat loss (W)**	**Radiative heat loss (W)**	**Passive heat loss (W)**	**Estimated error (W)**
25	13.58	29	43	72	25
10	13.59	46	64	110	29
-10	13.66	69	87	156	34

The final approximation that will be discussed is the pressure drop in the gas cooler. It is commonly assumed that the gas cooler is isobaric, therefore the same assumption was made for this research [1, 12, 14–16].

4.2.3. Predicting the cycle pressures

In order to approximate the isentropic efficiency of the compressor, it is necessary to predict the cycle pressures. The cycle pressures include the high side pressure and the low side pressure. The high side pressure refers to the pressures of state points 2, 3, and 4. Additionally, sometimes the high side pressure is referred to as the discharge pressure or the gas cooler pressure.

The low side pressure refers to the pressures of state points 1, 5, and 6. Other terms used to describe the low side pressure are the suction pressure or the evaporator pressure. The process in which the model uses to estimate the pressures will be outlined in this section.

The model first estimates the suction pressure by calculating the saturation pressure of the evaporator temperature (either T_5 or T_6). At times, there was a significant difference between the evaporator inlet (T_5) and the evaporator outlet temperature (T_6), therefore the lowest of T_5 and T_6 was used for the evaporator temperature. This ensures that the evaporator outlet temperature is either equal to or greater than the evaporator inlet temperature. Next, the enthalpy of state point 1 (h_1) is calculated by using the suction pressure and the measured temperature at state point 1 (T_1). Then, the enthalpy of state point 2 (h_2) is calculated using the reduced first law energy balance shown below, which is Equation 4.1 rearranged. The measured $\dot{W}_{\text{comp}}$ and estimated $\dot{m}$ are used when calculating h_2 with Equation 4.8.

$$h_2 = \frac{\dot{W}_{\text{comp}}}{\dot{m}} + h_1 \tag{4.8}$$

Then, h_2 is used in conjunction with other measured and estimated parameters to calculate the enthalpy at state point 3 (h_3). The included parameters are $\dot{Q}_{\text{out}}$, $\dot{m}$, and $\dot{Q}_{\text{losses}}$. Equation 4.9 is the first method used to calculate h_3, which is termed as $h_{3\text{L}}$ from this point on.

$$h_{3\text{L}} = h_2 - \frac{\dot{Q}_{\text{out}} + \dot{Q}_{\text{losses}}}{\dot{m}} \tag{4.9}$$

Thus far, the method for estimating the low side pressure, h_2 and $h_{3\text{L}}$ have been described. The purpose of calculating the enthalpy at state points 2 and 3 is to use them in conjunction with the measured temperatures at the corresponding state point to fix the state and estimate the high

side pressure. Therefore, h_2 and the measured compressor outlet temperature (T_2) are utilized to fix the state and estimate the high side pressure (P_2).

The high side pressure can be estimated again using h_{3L} and the measured gas cooler outlet temperature (T_3) to fix the state. This second estimate for the high side pressure is referred to as P_3. As was mentioned earlier, two estimates were also made for h_3. The second method to predict h_3 involves assuming the gas cooler is isobaric by using P_2 and the measured T_3 to fix the state. This second estimate for the enthalpy at state point 3 is termed h_{3P}. It is beneficial to have two estimates of the high side pressure and h_3 because of the significant bias of the measured data. The bias of the measured data propagates through the model calculations and can result in more significant errors for the model calculated values. Subsequently, two parameters were introduced to determine the accuracy of the discharge pressure and h_3 estimations. The first parameter is termed *dP* and is calculated by subtracting one pressure estimate from the other.

$$dP = P_2 - P_3 \tag{4.10}$$

The second parameter is termed *dh3* and is the difference between the two estimates of the gas cooler outlet enthalpy (h_3).

$$dh3 = h_{3L} - h_{3P} \tag{4.11}$$

The method for estimating the cycle pressures and the calculation of *dP* and *dh3* are visualized in Figure 4 - 2. In Figure 4 - 2, the measured data that was used in the estimation process is shown in purple while the modelled values are shown in black. The method in which *dh3* and *dP* are utilized in the model will be outlined in Section 4.6. For now, the discussion concerning how the HPWH components were modeled will continue with the electronic expansion valve.

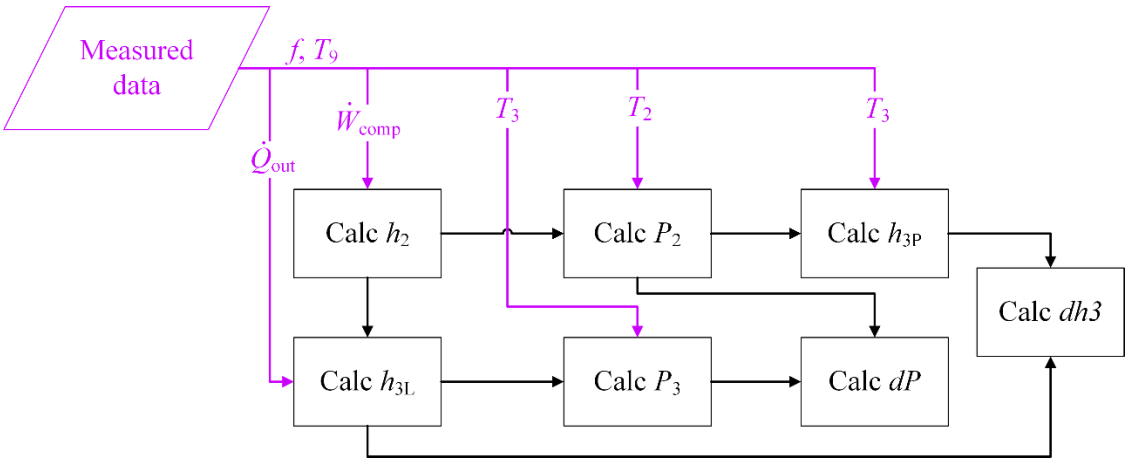

Figure 4 - 2: Visualization of the calculation method for *dh3* and *dP*

4.3. Electronic expansion valve

To fix state point 4 and to calculate its corresponding enthalpy (h_4), the estimated high side pressure and the measured expansion valve inlet temperature (T_4) were used. The electronic expansion valve (EEV) is assumed to be isenthalpic, therefore the enthalpy leaving the EEV (h_5) is equal to the enthalpy entering it (h_4) [10].

4.4. Evaporator

The governing equations that describe the evaporator, along with the necessary approximations, are described in the proceeding sections.

4.4.1. Evaporator equations

A first law energy balance was conducted on the evaporator and was reduced with the following assumptions to Equation 4.12. The assumptions concerning the evaporator are similar to the gas cooler assumptions in that kinetic and potential energy are both considered negligible. However, since the secondary fluid for the evaporator is the ambient air and is therefore warmer than the refrigerant, there is no passive heat loss term considered.

$$\dot{Q}_{in} = \dot{m}(h_6 - h_5) \tag{4.12}$$

Equation 4.12 was used to calculate $\dot{Q}_{\text{in}}$, where h_5 is the enthalpy entering the evaporator and h_6 is the enthalpy leaving the evaporator.

4.4.2. Evaporator approximations

To use Equation 4.12 in the model, several approximations were made concerning the evaporator pressure and outlet state. The pressure approximations are described first and are followed by the outlet state approximations. The evaporator pressure is calculated by finding the saturation pressure of the measured evaporator temperature (T_5 or T_6). Additionally, the evaporator is assumed to be isobaric, therefore the pressure of the refrigerant entering it (P_5) is equal to the pressure of the refrigerant leaving it (P_6). For the model's first iteration, it is assumed the refrigerant leaving the evaporator is a saturated vapour. If the model calculated $\dot{Q}_{\text{in}}$ is much larger than $\dot{Q}_{\text{in}}$ from a first law energy balance on the entire heat pump, then the quality of the evaporator outlet state (x_6) is reduced from 1 to a minimum value of 0.9 in subsequent iterations. It is a common assumption that the evaporator outlet is a saturated vapour or that is has some superheat [10], [62], [67]. However, the cycle in this research has an IHX which provides further heat to the working fluid after the evaporator outlet and before the compressor inlet. Therefore, it is possible for the refrigerant to leave the evaporator with a quality less than 1 and be superheated in the IHX. There are two reasons why this deviation was implemented into the model. The first reason is that when the model calculated state points (h_5 and h_6) are used in conjunction with Equation 4.12 to calculate $\dot{Q}_{\text{in}}$, the result can be significantly overestimated. By reducing the quality of the evaporator outlet, h_6 is also reduced and subsequently decreases $\dot{Q}_{\text{in}}$. The decrease in the enthalpy difference across the evaporator that corresponds to a decrease in x_6 can be visualized in Figure 4

- 3. In Figure 4 - 3, point 5 refers to the evaporator inlet, point 6a to the evaporator outlet with a quality of 90% and point 6b to the evaporator outlet with a quality of 100%. Process 5 – 6a results in a smaller enthalpy difference than process 5 – 6b. With a constant mass flow rate, a smaller enthalpy difference results in a decreased $\dot{Q}_{\text{in}}$.

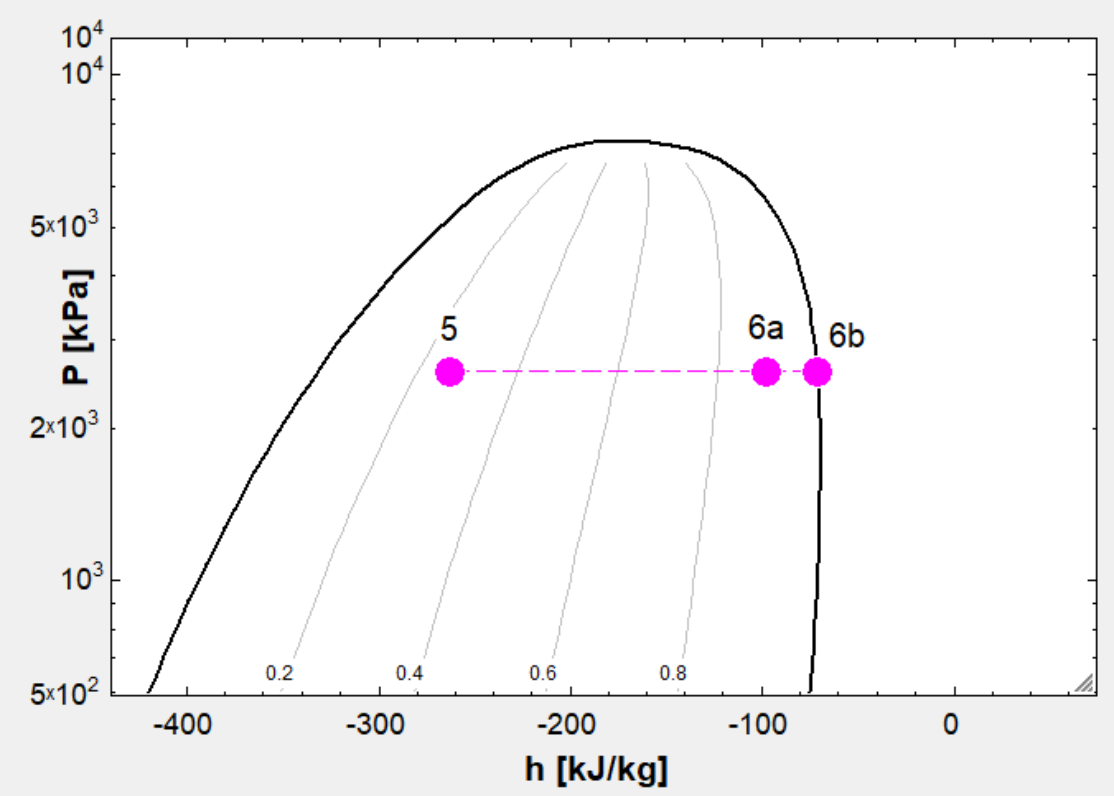

Figure 4 - 3: P-h diagram comparing different evaporator outlet states

The second reason for the variation of the evaporator outlet quality is due to the overestimation of h_1 in specific conditions. For reference, h_1 refers to the enthalpy of the compressor inlet. Because h_2 is calculated using h_1 (Equation 4.8), an overestimation in h_1 will cause an overestimation in h_2. Furthermore, the discharge pressure (P_2) is calculated as a function of h_2 and T_2. Due to the shape of the isotherms, an overestimated h_2 results in a discharge pressure that is smaller than the suction pressure, which is illustrated in Figure 4 - 4. Therefore, the

evaporator outlet is varied to ensure that the discharge pressure is greater than the suction pressure. By decreasing the quality of the evaporator outlet, h_1 is decreased and causes a decrease in h_2, which results in an increased P_2 for the same T_2. Figure 4 - 4 illustrates this process, where both 1 – 2 processes represent the work of the compressor. The orange squares represent the resulting work with h_1 calculated using the evaporator pressure and measured T_1. In this first process, h_6 is calculated with a quality of one. In contrast, the pink diamonds represent the work with h_1 calculated using the effectiveness method and h_6. In this second process, h_6 is calculated using a quality of less than one. The effectiveness method will be described in the following section.

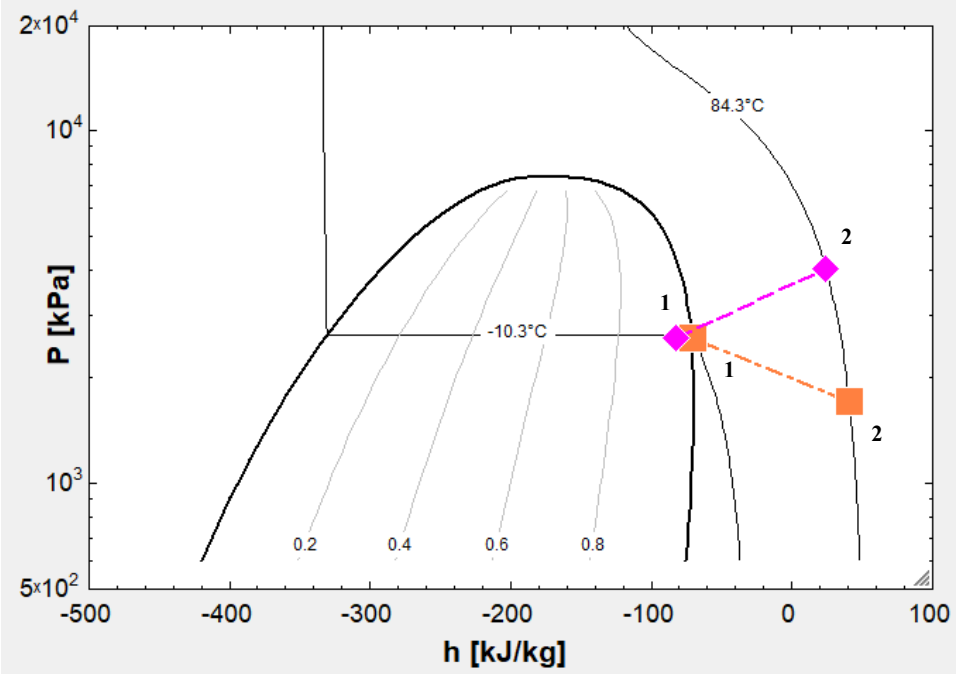

Figure 4 - 4: P - h diagram depicting the effects differing compressor suction states have on the discharge state

Thus, the quality of the refrigerant leaving the evaporator is sometimes assumed to be less than 1 to provide more accurate estimates for $\dot{Q}_{\text{in}}$ and P_2. Notably, this deviation only occurs when

extreme conditions occur, such as the situation that led to Figure 4 - 4 or a significantly overestimated $\dot{Q}_{\text{in}}$.

4.5. Internal heat exchanger

The equations and approximations regarding the IHX will be described in this section. The discussion will begin with the effectiveness method that was mentioned in the previous section. The effectiveness method is used to analyze the IHX and to calculate the enthalpy of the compressor inlet (h_1) for any subsequent iterations. This ensures that any changes in the quality of the evaporator outlet (h_6) are reflected in the rest of the state points. The effectiveness method involves dividing the heat transfer rate from the high pressure side to the low pressure side by the theoretical maximum heat transfer rate. The effectiveness method is shown in Equation 4.13, where $\dot{Q}_{\text{IHX}}$ represents the heat transfer from the high pressure stream to the low pressure stream, $\dot{Q}_{\text{max}}$ represents the theoretical maximum heat transfer rate., and ε represents the heat exchanger effectiveness.

$$\varepsilon = \frac{\dot{Q}_{\text{IHX}}}{\dot{Q}_{\text{max}}} \tag{4.13}$$

A first law energy balance can be performed on the low pressure side of the IHX and reduced to Equation 4.14. The assumptions involved in the simplification of the energy balance include no work, negligible heat losses to the surroundings, and negligible potential and kinetic energy.

$$\dot{Q}_{\text{IHX}} = \dot{m}(h_1 - h_6) \tag{4.14}$$

The theoretical maximum heat transfer rate assumes that all heat transfer possible has occurred when the outlet temperature of the cold stream is equal to the inlet temperature of the hot

stream [65]. However, the specific heat was not assumed to be constant because great variation exists in the specific heat around the critical point. Therefore, Equation 4.15 was used to calculate the maximum heat transfer rate. It is important to note that enthalpy is a function of both temperature and pressure. Thus, even if the outlet temperature of the cold stream equaled the inlet temperature of the hot stream, it would be impossible for their pressures to be equal. Therefore, in Equation 4.15, the gas cooler outlet enthalpy is termed $h_{3,m}$ and is calculated using the measured gas cooler outlet temperature (T_3) and the low side pressure.

$$\dot{Q}_{\max} = \dot{m}\left(h_{3,m} - h_6\right) \tag{4.15}$$

Combining Equations 4.14 and 4.15 with Equation 4.13 gives Equation 4.16, which was utilized to calculate the compressor inlet enthalpy (h_1).

$$\varepsilon = \frac{h_1 - h_6}{h_3 - h_6} \tag{4.16}$$

The final approximation is that the IHX effectiveness was assumed to be 0.2. This value was chosen because previous work on a comparable system found that the IHX had an effectiveness of 0.2 [10]. Notably, different values were attempted but it was found that an effectiveness of 0.2 fit the data the most appropriately. This concludes the discussion concerning each individual component's modelling methodology.

4.6. Model convergence and verification

The experimentally measured data was limited, therefore theoretical methods were employed to ensure the estimated cycle pressures and calculated state points were reasonable. Both model convergence and verification methods involve calculating specific state points or heat transfer rates twice and subtracting one from the other. For reference, *dP* and *dh3* are two such

parameters and are described by Equations 4.10 and 4.11. Another parameter is termed *dQ* and is described in this section. It is necessary to calculate certain parameters twice because of the considerable uncertainty of the measured data. The measured data is used to calibrate the model, therefore any uncertainty in the data propagates through to the estimated pressures and enthalpies. By calculating certain state points twice and ensuring the difference between each method approaches zero, it is assumed that a reasonable value has been found for each state point. The approach used to confirm model convergence will be reviewed in detail and followed with the model verification.

4.6.1. Model convergence

In the context of this thesis, model convergence refers to when the value of *dh3* approaches zero. For reference, *dh3* is calculated by estimating the gas cooler outlet enthalpy (h_3) with two methods and finding the difference between the estimations. Section 4.2.3 describes *dh3* in more detail. In certain conditions, *dh3* resulted in a very large value and thus indicated the model had not converged and that the estimated discharge pressure was unreasonable. However, *dP* could result in a value as large as 2,000 kPa even when the model had converged and a reasonable discharge pressure had been found. This occurs when the phase of the gas cooler outlet state is a subcooled liquid. It was observed that in the subcooled region the enthalpy is a strong function of temperature but a weak function of pressure. Therefore, if the enthalpy and temperature are used to calculate the pressure of the subcooled liquid, then a very small error in either enthalpy or temperature can result in a very large difference in pressure. This can be seen in Table 4 - 2 and Figure 4 - 5. Table 4 - 2 shows that for constant enthalpy in the subcooled region, the calculated pressure can sometimes change by one MPa for a one degree change in temperature.

Table 4 - 2: Pressure variations in the subcooled region

#	P (MPa)	T (°C)	h (kJ/kg)
1	7.0	22	-250
2	7.8	23	-250
3	8.8	24	-250
4	9.8	25	-250

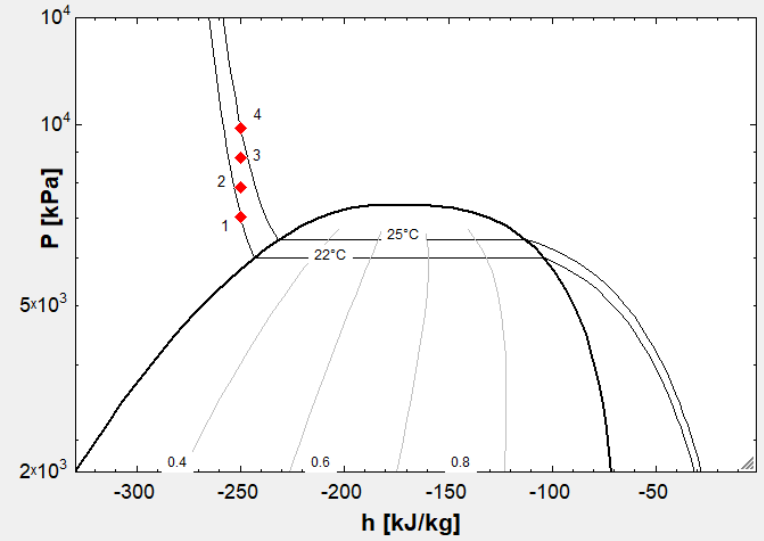

Figure 4 - 5: P - h diagram depicting pressure increase with an increase in temperature and constant enthalpy

Consequently, *dh3* was chosen as the parameter to determine model convergence. Additionally, a limit of 3 kJ/kg was chosen for *dh3* because a limit of approximately 0 kJ/kg was unreasonable for many data points due to the significant biases of the measured data. Accordingly, iterations stop once *dh3* is equal to or less than 3 kJ/kg or when no more iterations are possible. Yet, *dh3* for many data points did not converge to the limit but came within a reasonable value, an example is shown in Table 4 - 3. In these cases, the discharge pressure that corresponds to the smallest *dh3* is considered to be the most accurate estimate. Table 4 - 3 illustrates a brief sensitivity study that shows the isentropic efficiency changing minimally as *dh3* converges to its minimum value. In summary, the parameter *dh3* was used to determine if reasonable estimates had been found for the discharge pressure.

Table 4 - 3: Changing isentropic efficiency with converging dh3

Iteration #	*dh3*	Isentropic efficiency
1	14.23	0.5619
2	13.94	0.5604
3	13.66	0.5589
4	13.38	0.5575
5	13.09	0.556
	…	
limit	7.62	0.5472

4.6.2. Model verification

The theoretical approach that was used to verify the model involved calculating the evaporator heat transfer rate ($\dot{Q}_{\text{in}}$) with two methods. The first method included deriving $\dot{Q}_{\text{in}}$ from measured and estimated data. Consequently, a first law energy balance was conducted on the entire heat pump and therefore used Equation 4.17 with the measured $\dot{Q}_{\text{out}}$, $\dot{W}_{\text{comp}}$ and the estimated $\dot{Q}_{\text{losses}}$. Figure 4 - 6 illustrates the first law energy balance on the entire heat pump. This first $\dot{Q}_{\text{in}}$ is referred to as derived from measurements and is represented by $\dot{Q}_{\text{in,f}}$.

$$\dot{Q}_{\text{in,f}} = \dot{Q}_{\text{out}} + \dot{Q}_{\text{losses}} - \dot{W}_{\text{comp}} \tag{4.17}$$

The second method in which $\dot{Q}_{\text{in}}$ was calculated used Equation 4.12 and is referred to as the model calculated $\dot{Q}_{\text{in}}$. The model calculated $\dot{Q}_{\text{in}}$ is represented by $\dot{Q}_{\text{in,m}}$. The difference between $\dot{Q}_{\text{in,f}}$ and $\dot{Q}_{\text{in,m}}$ is termed *dQ*.

$$dQ = \dot{Q}_{\text{in,m}} - \dot{Q}_{\text{in,f}} \tag{4.18}$$

If dQ is zero or within the uncertainty calculated for $\dot{Q}_{\text{in,f}}$, then the estimated evaporator state points are considered reasonable because there is no unaccounted energy transfer to or from the evaporator. The premise behind this verification is that when both *dh3* and dQ are close to zero, or within their limits, the best possible estimate of the discharge pressure, suction pressure and evaporator state points have been found. In turn, this gives the best estimate for the isentropic efficiency. This concludes the discussion on the model convergence and verification. The proceeding section describes the computational flow and logic of the model.

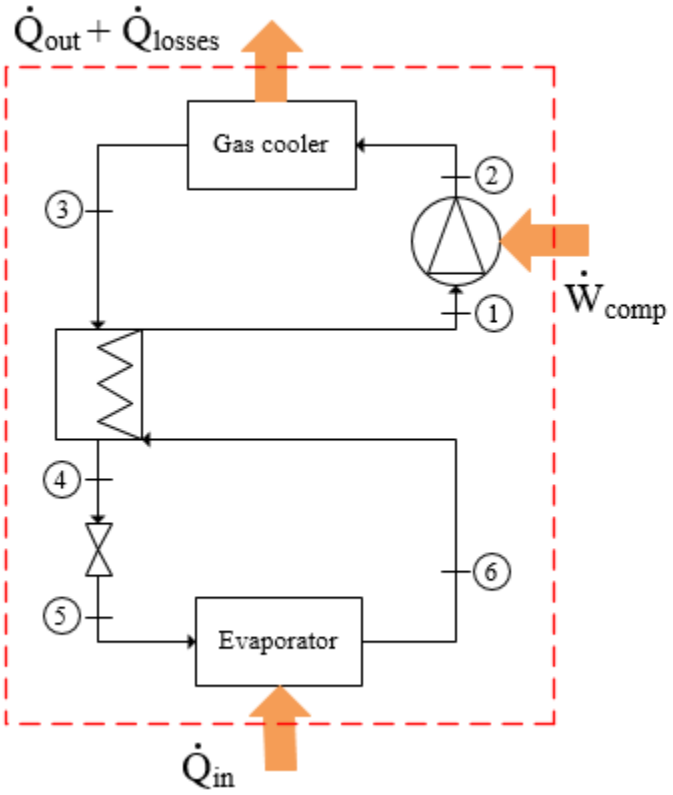

Figure 4 - 6: First law energy balance on the HPWH

4.7. Model logic

An overview of the iterative process and computational flow is described in this section and in Figure 4 - 7 and Figure 4 - 10. This model logic was developed to find reasonable estimates of the discharge pressure and isentropic efficiency that satisfy the first law equations within the bias of the measured data.

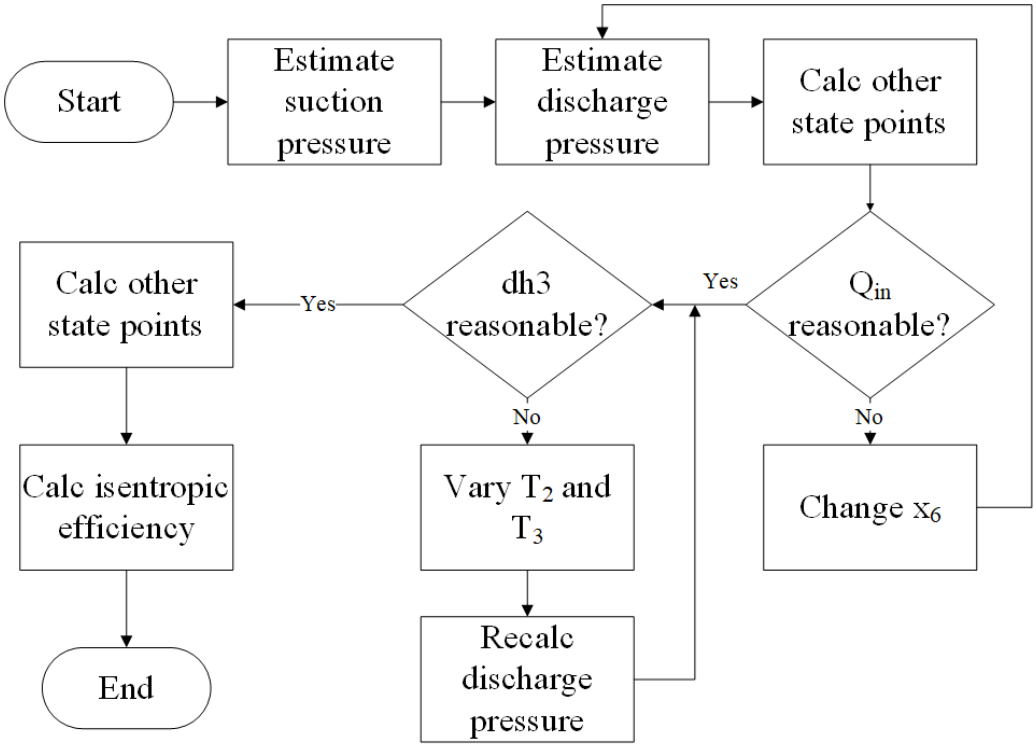

Figure 4 - 7: EES model overview of computational flow

The model begins by calculating the suction pressure using the evaporator temperature. Next, the enthalpy of the compressor inlet (h_1) is calculated and used in the compressor and gas cooler models, which results in the estimation of the discharge pressure. After, the enthalpy of the expansion valve inlet (h_4) is calculated and used in the expansion valve and evaporator submodels, thus completing the first iteration. In subsequent iterations, two methods were used to encourage convergence of the model. The first method involves varying the quality of the evaporator outlet

(x_6) and recalculating the enthalpy of the compressor inlet (h_1). This first method is only used if the model calculated $\dot{Q}_{\text{in}}$ is significantly larger than the measurement derived $\dot{Q}_{\text{in}}$ or if *dh3* is greater than 100 kJ/kg. Each time x_6 is varied, a new iteration is completed to recalculate the state points and the model calculated $\dot{Q}_{\text{in}}$. The second method involves varying the compressor outlet temperature (T_2) and the gas cooler outlet temperature (T_3) within their uncertainty. In Chapter 3, the uncertainty was described for the measured refrigerant temperatures, including T_2 and T_3. The uncertainty for these two temperatures is relatively large; depending on the conditions it ranges from 0.5°C to 8°C. These significant measurement errors can propagate into larger errors in the model calculated pressures and enthalpies. Therefore, to find the best estimate for the discharge pressure using the experimental data, T_2 and T_3 are varied within their uncertainty to find the minimum *dh3*. Figure 4 - 8 describes the method in which the temperatures T_2 and T_3 are varied.

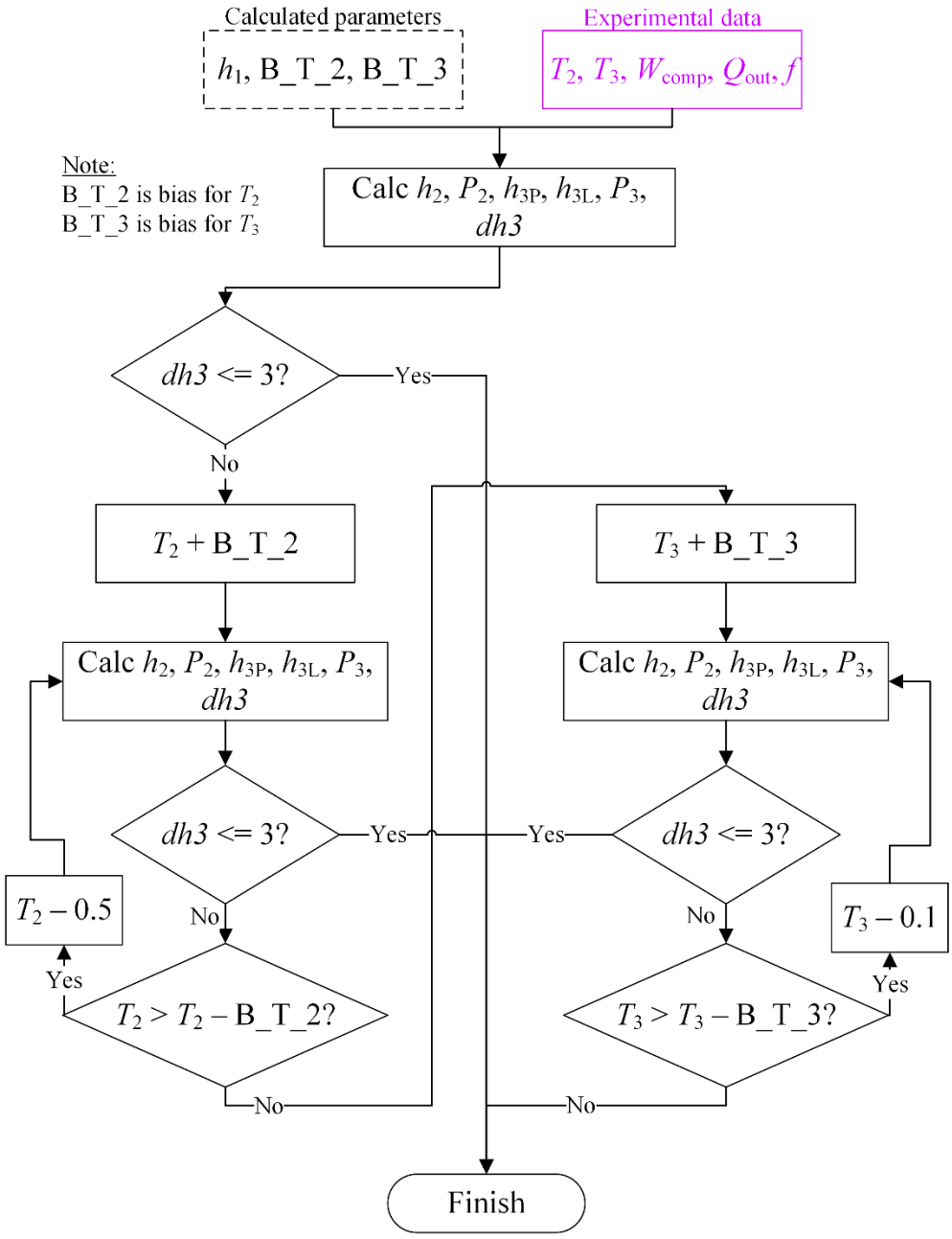

Figure 4 - 8: Method 2 for EES model convergence - variation of T_2 and T_3

After each variation of these two temperatures, the rest of the state points are recalculated. The employment of these two methods causes *dh3* and *dQ* to approach zero and thereby results in a better estimate for the discharge pressure and isentropic efficiency. The model terminates once *dh3* is equal to or less than 3 kJ/kg, or once there are no more possible iterations. In turn, the

conditions that resulted in the minimum *dh3* are used to calculate the isentropic efficiency. The transfer of parameter values between each component's submodel is illustrated in Figure 4 - 9 while the iterative process of the model is depicted in Figure 4 - 10.

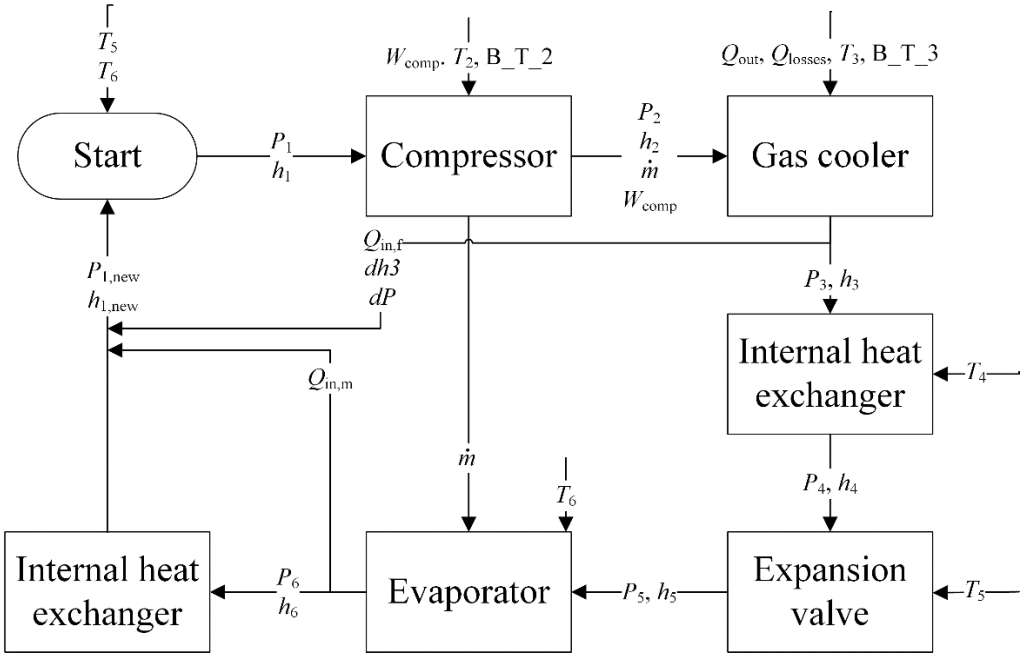

Figure 4 - 9: Transfer of measured data and estimated parameters between component submodels for numerical model

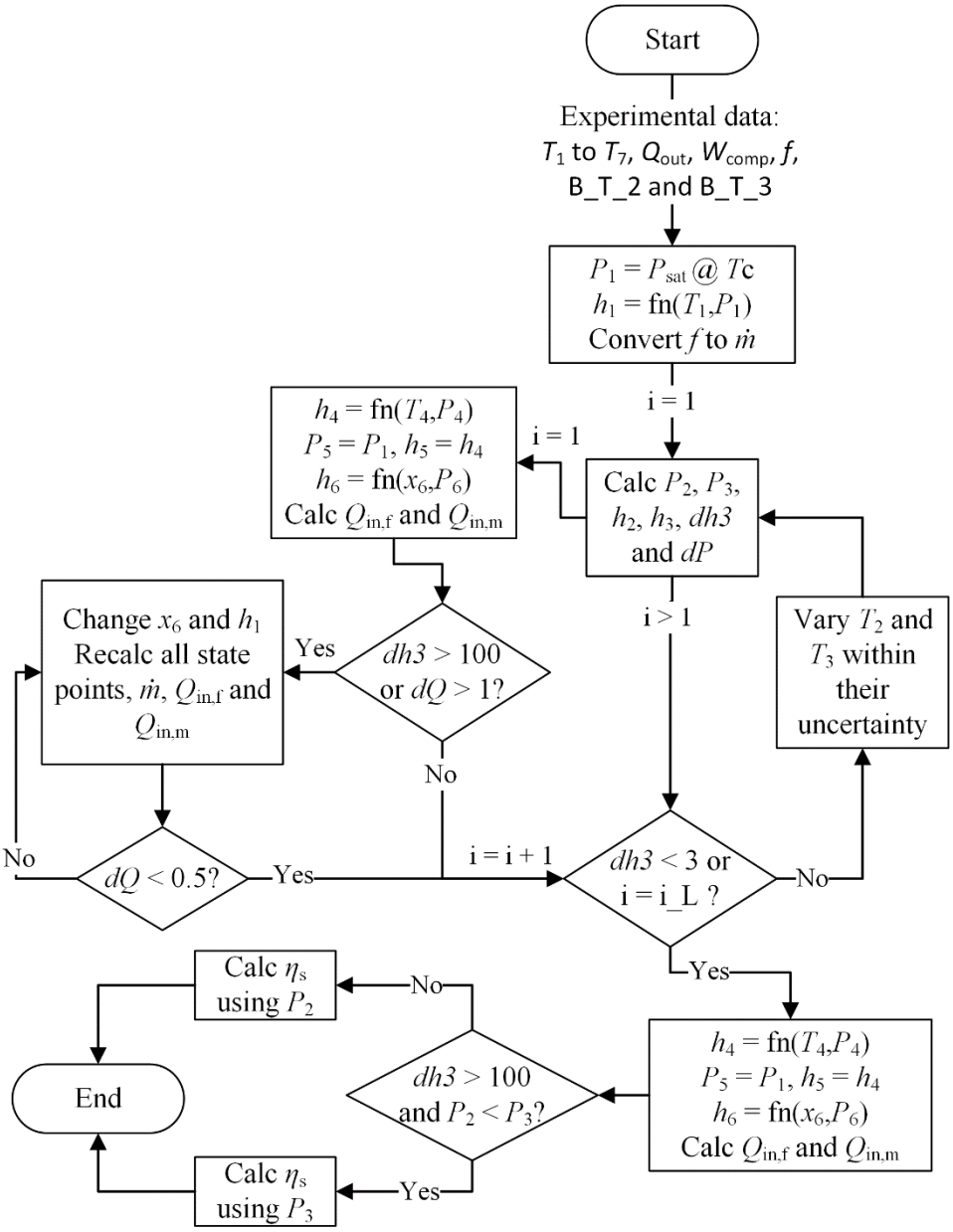

Figure 4 - 10: Logic of isentropic efficiency model

The final item to discuss involves *dP* - in some conditions *dP* was very large (greater than 1500 kPa). This created the dilemma of which discharge pressure estimate to use to calculate the isentropic efficiency. Generally, the estimate of P_2 was used because the phase of the refrigerant at state 2 is always either a supercritical fluid or a superheated steam. The enthalpy of supercritical and superheated fluids is more strongly correlated to pressure than a subcooled liquid is. Using P_2

in the correct conditions reduces the error of the final isentropic efficiency. However, P_3 is utilized to calculate the isentropic efficiency in conditions where dP is very large and P_2 is significantly underestimated.

4.8. Assumptions and limitations

Several assumptions and limitations were inherent in the development of this model. These were related to steady state analysis and the limits concerning the measured data.

It was assumed for this model that the HPWH and all its associated components were at steady state. While the ambient temperature remained relatively constant, the water inlet temperature was steadily increasing throughout each test. There was a temperature rise of approximately 45°C in a period ranging from one to two hours. As the water inlet temperature increases, so too would the temperature of the heat exchanger material. It was assumed that the transients involved in the heat exchangers and pipes were negligible. Additionally, the heat loss from the components other than the gas cooler (such as the lines between components and the compressor) were considered negligible compared to the heat loss from the gas cooler. The passive heat loss from the gas cooler was estimated and is covered in Section 4.2.2.

Motor frequency data was measured for the ambient temperatures of 25°C and -10°C, but not for 10°C. However, experimental data for all other necessary variables was measured for the ambient temperature of 10°C. Rather than having isentropic efficiencies for only the temperatures of 25°C and -10°C, a linear relationship was assumed for the motor frequency as a function of ambient temperature between 25°C and -10°C. Subsequently, with the assumed motor frequency, isentropic efficiency data was calculated for 10°C. Furthermore, due to the limited motor frequency data, the isentropic efficiency was only calculated for the ambient temperatures 25°C,

10°C, and -10°C. While performance data is available for more extensive ranges than that, the isentropic efficiency is limited to the abovementioned ambient temperatures.

The verification for the model did not include experimentally measured data for the pressure and isentropic efficiency. Measured data for these parameters was not available due to NRCan's restrictions for their HPWH and experimental facilities. Therefore, theoretical concepts of thermodynamics and parameters derived from the measurements were used to verify the model. Thus, the model is not experimentally validated and requires further work, as described in Chapter 6.

The considerable uncertainty associated with the measured data is an additional limitation. The uncertainty of the measured data propagates through to the estimated pressures and enthalpies and can cause significant errors in the final results. The process through which this uncertainty was quantified is covered in Chapter 3 and the process through which reasonable model estimates were found was described in this chapter. However, reasonable estimates were not always possible because of the significant uncertainty. Accordingly, Chapter 6 includes recommendations on uncertainty limits for future experimental work.

4.9. Summary of model

In this chapter, the model that was used to approximate the isentropic efficiency of the compressor and the cycle pressures was described. Each individual component of the HPWH and its associated equations and assumptions were included. Furthermore, the overall model logic, iterative process, means of convergence and verification were described in detail. Going forward, the estimated isentropic efficiency and cycle pressures can be used in a numerical model to

estimate the cycle state points and performance of the HPWH in a water-source configuration. The model generated results and all subsequent discussion are contained in the next chapter.

5. Results and discussion

The results for this research include the verification of the numerical model, the model results, and extensive performance data. The model results are comprised of predicted cycle pressures and compressor isentropic efficiency for different ambient air temperatures. Additionally, experimental data is reviewed and discussed in the context of the system's control logic. This section covers these results and any corresponding discussion in depth. Furthermore, the state points in this section are the same state points from Figure 4 - 1.

5.1. Model verification

In this section, the results for *dh3* and *dQ* are reviewed. These parameters were used to determine model convergence and verification and are described in detail in Section 4.6. For reference, the tests performed at the ambient temperatures of 25°C, 10°C, and -10°C are referred to as case A, case B, and case C from here on.

5.1.1. Verification results and trends

This section presents the results and overall trends for *dh3* and then for $\dot{Q}_{\text{in}}$. The details regarding the calculation of *dh3* are described in Section 4.2.3. It was assumed that when *dh3* approached 0 kJ/kg that a reasonable estimate for the discharge pressure had been found. However, it was not always possible or necessary for each *dh3* to converge to 0 kJ/kg, therefore it was considered to have converged once *dh3* was equal to or less than 3 kJ/kg. It was not always necessary for *dh3* to converge to 0 kJ/kg due to the minimal change that was observed in the resulting isentropic efficiency from each iteration. Figure 5 - 1 illustrates the results for *dh3* for case A, B, and C. For case A, the majority of the results remain between 1 kJ/kg and 20 kJ/kg with the minimum and maximum of 0.02 kJ/kg and 26 kJ/kg, respectively. For case B, *dh3* ranges

between 10 kJ/kg and 30 kJ/kg until the water inlet temperature reaches 30°C, after which *dh3* converges approximately to the set limit of 3 kJ/kg. For case C, *dh3* ranges between 100 kJ/kg to 200 kJ/kg with the exception of six points that approach zero. There are several reasons why *dh3* is greater than 3 kJ/kg and these will be covered in Section 5.1.2.

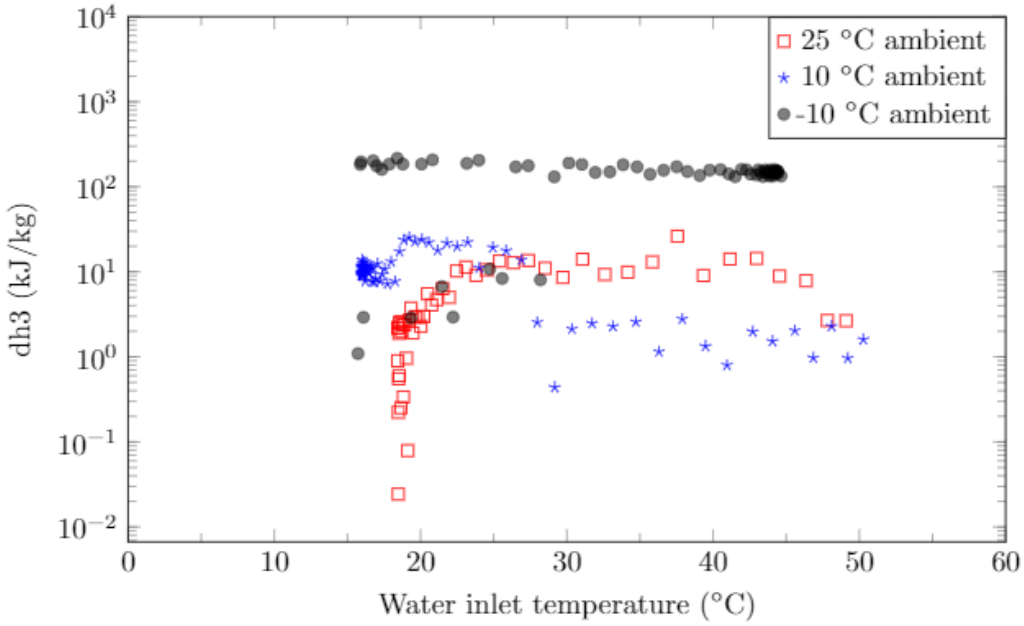

Figure 5 - 1: Model results for dh3

The results and overall trends for $\dot{Q}_{\text{in}}$ will be covered next. The first law of thermodynamics was used to verify the model by calculating the heat transfer rate into the evaporator, $\dot{Q}_{\text{in}}$, with two separate methods. The first method included a first law energy balance on the entire system (derived from measurements) and the second method included a first law energy balance on just the evaporator (model calculated). Section 4.6.2 reviews these calculations in more detail. The derived from measurements and model calculated $\dot{Q}_{\text{in}}$ are shown in Figure 5 - 2, Figure 5 - 3, and Figure 5 - 4 for case A, B, and C, respectively. While the model calculated $\dot{Q}_{\text{in}}$ is very close to the derived from measurements $\dot{Q}_{\text{in}}$ for case A, the same cannot be said for case B and C. The largest

bias associated with the derived from measurements $\dot{Q}_{in}$ for case A, B, and C are 0.22 kW, 0.23 kW, and 0.26 kW, respectively. The largest difference between the derived from measurements and model calculated $\dot{Q}_{in}$ for case A, B, and C are 0.24 kW, 1.36 kW, and 1.08 kW, respectively. While the derived from measurements $\dot{Q}_{in}$ shows a decreasing trend for each case, the model calculated $\dot{Q}_{in}$ decreases only for case A and C. Specifically, the model calculated $\dot{Q}_{in}$ for case B initially decreases but remains relatively constant once the water inlet temperature reaches 25°C.

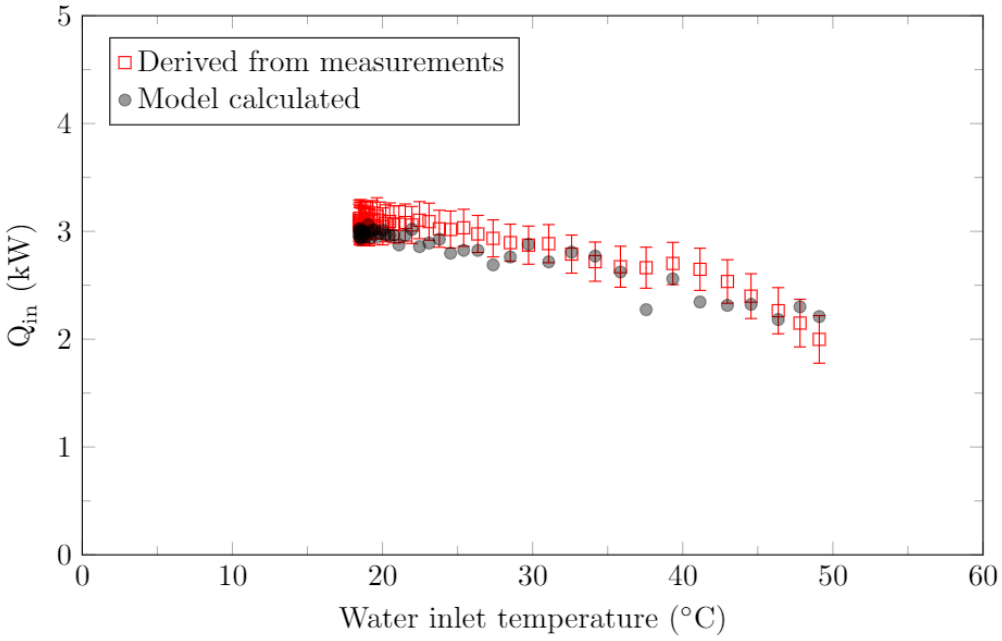

Figure 5 - 2: Evaporator heat transfer results for case A (25°C ambient air)

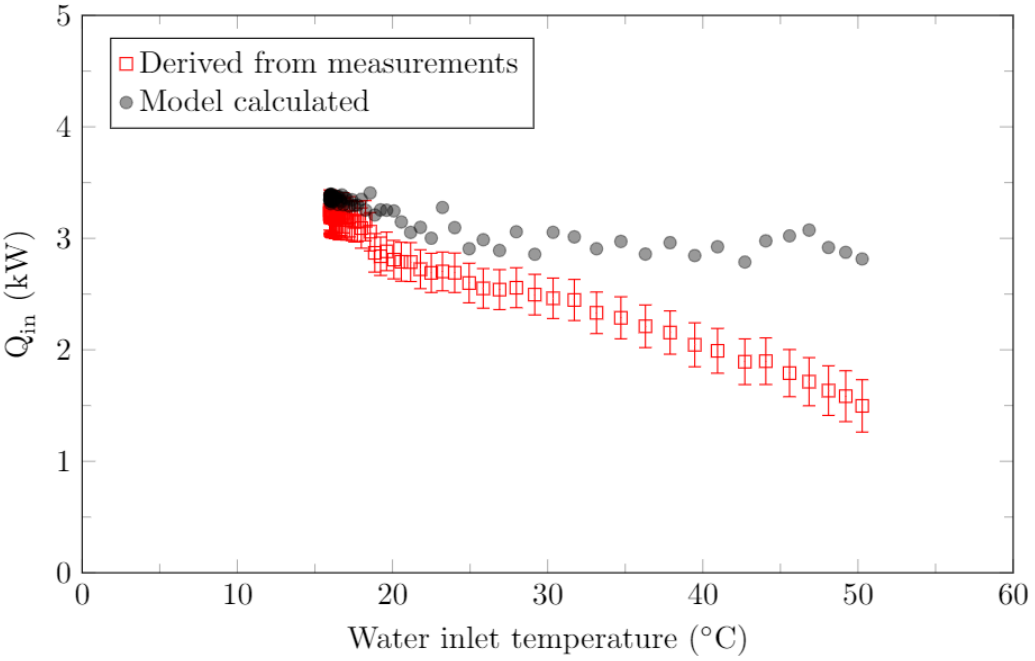

Figure 5 - 3: Evaporator heat transfer results for case B (10°C ambient air)

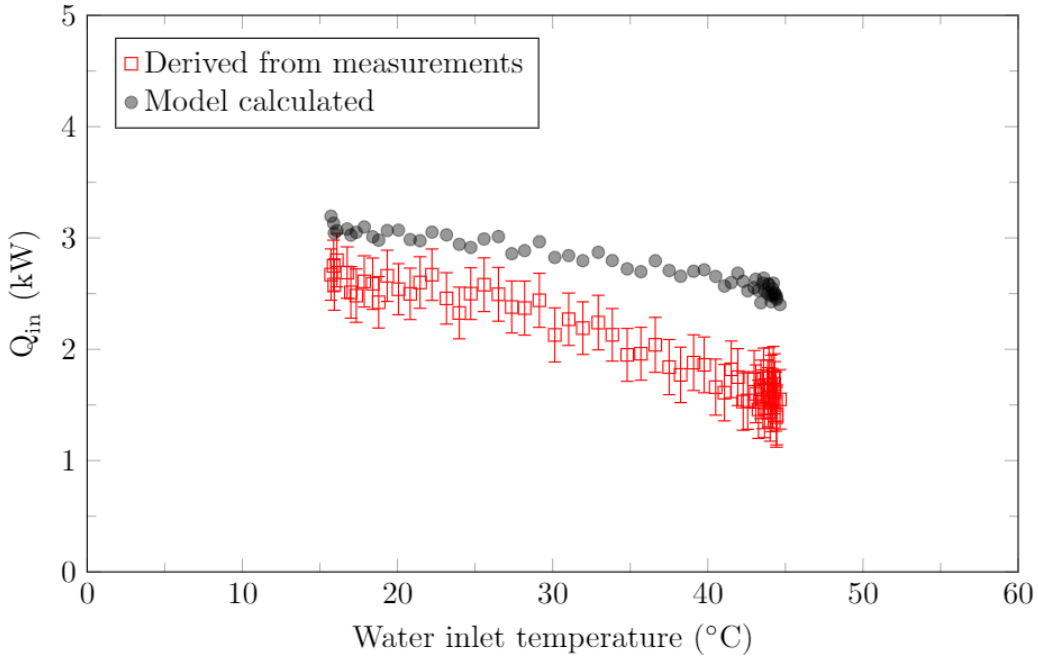

Figure 5 - 4: Evaporator heat transfer results for case C (-10°C ambient air)

Furthermore, the overall decreasing trend of both the derived from measurements and model calculated $\dot{Q}_{\text{in}}$ with an increased water inlet temperature is expected when the evaporator inlet temperature is observed. The evaporator inlet temperature increases with an increasing water inlet temperature, which causes a decreased temperature difference between the refrigerant and air stream. In this scenario, the refrigerant inlet temperature is the cold inlet temperature and the air temperature is the hot inlet temperature. Moreover, the maximum possible heat transfer is dependent upon the temperature difference between the hot inlet temperature and the cold inlet temperature. Therefore, it is expected that $\dot{Q}_{\text{in}}$ would decrease with an increase in evaporator inlet temperature. The evaporator inlet temperature and ambient air temperature for case A, B, and C are depicted in Figure 5 - 5, Figure 5 - 6, and Figure 5 - 7, respectively.

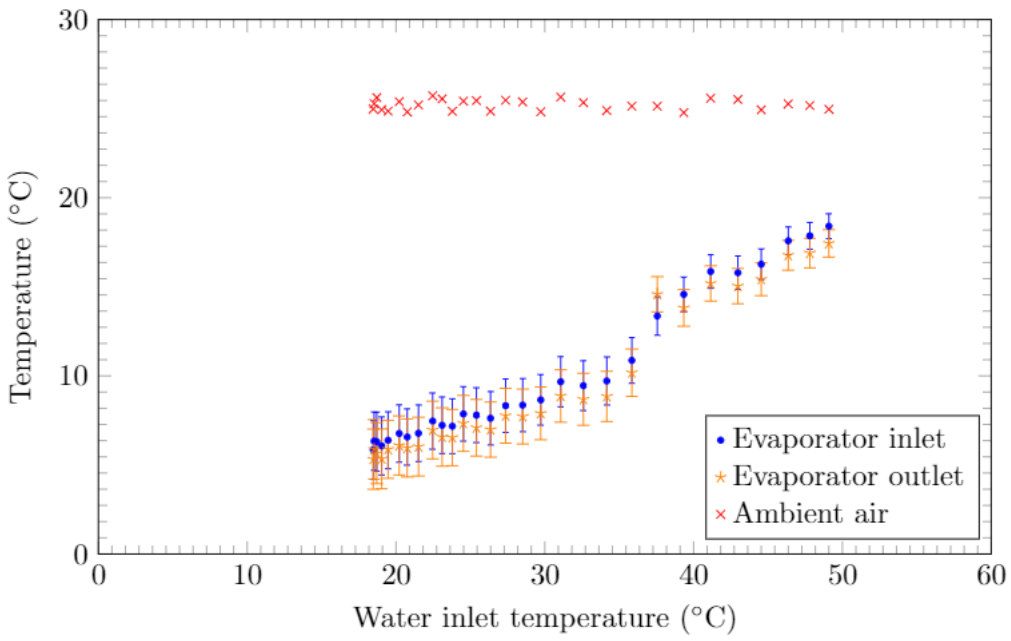

Figure 5 - 5: Evaporator refrigerant inlet and outlet temperatures for case A (25°C ambient air)

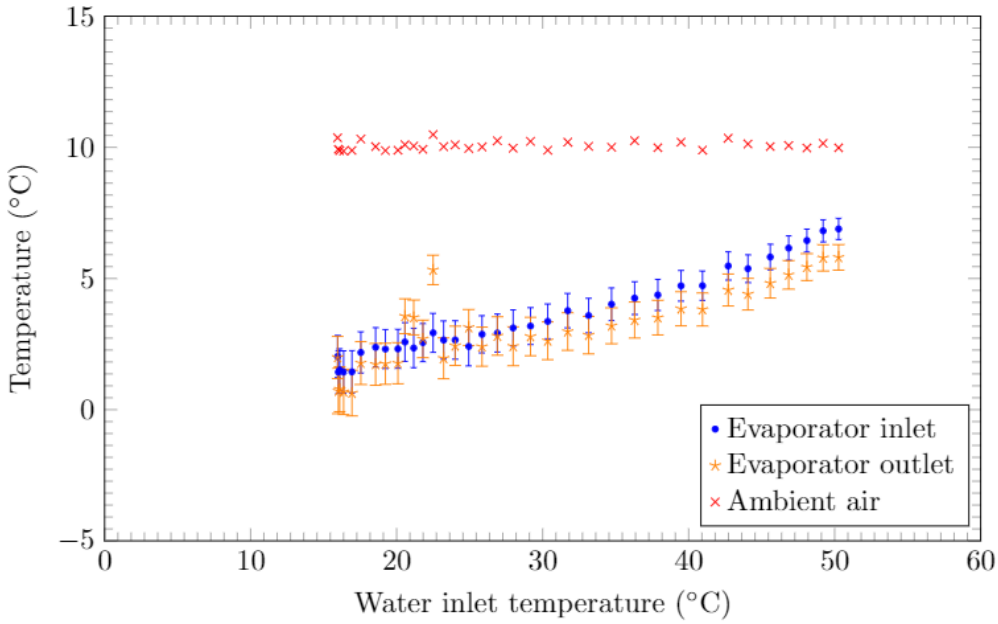

Figure 5 - 6: Evaporator refrigerant inlet and outlet temperatures for case B (10°C ambient air)

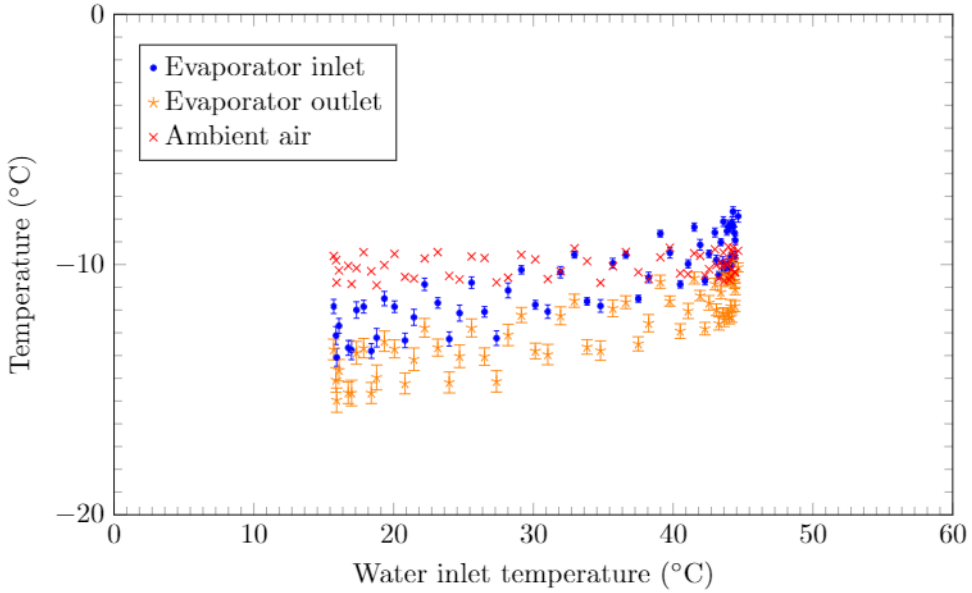

Figure 5 - 7: Evaporator refrigerant inlet and outlet temperatures for case C (-10°C ambient air)

5.1.2. Verification discussion

The prior results reveal that the model did not always converge to the specified limits. There are several variables in the model that would affect the calculated results. Those variables

include the motor speed, the evaporator pressure, the phase of state 1, and the pressure of the expansion valve inlet. This section will discuss how these variables impact the model results and change its convergence.

The effects of the compressor motor speed on the model results will be described first. For cases A and C, the measured motor speed was used as an input to estimate the mass flow rate. However, the motor speed was not measured for case B. Subsequently, a linear relationship was assumed between cases A and C to approximate the motor speed for case B. Figure 5 - 8 depicts the measured motor speed for cases A and C. The bias associated with the motor frequency is 0.05% for each measurement and is therefore too small to appear on the graph.

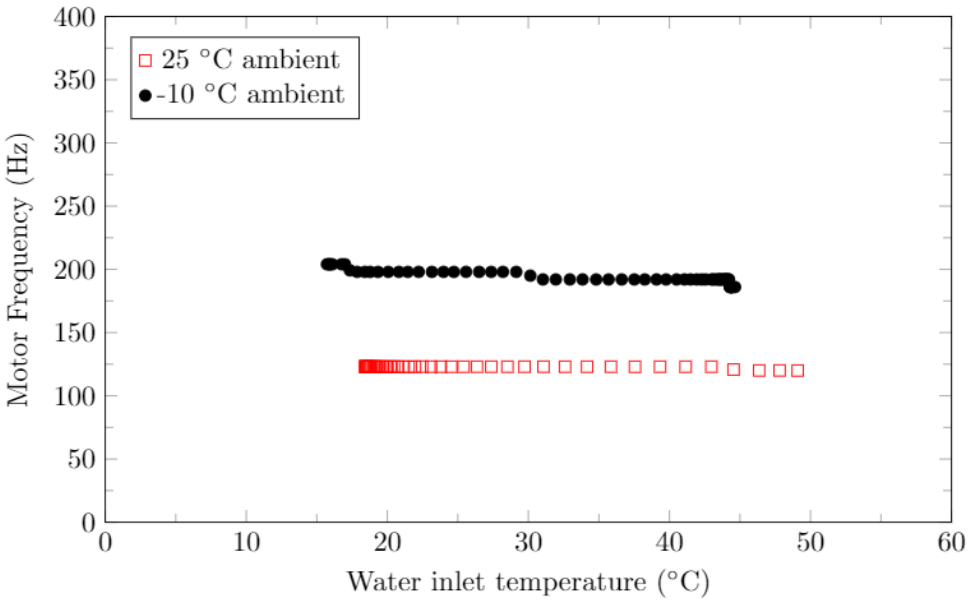

Figure 5 - 8: Measured compressor motor frequency data with respect to the water inlet temperature

While one can observe that the speed remains relatively constant as a function of water inlet temperature, it actually varies up to 10% for cases A and C. Nevertheless, because the motor frequency was not measured for case B and because of the consequent assumed linear relationship,

a constant motor speed was used for every data point for case B. Consequently, the constant, approximated motor speed contributes to the overestimated model calculated $\dot{Q}_{\text{in}}$ and *dh3* for case B. An overestimated motor speed results in an overestimated mass flow rate, which leads to an overestimated $\dot{Q}_{\text{in}}$. An example of this is shown in Table 5 - 1, which presents the model results for one data point with two different motor frequencies from case B. The model results in Figure 5 - 3 were calculated with a motor frequency of 155 Hz. Therefore, the results for the same data point were recalculated using a smaller motor frequency of 145 Hz and shown in Table 5 - 1. This 6% reduction in motor frequency reduces the model calculated $\dot{Q}_{\text{in}}$ by 7% and *dh3* by 65%. Therefore, the approximated motor speed for case B contributes to the considerably large results for *dQ* and *dh3*.

Table 5 - 1: Effect of compressor motor frequency on model verification parameters

Motor frequency (Hz)	155	145
Mass flow rate (kg/s)	0.0169	0.0159
Model calculated $\dot{Q}_{\text{in}}$ (kW)	3.27	3.05
***dQ* (kW)**	0.573	0.347
***dh3* (kJ/kg)**	22	7.75

The effects of the evaporator pressure on the model results will now be described. The evaporator pressure is calculated by finding the saturation pressure of the evaporator refrigerant temperature. Additionally, the suction enthalpy (h_1) is then calculated using the evaporator pressure. Therefore, error in the evaporator refrigerant temperature will result in error in the evaporator pressure and suction enthalpy. Figure 5 - 5 to Figure 5 - 7 compare the evaporator refrigerant inlet and outlet temperatures to the ambient air temperature. It is important to note that

in Figure 5 - 5 to Figure 5 - 7, some of the beginning points were removed to increase the graph clarity.

For each case, the evaporator outlet temperature is colder than the evaporator inlet temperature. This is not possible as the evaporator's function is to change the phase of the refrigerant from a mixture to a saturated vapour or to a superheated steam. Therefore, one would expect the outlet temperature to be either equal to or greater than the inlet temperature. Furthermore, as the ambient temperature decreases, the difference between the inlet and outlet temperature becomes greater. Thus, these temperature differences are greatest for case C. It is expected that the evaporator pressure would correspond to the saturation pressure within the temperature ranges of the evaporator inlet and outlet, however, the temperature difference for case C is approximately 2°C. The change in saturation pressure that corresponds to this temperature difference is 150 kPa, which is three times the expected evaporator pressure drop according to Subei [68]. Therefore, the temperature drop measured over the evaporator cannot be assumed to be caused by the evaporator pressure drop. Thus, there is significant uncertainty concerning the evaporator pressure. Additionally, the model is highly sensitive to the evaporator pressure. An example of the model's sensitivity to the pressure is shown for a data point from case C in Table 5 - 2. By increasing the evaporator pressure by 130 kPa (5.6%), the resulting discharge enthalpy decreases by 20%, the discharge pressure increases by 292%, *dh3* decreases by 15%, and *dQ* increases by 58%. The evaporator pressure uncertainty, coupled with the model's sensitivity to said pressure, is a significant source of error in the model.

Table 5 - 2: Model sensitivity to the evaporator pressure

Evaporator pressure (kPa)	2300	2430	5.6% ↑
h_2 **(kJ/kg)**	65.12	52.39	20% ↓
P_2 **(kPa)**	729.9	2863	292% ↑
dh3 **(kJ/kg)**	235.2	200.7	15% ↓
dQ **(kW)**	0.383	0.607	58% ↑

The next variable reviewed is the phase of state 1. Conventionally, it is assumed that the refrigerant entering a compressor in a HPWH would be a superheated vapour. Figure 5 - 9 through Figure 5 - 11 compare the suction temperature to the evaporator outlet temperature. The suction temperature is significantly larger than the evaporator outlet temperature for case A and B. In contrast, the suction temperature is barely larger than the outlet temperature for case C. The model assumed that the evaporator outlet state was a saturated vapour (or had a quality between 0.9 to 1) and that the refrigerant became superheated in the IHX. Furthermore, the model calculated the enthalpy of state 1 by using the evaporator pressure and the measured suction temperature. For cases A and B, significant superheat would occur given that the suction temperature is at least a few degrees warmer than the evaporator outlet temperature. On the other hand, a very small amount of superheat would occur given that the suction temperature is barely greater than the evaporator outlet temperature for case C and for the final points in case B. Moreover, depending on what the phase of the evaporator outlet was, its entirely possible that no superheat would occur for state 1. Correspondingly, it was observed that the largest values of *dQ* and *dh3* were observed

for points when the compressor inlet temperature (T_1) was very close to the evaporator temperature. Therefore, this is a component of the HPWH that requires further investigation.

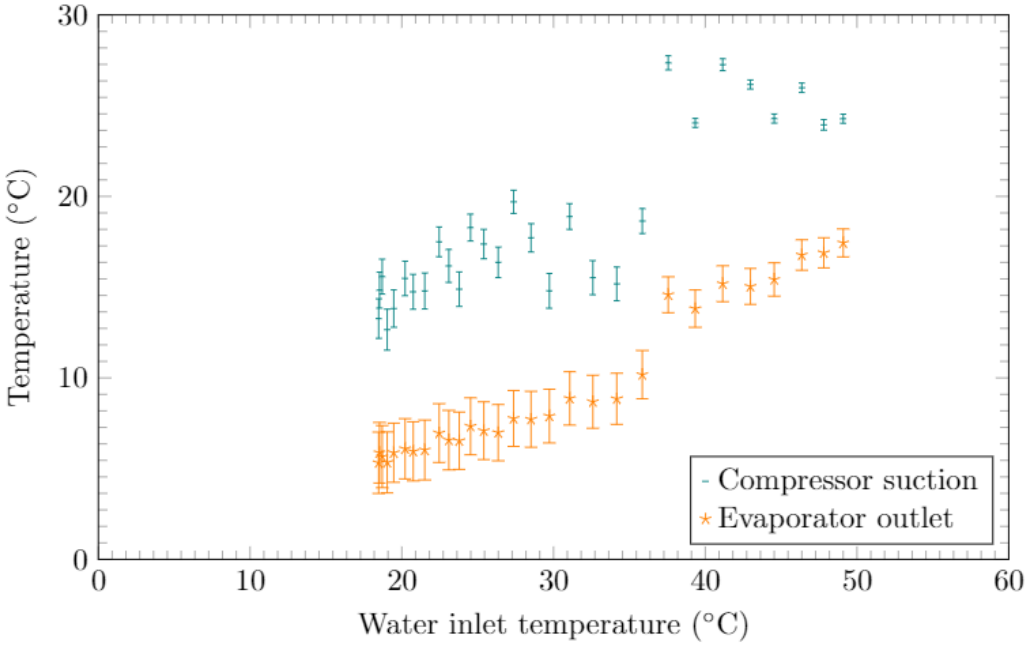

Figure 5 - 9: Comparison of compressor suction temperature to evaporator outlet temperature for case A (25°C ambient air)

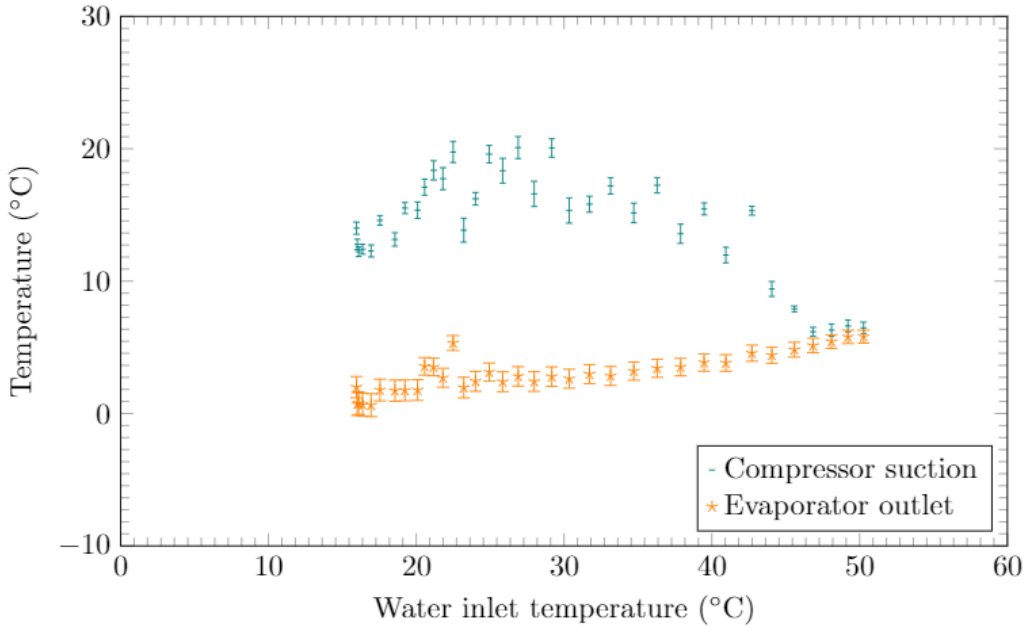

Figure 5 - 10: Comparison of compressor suction temperature to evaporator outlet temperature for case B (10°C ambient air)

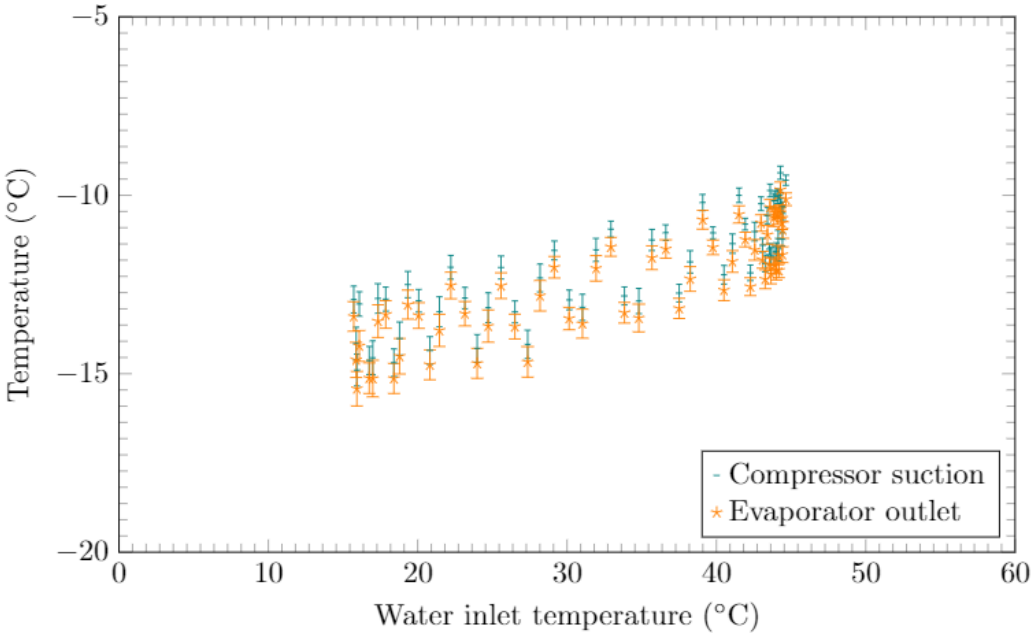

Figure 5 - 11: Comparison of compressor suction temperature to evaporator outlet temperature for case C (-10°C ambient air)

The last variable that will be discussed is the electronic expansion valve (EEV) inlet pressure. To calculate the enthalpy at the EEV inlet (h_4), either P_2 or P_3 was used. For some data points, the difference between the estimated P_2 and P_3 ranged from 300 kPa to 5,000 kPa. Notably, the enthalpy of the expansion valve inlet is equal to the enthalpy of the evaporator inlet. Therefore, the chosen pressure ultimately affects the enthalpy of the evaporator inlet (h_5). When a significant difference between P_2 and P_3 exists, a decision must be made as to which one will be utilized in the calculation of h_4. When *dh3* exceeded 75 kJ/kg, this indicated that P_2 was significantly underestimated and therefore P_3 was used to calculate h_4. If P_2 were used in this scenario, the evaporator inlet phase would be a superheated steam instead of a liquid-vapour mixture. Consequently, P_2 was used to calculate h_4 only when *dh3* was less than 75 kJ/kg. An additional unwanted result from using P_2 when *dh3* is greater than 75 kJ/kg is that the model underpredicts the temperature difference across the EEV compared to the measured temperature difference.

Figure 5 - 12 depicts these consequences. In Figure 5 - 12, h_4 calculated using P_3 and the resulting h_5 are depicted with the dotted line. In the same figure, h_4 calculated with P_2 and the resulting h_5 are depicted by the tiny magenta dot, which is circled in red for clarity. Therefore, P_3 is used when *dh3* is greater than 75 kJ/kg because it offers a better estimate of the evaporator inlet enthalpy. However, the issue with using P_3 is that h_4 can be underpredicted – thereby resulting in a larger calculated $\dot{Q}_{\text{in}}$. It stands to reason that the true discharge pressure lies between the estimates of P_2 and P_3, thereby giving an increased h_4 and h_5 and a decreased model calculated $\dot{Q}_{\text{in}}$. This assumption contributes to the overcalculation of $\dot{Q}_{\text{in}}$ in the case C results.

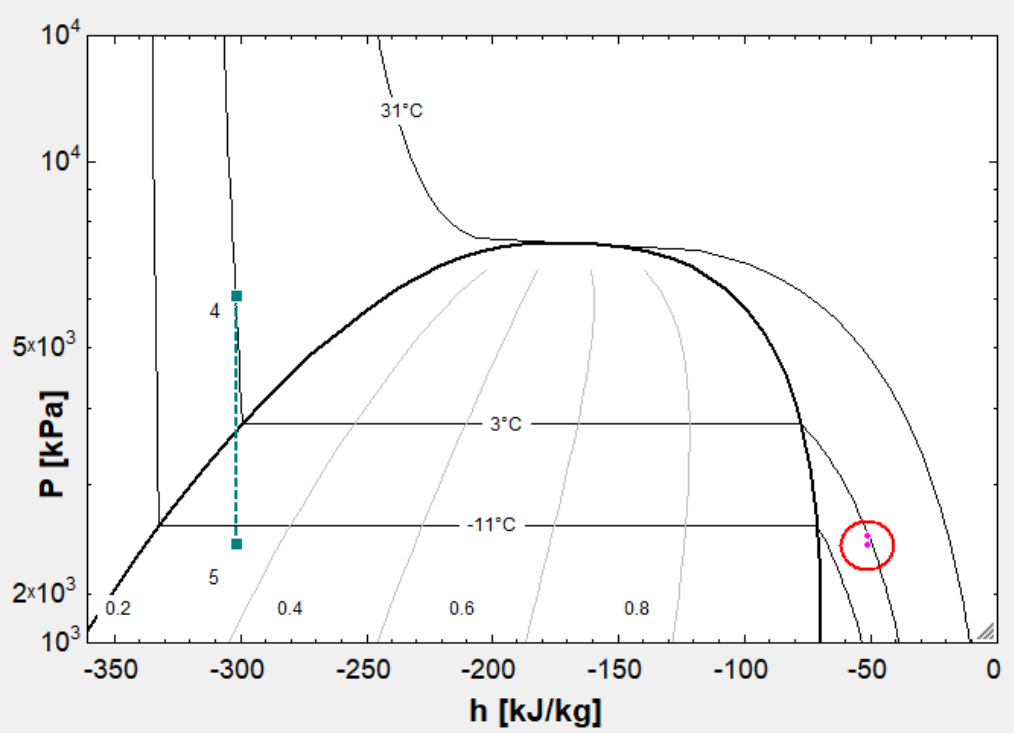

Figure 5 - 12: P - h diagram comparing locations of expansion valve inlet and outlet for different discharge pressure

In summary, the enthalpy of state point 3 and the evaporator heat transfer rate were calculated in two separate ways to verify the model. For cases B and C, there is significant

uncertainty associated with the model and its results. Accordingly, it was identified that the variables and associated approximations that contribute to the model uncertainty are the motor speed, the evaporator pressure, the phase of state 1, and the pressure of the expansion valve inlet. Subsequent recommendations on increasing the model accuracy are given in Chapter 6. Next, the control logic and the relevant experimental data are reviewed.

5.2. Control logic

The HPWH used in this research has three variable speed components, an EEV, and a built-in control program. The control program varies the speeds of the components to ensure safe operation and optimal performance. The three variable speed components include the water pump, evaporator fan, and compressor. This section discusses these three components and the EEV in the context of the control program, beginning with the water pump.

5.2.1. Water pump

The purpose of the water pump is to circulate the water from the bottom of the water tank, through the gas cooler, and back into the top of the water tank. The water pump is controlled by the water set point temperature, which is also referred to as the gas cooler water outlet temperature (T_8). The heat transfer rate from the refrigerant to the water is described by Equation 5.1.

$$\dot{Q}_{\text{out}} = \dot{m}_{\text{water}} c_{\text{p}} (T_8 - T_7) \tag{5.1}$$

As the water tank is heated, the water inlet temperature (T_7) increases. According to the above equation, if T_7 increases and both the mass flow rate and $\dot{Q}_{\text{out}}$ remain constant, this will cause an increase in T_8. It is observed from the experimental data that T_8 does not increase but remains relatively constant at 60°C. To ensure T_8 remains stable at 60°C, the pump power increases which causes an increase in mass flow rate. This can be seen in Figure 5 - 13 where water flow

rate is graphed as a function of water inlet temperature (T_7). The largest bias associated with the water flow measurements is 1.5%.

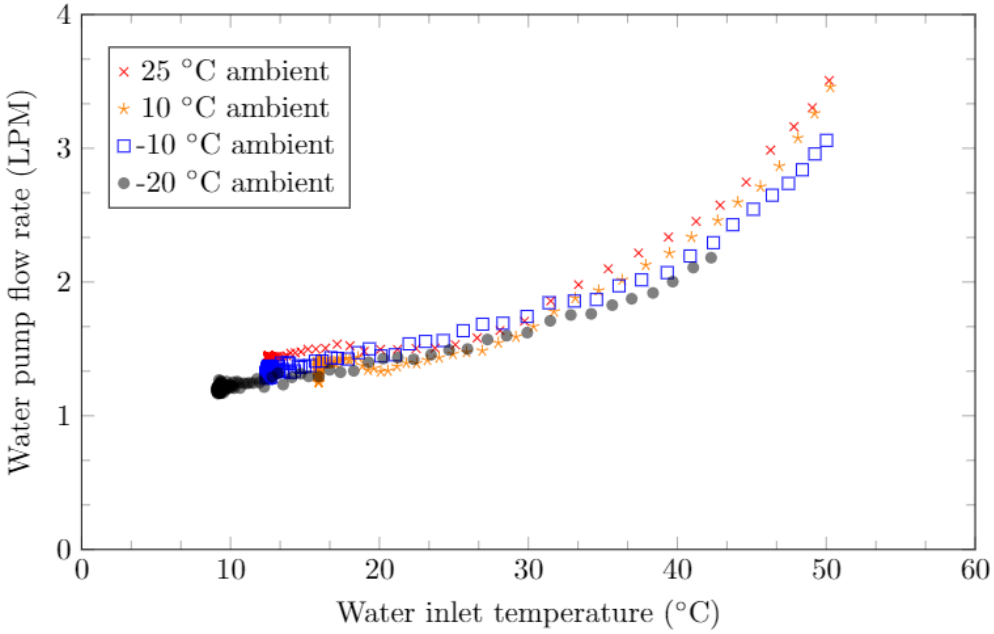

Figure 5 - 13: Water flow rate as a function of water inlet temperature

The figure above shows an increase in water flow rate as the water inlet temperature (T_7) increases. Additionally, the manufacturer's literature confirms that the speed of the water pump is controlled by the gas cooler water outlet temperature (T_8). Next, the control logic of the evaporator fan will be briefly covered.

5.2.2. Evaporator fan

Neither the evaporator fan power nor the air flow rate were measured. Therefore, the control logic for the fan could not be verified experimentally. However, the manufacturer's literature states that the evaporator fan speed is controlled by the ambient air temperature to maximize heating capacity and efficiency [17]. It is hypothesized that as the ambient air temperature decreases, the fan speed increases which causes a resulting increase in the mass flow

rate of the air. The increased air flow rate could maintain the rate of heat transfer for decreased ambient temperatures.

5.2.3. Compressor and expansion valve

The controls for the compressor, unlike the water pump and evaporator fan, were not available from the manufacturer's literature. Therefore, the compressor and any associated parameters or components were observed to determine the compressor controls. These relevant parameters and component include the water inlet temperature, gas cooler outlet temperature, the discharge pressure, and the expansion valve. The discharge pressure is relevant to the discussion because it is either controlled by the compressor or it affects the compressor. Therefore, the discussion will begin with the discharge pressure.

Precise control of the discharge pressure is necessary because if the discharge pressure did not increase with the water inlet temperature, the heat transfer rate out of the gas cooler would be insufficient to maintain the water outlet temperature (T_8) at its setpoint of 60°C due to the decreased water temperature difference. This is caused by the increase in gas cooler outlet temperature (T_3) with T_7, which is depicted in Figure 5 - 14. The smallest temperature bias occurred for the ambient temperature of 25°C and range between the minimum of 0.2°C and maximum of 2.1°C. The most significant temperature errors occurred for the ambient temperature of -20°C and range between the minimum of 2.5°C and maximum of 4.9°C.

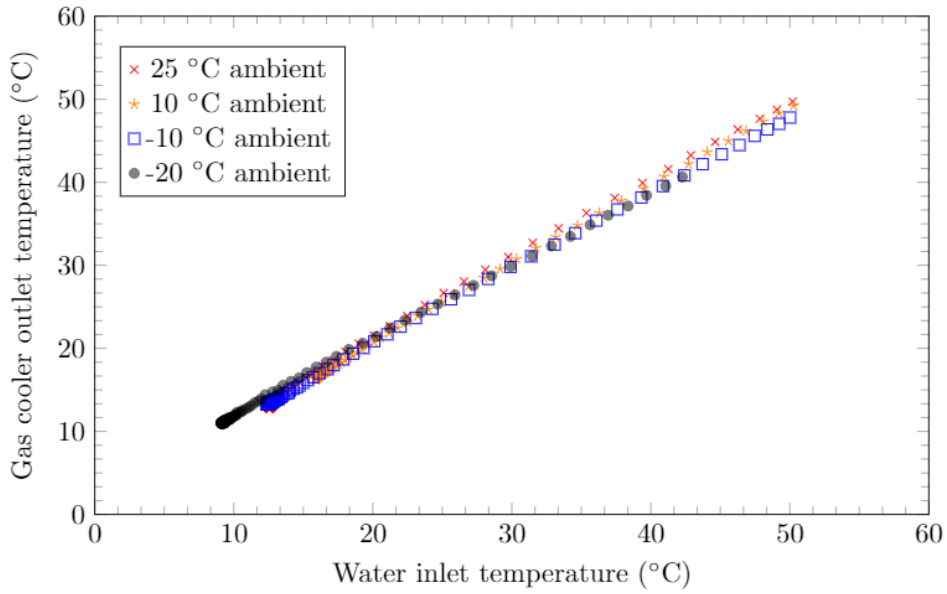

Figure 5 - 14: Gas cooler outlet temperature vs water inlet temperature

Furthermore, an increase in T_3 causes an increase in the gas cooler outlet enthalpy (h_3). Consequently, an increase in either the mass flow rate or the compressor discharge enthalpy (h_2) is necessary to ensure the gas cooler heat transfer rate ($\dot{Q}_{\text{out}}$) remains constant when h_3 increases. This is because $\dot{Q}_{\text{out}}$ is governed by Equation 5.2 and because the HPWH is capacity controlled.

$$\dot{Q}_{\text{out}} = \dot{m}(h_2 - h_3) \tag{5.2}$$

Therefore, either the mass flow rate or h_2 must increase to maintain $\dot{Q}_{\text{out}}$. If the compressor were used to maintain $\dot{Q}_{\text{out}}$ in response to an increase in T_7, the compressor speed would increase to provide a greater mass flow rate and an increased high side pressure. However, the measured motor frequency data paints a different picture – the motor frequency is a strong function of the ambient air temperature, which is depicted in Figure 5 - 8. Thus, the compressor is controlled in response to the ambient air temperature, not the high side pressure. It has been established that the compressor speed is relatively constant with a changing T_7, therefore it is unlikely the mass flow

rate is changing enough to maintain $\dot{Q}_{out}$ with the drastic changes that are seen in h_3. Therefore, h_2 must be increasing to maintain $\dot{Q}_{out}$. There are now two scenarios that would result in an increased h_2, either the discharge temperature or the discharge pressure will increase. The experimental data portrays a varying discharge temperature in Figure 5 - 15, but not a clear increase in discharge temperature in response to an increase in water inlet temperature. Thus, it is assumed the discharge pressure must be the variable that is increasing. The smallest and largest bias error for the temperatures in Figure 5 - 15 is 4.5°C and 10°C, respectively.

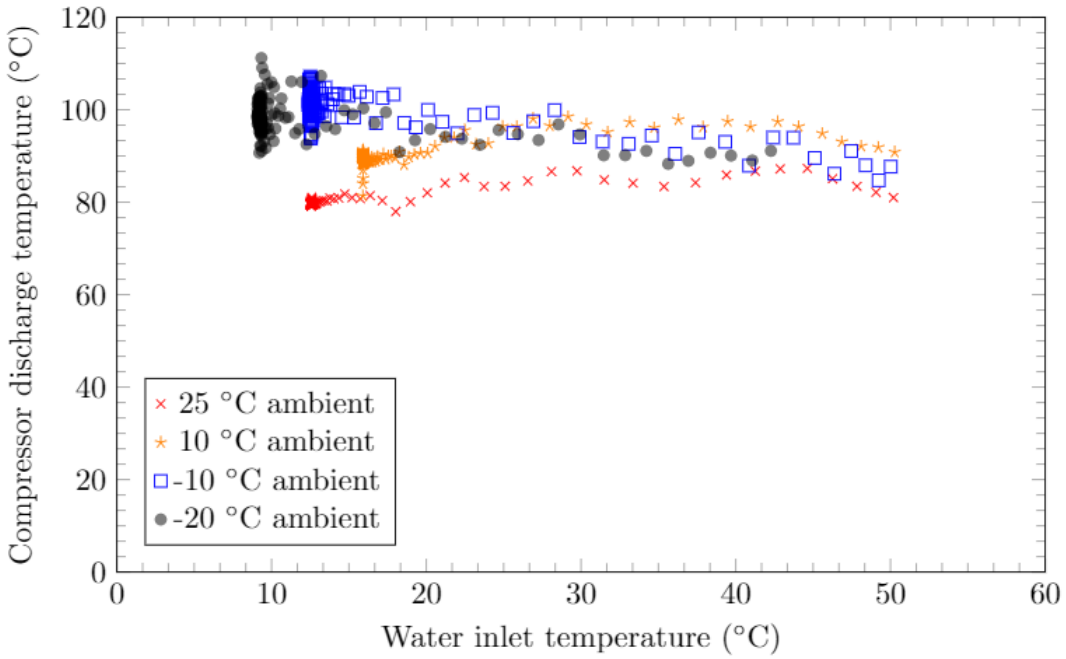

Figure 5 - 15: Compressor discharge temperature vs water inlet temperature

Moreover, if T_3 is increased and there is no corresponding increase in discharge pressure, then the resulting h_3 is very large. This is depicted in Figure 5 - 16, where T_3 is increased from 18°C to 48°C with no increase in discharge pressure. As was mentioned earlier, because the compressor speed remains constant with an increasing T_3, it is highly unlikely that the mass flow rate increases any significant amount. Therefore, with the observed minimal change in discharge

temperature, this massive increase in h_3 would result in a very small $\dot{Q}_{\text{out}}$. The $\dot{Q}_{\text{out}}$ resulting from this scenario is significantly smaller than the measured $\dot{Q}_{\text{out}}$ for the same T_7.

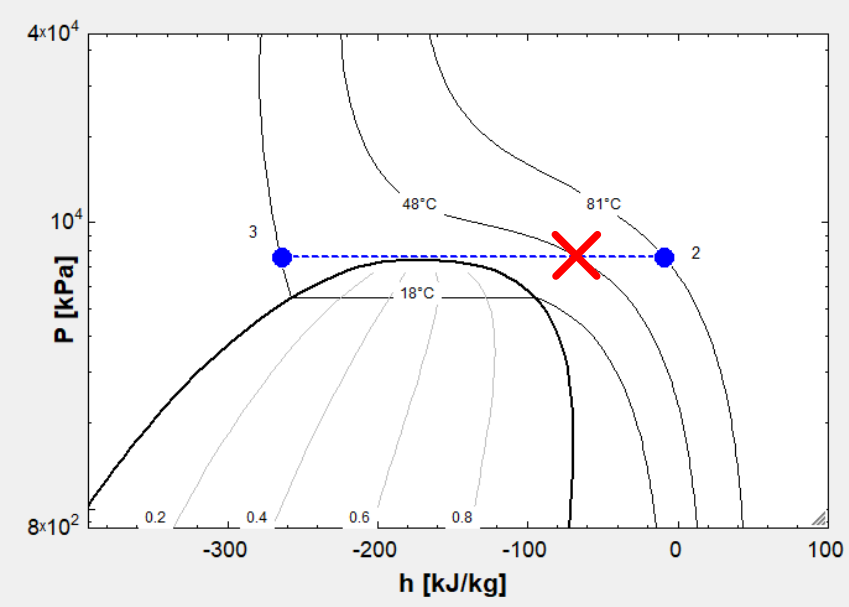

Figure 5 - 16: P - h diagram illustrating the effect of an increasing gas cooler temperature with a constant discharge pressure

Thus far, it has been assumed that h_2 must increase to maintain $\dot{Q}_{\text{out}}$. However, upon closer examination of Figure 5 - 16, it can be observed that if T_2 remains relatively constant, an increase in discharge pressure will cause a decrease in h_2 because of the curve of the isotherm. Yet, an increase in discharge pressure will have the same effect on h_3. Therefore, while both h_2 and h_3 will decrease with an increase in pressure, the overall difference between them will be increased. It can be observed from Figure 5 - 17 that the gap between the two isotherms for 48°C and 81°C increases with an increase in discharge pressure. Thus, the $\dot{Q}_{\text{out}}$ process corresponding to the higher water inlet temperature is identified as the 2 – 3 process depicted with the red squares in Figure 5 - 17. This process shows a higher discharge pressure than the circle 2 – 3 process, but a smaller h_2 due to the increased pressure.

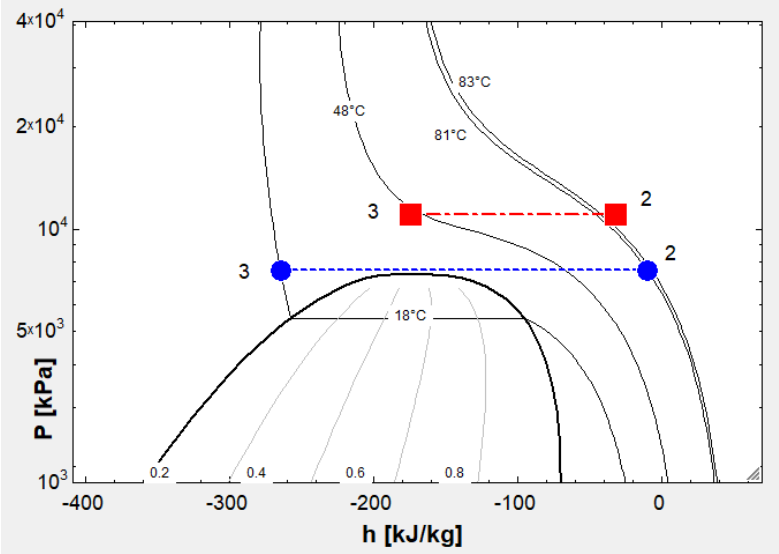

Figure 5 - 17: P - h diagram illustrating how the enthalpy difference changes with an increase in discharge pressure

Given these points, it is reasonable to assume that the compressor does not increase the discharge pressure in response to an increasing water inlet temperature, even though numerous control schemes have been developed to do so [3–5]. However, the question remains as to which component does increase the discharge pressure. In the literature, control schemes have been proposed that use a variable speed water pump and an electronic expansion valve (EEV) to control the discharge pressure [6–10]. A reduction in the opening of the EEV would cause an increase of pressure on the gas cooler side and a larger temperature drop over the EEV. For the temperature drop to increase, the pressure drop must also increase. Figure 5 - 18 depicts the increasing temperature drop over the EEV and the error for these measurements range between the minimum of 0.5°C and the maximum of 2.8°C. Thus, through data observation it is hypothesized that the discharge pressure is controlled by the EEV. Additionally, this increasing temperature drop over the EEV with respect to T_7 is necessary to ensure the evaporator temperature remains colder than

the ambient air temperature. This guarantees that heat is transferred from the air to the refrigerant in the evaporator.

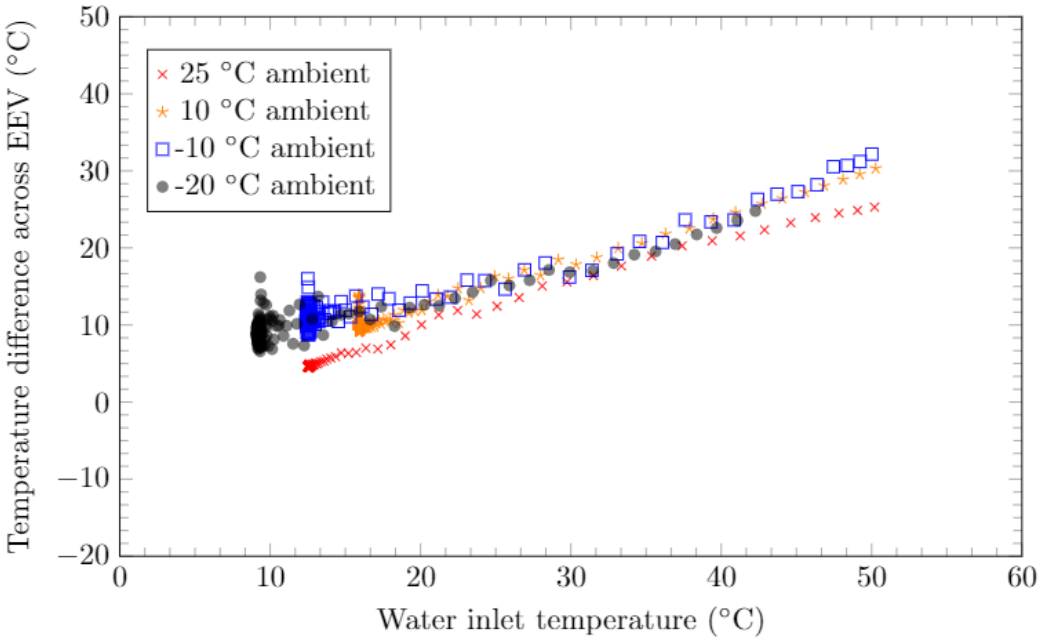

Figure 5 - 18: Measured temperature difference across the electronic expansion valve

The final thing to mention in the discussion regarding the compressor is the effect an increased discharge pressure would have on the compressor work. An increase in the compressor work with an increase in discharge pressure is expected because when the pressure ratio increases, the compressor requires more power to achieve the discharge pressure. Interestingly, the measured data shows an increase in compressor work with an increase in water inlet temperature. The increase in work is small relative to the measurement bias but the trend is observed for each ambient temperature that was tested. The measured compressor work is shown as a function of water inlet temperature in Figure 5 - 19. The increase in compressor work is 17%, 28%, 10%, and 14% for the ambient temperatures of 25°C, 10°C, -10°C, and -20°C, respectively. The most

significant bias for the compressor work is 17%, 16%, 13%, and 12% for the ambient temperatures of 25°C, 10°C, -10°C, and -20°C, respectively.

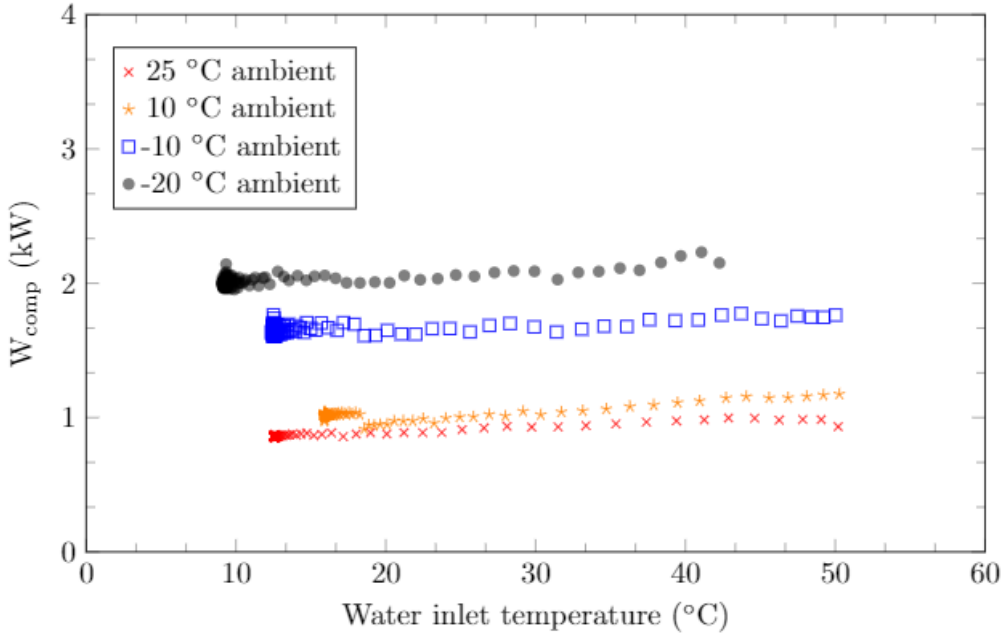

Figure 5 - 19: Compressor work as a function of ambient air and water inlet temperature

Therefore, it was concluded that the compressor is controlled in response the ambient temperature and hypothesized that the expansion valve controls the discharge pressure. This is because the motor frequency varies more with ambient temperature than it does with water inlet temperature. Furthermore, an increase in discharge pressure must be observed with an increase in water inlet temperature to maintain the levels of heat transfer rate that were measured. In addition, this increase in the discharge pressure is seen in the slight increase in the work of the compressor associated with higher water inlet temperatures. Knowledge of the increase in discharge pressure was vital to the creation of the numerical model and understanding the model results, which are presented and discussed in the following section.

5.3. Model results

The numerical model was used to predict the cycle pressures and the isentropic efficiency of the compressor for various ambient air and water inlet temperatures. The water inlet temperatures varied from 15°C to 50°C and the included ambient air temperatures are 25°C, 10°C, and -10°C, which, for reference, are referred to as case A, case B, and case C, respectively. The pressure and isentropic efficiency results will be covered in this section, beginning with the method in which the error was estimated for these results.

5.3.1. Approximation of error for model results

A sensitivity analysis was performed to approximate the error of the pressure and isentropic efficiency predictions. The experimental data that was used to calibrate the model involved significant measurement bias. Consequently, the model results were recalculated by using the highest and lowest value for each measured data point given its measurement bias. The analysis included testing the sensitivity of the model to temperatures 1 – 6 (the same temperatures from Figure 4 - 1), the compressor work, the gas cooler heat transfer rate, and the motor frequency. Then, the changes that were observed in the final result for the pressure and efficiency were combined in the root sum of square method. Additionally, the analysis was completed for one data point from each case with the most influential parameters presented in Table 5 - 3. It is observed from Table 5 - 3 that for each case, the model is very sensitive to the discharge temperature (T_2) and to the compressor work. Furthermore, the gas cooler heat transfer and gas cooler outlet temperature (T_3) can also affect significant changes in the pressure and isentropic efficiency results.

Table 5 - 3: Model sensitivity analysis results and most influential parameters

Ambient Temperature (°C)	Parameter	Measurement bias	% change in P_2	% change in η_s
25	T_2	4.7°C	10	17
	W_{comp}	17%	23	66
	Q_{out}	2.5%	11	18
10	T_2	7.2°C	24	37
	T_3	1.7°C	6	10
	W_{comp}	15%	7	31
(-10)	T_2	9.2°C	71	84
	T_3	2.4°C	52	56
	W_{comp}	13%	30	33

5.3.2. Pressure results

The approximated low side pressures are shown in Figure 5 - 20 while the high side pressures are shown in Figure 5 - 21. As has been mentioned before, there were no measured pressures to compare the calculated values to. Therefore, the pressures have been compared to the manufacturer's range of allowable pressures for the system. The allowable pressure range on the evaporator side is 1.7 MPa to 5.5 MPa [17]. Figure 5 - 20 illustrates that the approximated suction pressures remain within the manufacturer's range, with the exception of one data point for case A. For cases A, B, and C, each suction pressure increases slightly with the increase in water inlet temperature, which is expected because the evaporator inlet temperature increases with the water inlet temperature. This is illustrated in Figure 5 - 5, Figure 5 - 6, and Figure 5 - 7. The more notable increase in suction pressure for case A is due to the larger temperature differential between the

ambient temperature and the evaporator inlet temperature, which is illustrated in Figure 5 - 5. The suction pressure bias was approximated by calculating the highest possible evaporator pressure and the lowest possible evaporator pressure with the measured evaporator inlet and outlet temperatures. The bias for case A ranged from 102 kPa to 417 kPa, for case B ranged from 110 kPa to 234 kPa, and for case C ranged from 160 kPa to 192 kPa.

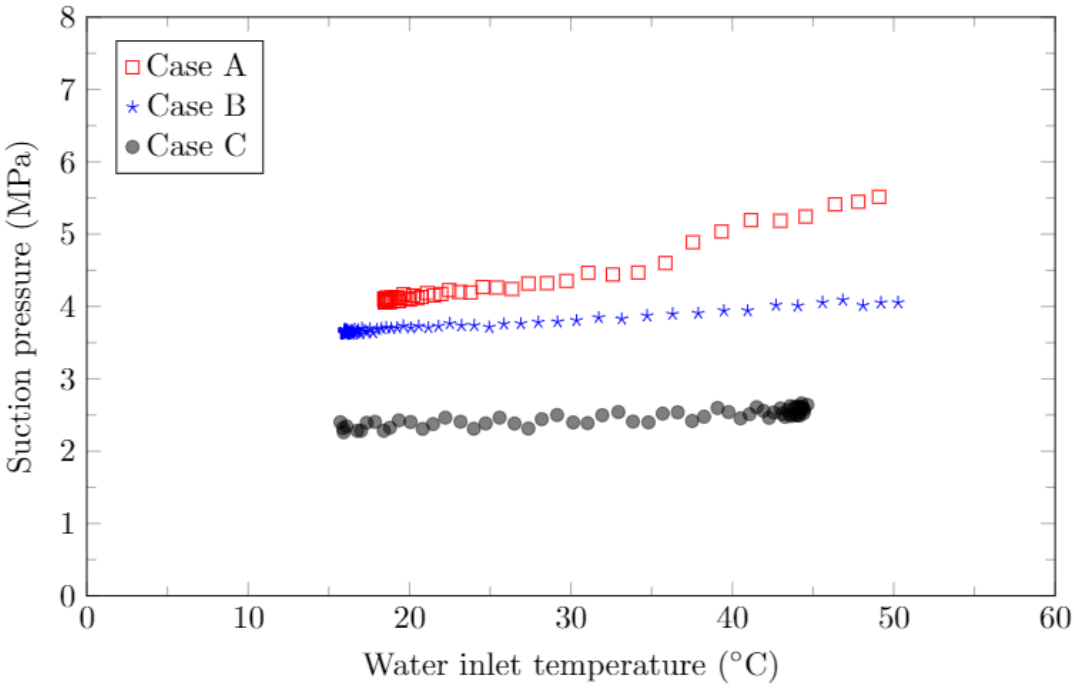

Figure 5 - 20: Model results for suction pressure

For the gas cooler side, the maximum allowable pressure is 12 MPa and there is no low end specified. It can be seen from Figure 5 - 21 that all the calculated high side pressures remained below this upper limit. There is no lower allowable value because the unit does not always operate transcritically. This was confirmed with industry professionals who develop and build transcritical systems: transcritical cycles will operate subcritically as an energy saving measure if the conditions allow for it. Case A and B show the expected trend of an increased discharge pressure with an increased water inlet temperature. In contrast, case C does not show a clear trend. The estimated

bias for the discharge pressure for cases A, B, and C are 2060 kPa, 1920 kPa, and 7310 kPa, respectively.

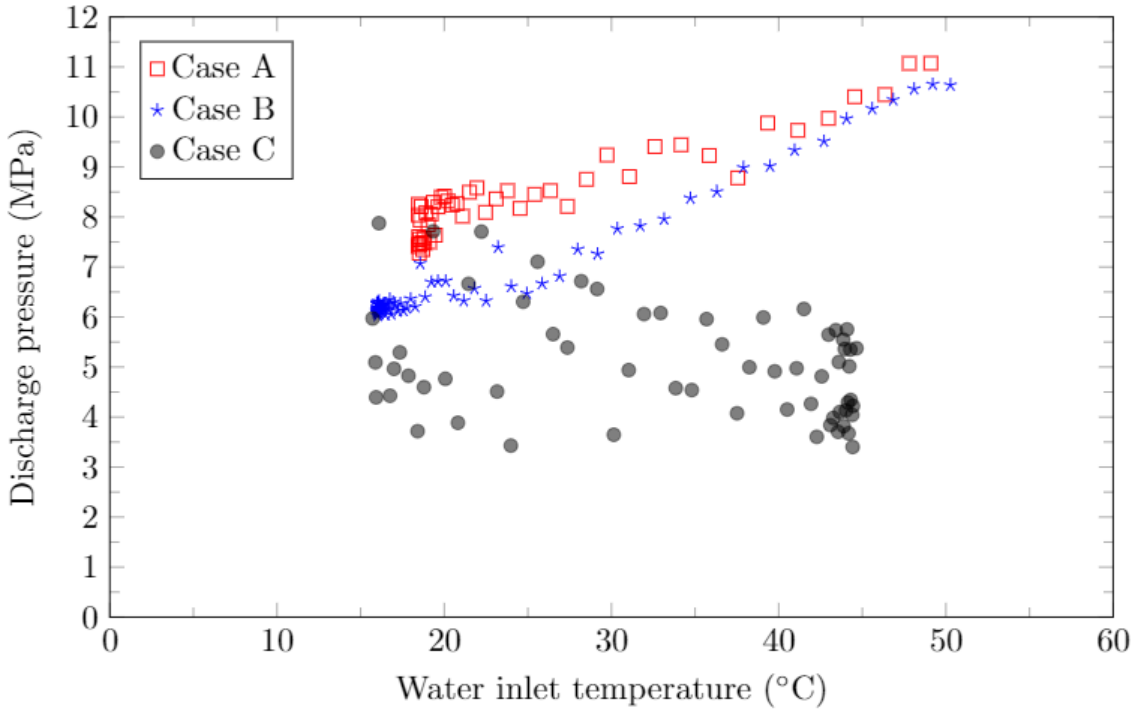

Figure 5 - 21: Model results for discharge pressure

5.3.3. Isentropic efficiency results

The compressor isentropic efficiency was approximated using the cycle pressure estimates. In the literature, it was common to use correlations that calculate the isentropic efficiency as a function of pressure ratio [3, 11–15]. Accordingly, the isentropic efficiency was calculated over a large range of values because it was expected that the pressure ratio would change significantly with changes in the water inlet temperature. In this section, the isentropic efficiency will be visualized in two different ways: 1) as a function of water inlet temperature in Figure 5 - 22 and 2) as a function of pressure ratio in Figure 5 - 23. The approximated bias for the isentropic efficiency for cases A, B, and C is 31%, 23%, and 61%, respectively.

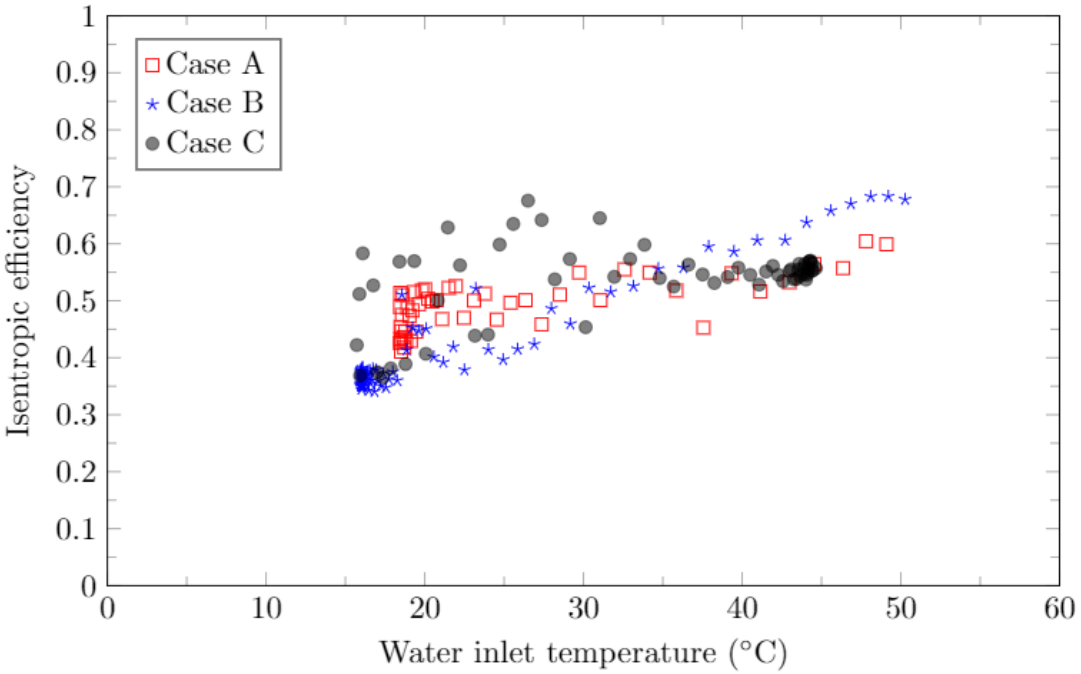

Figure 5 - 22: Model results for isentropic efficiency as a function of water inlet temperature

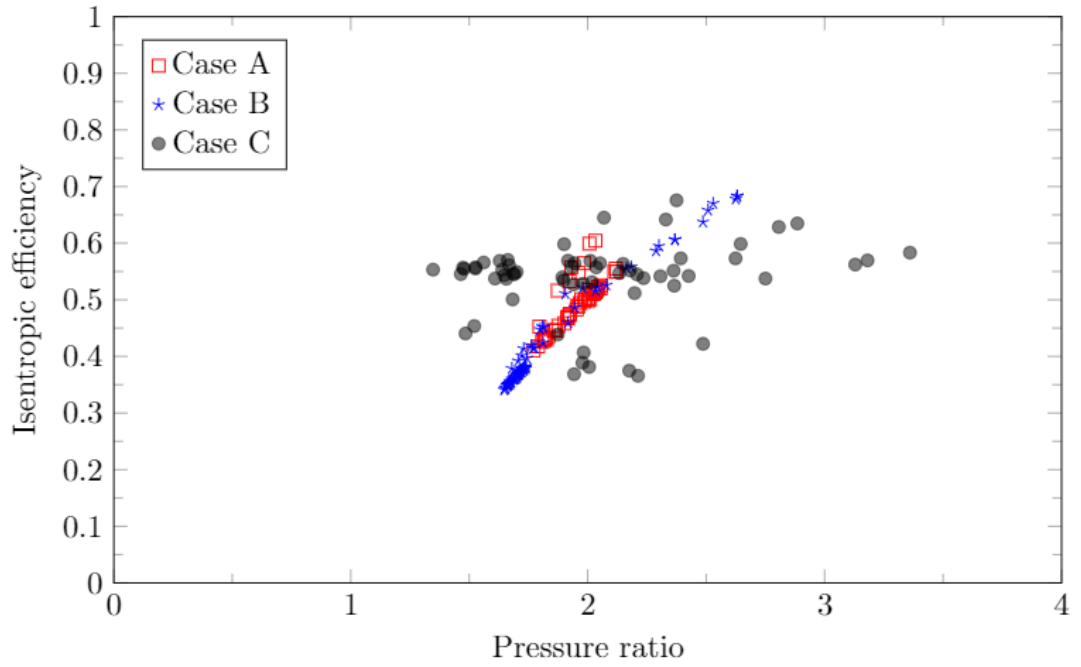

Figure 5 - 23: Model results for isentropic efficiency as a function of pressure ratio

The isentropic efficiency is graphed as a function of water inlet temperature and ambient temperature because of the burgeoning amount of research involved with determining transcritical CO_2 HPWHs feasibility for providing space heating in cold climates. In these types of research, it is desirable to understand how the HPWH will perform with a given source and water inlet temperature, therefore the isentropic efficiency is graphed as a function of such. Furthermore, the isentropic efficiency was graphed as a function of pressure ratio because a large proportion of the compressor data that exists shows the isentropic efficiency as a function of it. This is useful for comparing different performance metrics between compressors and to ensure that the trends of the calculated isentropic efficiency are qualitatively the same as other compressors.

For cases A and B, Figure 5 - 23 shows that the isentropic efficiency increases with pressure ratio. According to Brodal et al.[73], this trend is observed for other transcritical CO_2 compressors leading up to the compressor's optimum isentropic efficiency. Furthermore, Figure 5 - 21 shows an increase in discharge pressure with an increase in water inlet temperature. Therefore, the trend of increasing isentropic efficiency with increasing water inlet temperature is expected for cases A and B, which is shown in Figure 5 - 22. Due to the significant uncertainty regarding case C, there is no distinguishable trend shown for the isentropic efficiency or discharge pressure results for case C.

5.4. Performance data

Performance data was measured for the HPWH for an extensive range of ambient air and water inlet temperatures. The collated performance data includes the COP, the gas cooler heat transfer, and the unit work. This data was used to create performance maps by linearly interpolating between data points. Accordingly, the performance maps plot the data as functions of the two temperatures that have the greatest effect on the unit's performance and heating capacity: the

ambient air and water inlet temperature. Consequently, the effects of these temperatures on the performance of the unit will be described. Performance data was measured for nine ambient air temperatures, -29°C, -20°C, -15°C, -10°C, 1.1°C, 10°C, 20°C, 25°C, and 35°C and for a range of water inlet temperatures from 10°C to 50°C. Notably, not every ambient air temperature has performance data for every water inlet temperature within that range. This section presents the performance maps and discusses the observed trends.

5.4.1. HPWH power performance map

The performance data concerning the unit power will be reviewed first. Figure 5 - 24 displays the unit power as a function of both ambient air and water inlet temperature. Additionally, Figure 5 - 25 shows the compressor power for the four air temperatures that it was measured for. It is observed that the unit power is a strong function of the ambient air temperature. For example, for the water inlet temperature of 25°C, the unit power increases by 114% when the ambient air decreases from 35°C to -29°C. On the other hand, for the air temperature of 10°C, the unit power increases by 16% when the water inlet temperature increases from 15°C to 50°C. This trend is expected because the unit power is mostly comprised of the compressor power and the compressor speed is more a function of ambient air temperature than water inlet temperature. Additionally, the unit power is lesser for warmer ambient air temperatures because the compressor requires less power at these conditions. This is due to the evaporator pressure being higher at warmer ambient temperatures and therefore the compressor operates at lower pressure ratios than it does for the colder ambient temperatures.

W_{in} (kW)									
Water inlet temp (°C)	Ambient air temp (°C)								
	(-29)	(-20)	(-15)	(-10)	1.1	10	20	25	35
10		2.18							
15	2.17	2.19	2.22	1.78	1.44	1.07		0.92	
20	2.20	2.21	2.26	1.80	1.46	1.09	0.89	0.95	
25	2.23	2.22	2.29	1.82	1.48	1.12	0.92	0.97	1.04
30	2.26	2.24	2.33	1.84	1.50	1.14	0.94	0.99	1.11
35	2.29	2.25	2.36	1.86	1.52	1.17	0.97	1.01	1.19
40	2.32	2.27	2.40	1.88	1.54	1.19	0.99	1.03	1.27
45			2.43	1.90	1.56	1.22	1.02	1.06	1.34
50			2.47	1.92	1.59	1.24	1.05	1.08	1.42
Measurement bias (%)	11	11	11	12	13	15	16	16	15

Legend
No data

Figure 5 - 24: HPWH power performance map

W_{comp} (kW)				
Water inlet temp (°C)	Ambient air temp (°C)			
	(-20)	(-10)	10	25
10	2.01			
15	2.03	1.64	1.00	0.87
20	2.05	1.66	1.02	0.89
25	2.07	1.67	1.04	0.91
30	2.09	1.69	1.06	0.93
35	2.11	1.70	1.08	0.94
40	2.12	1.72	1.10	0.96
45		1.73	1.12	0.98
50		1.75	1.14	1.00
Measurement bias (%)	12	13	16	17

Legend
No data

Figure 5 - 25: HPWH compressor power performance map

While the unit and compressor power are most significantly influenced by the ambient air temperature, the influence exhibited by the water inlet temperature is also notable. When the water inlet temperature increases, a corresponding increase in the discharge pressure is expected. This

pressure increase results in an increased pressure ratio and thereby causes an increase in compressor power. This is explained more thoroughly in Section 5.2.3. Figure 5 - 24 illustrates this small increase in total unit power as a response to the water inlet temperature increase and consequent discharge pressure increase. The increase in total unit power is also a consequence of the increasing water pump flow rate – as the flow rate increases the pump power increases. The power increase is similar to the uncertainty for the unit power, however, this is a trend observed for every ambient temperature tested. For example, the unit power increases by 17% when the water inlet temperature increases from 15°C to 50°C for the air temperature of 25°C while the corresponding measurement bias is 16%.

5.4.2. Gas cooler heat transfer rate performance map

Next, the performance data for the gas cooler heat transfer ($\dot{Q}_{\mathrm{out}}$) will be reviewed. $\dot{Q}_{\mathrm{out}}$ is depicted in Figure 5 - 26 as a function of air and water inlet temperature. Opposite from the trends observed for the unit power, the gas cooler heat transfer rate is more a function of water inlet temperature than ambient air temperature. Figure 5 - 26 shows a clear decrease in heat transfer with an increase in water inlet temperature. For example, $\dot{Q}_{\mathrm{out}}$ decreases by 43% for the ambient temperature of 25°C when the water inlet temperature increases from 15°C to 50°C. The heat transfer decrease is due to the diminishing temperature difference between the inlet and outlet water temperature across the gas cooler. As the water inlet temperature increases, the heat transfer required to lift the water temperature to the defined setpoint for the outlet decreases. Furthermore, while $\dot{Q}_{\mathrm{out}}$ remains relatively constant between different ambient air temperatures, a significant decrease in heating capacity is observed for the ambient temperature of -29°C.

Q_{out} (kW)									
Water inlet temp (°C)	Ambient air temp (°C)								
	(-29)	(-20)	(-15)	(-10)	1.1	10	20	25	35
10		4.20							
15	2.72	4.00	4.71	4.32	4.48	4.12		4.37	
20	2.71	3.79	4.44	4.06	4.25	3.89	4.43	4.13	
25	2.70	3.58	4.17	3.79	4.02	3.67	4.14	3.89	3.96
30	2.69	3.38	3.89	3.53	3.78	3.45	3.84	3.65	3.93
35	2.69	3.17	3.62	3.27	3.55	3.22	3.54	3.41	3.90
40	2.68	2.96	3.35	3.01	3.32	3.00	3.24	3.16	3.87
45			3.08	2.75	3.09	2.77	2.94	2.92	3.84
50			2.80	2.49	2.85	2.55	2.64	2.68	3.80
Measurement bias (%)	3.1	4.5	6.4	6.6	4.7	4.7	7.3	5.9	5.1

Legend
No data

Figure 5 - 26: Gas cooler heat transfer rate performance map for HPWH

5.4.3. HPWH performance map

Figure 5 - 27 illustrates the COP over various conditions. It is observed that the COP is influenced by both the ambient air and water inlet temperatures. Generally, for each ambient temperature, the highest COPs are observed at the coldest water inlet temperatures. This occurs because the maximum values of $\dot{Q}_{\text{out}}$ and the minimum values for the unit power are observed at the coldest water inlet temperatures. In addition, the maximum COP is observed for an ambient and water inlet temperature of 20°C while the minimum COP corresponds to an ambient temperature of -15°C and a water temperature of 50°C. The highest average COP is 3.69 and corresponds to the air temperature of 20°C while the lowest average COP is 1.20 and corresponds to the air temperature of -29°C.

COP									
Water inlet temp (°C)	Ambient air temp (°C)								
	(-29)	(-20)	(-15)	(-10)	1.1	10	20	25	35
10		1.93							
15	1.25	1.82	2.11	2.41	3.10	3.83		4.69	
20	1.23	1.72	1.97	2.25	2.91	3.57	4.90	4.37	
25	1.21	1.62	1.83	2.09	2.73	3.31	4.50	4.05	3.81
30	1.19	1.51	1.69	1.93	2.54	3.06	4.09	3.72	3.57
35	1.17	1.41	1.55	1.77	2.35	2.80	3.69	3.40	3.32
40	1.15	1.30	1.41	1.61	2.16	2.54	3.28	3.07	3.08
45			1.27	1.45	1.97	2.28	2.88	2.75	2.84
50			1.13	1.29	1.78	2.02	2.47	2.43	2.60
Measurement Bias (%)	11	11	12	13	13	15	16	16	15

Legend
No data

Figure 5 - 27: Performance map for HPWH

Figure 5 - 27 shows the highest COPs are for source temperatures above 0°C. This is ideal for a water-source HPWH as the source temperatures are generally above 0°C. Furthermore, the highest COPs are also for colder water inlet temperatures. Hydronic space heating can be achieved in many ways and the water inlet temperature will be greatly affected by the method chosen. For example, if hydronic heating is achieved through the floors, then an expected water inlet temperature would be between 25°C and 30°C [33] and would give COPs on the higher end of the range. However, if the heated water was used in forced air heating, the water inlet temperature would be expected to be between 37°C to 50°C [33] and the resulting COPs would be smaller. Therefore, the HPWH in this study performs best with cold water inlet temperatures and above 0°C ambient air temperatures. Consequently, configurations with low water inlet temperatures and high ambient air temperatures are preferable to maximize its performance. Based upon the above steady state performance data, it appears the HPWH used in this study is well suited to operate in a water-source configuration and to provide hydronic floor heating. Further research is required to

understand the seasonal performance and to collect performance data for the water-source configuration, as described in Chapter 6.

5.5. Summary of key findings

There were several key findings regarding the analyses of the model accuracy, model results, HPWH control logic, and HPWH performance. For the model accuracy, it was observed that the combination of the model's sensitivity and the bias of the measured data resulted with very high error for the pressure and isentropic efficiency results. Furthermore, it was found that the model is highly sensitive to the evaporator pressure, discharge temperature, gas cooler outlet temperature, compressor work, and gas cooler heat transfer rate.

The analysis of the experimental data and model creation showed that the compressor is controlled by the ambient air and that the expansion valve controls the high side pressure. Additionally, the water pump is controlled by the water inlet temperature to maintain a water outlet temperature of 60°C and the evaporator fan is controlled by the ambient air temperature.

Study of the HPWH performance data shows that the maximum COPs are observed at ambient air temperatures greater than 0°C and at colder water inlet temperatures. This is due to two reasons, 1) the minimum compressor powers correspond to the warmer ambient air temperatures and the colder water inlet temperatures and 2) $\dot{Q}_{\text{out}}$ is greatest for the coldest water inlet temperatures. Furthermore, the steady state data shows promising performance of the HPWH in a water-source configuration for the application of hydronic floor heating. The next steps in determining the feasibility of the HPWH for this application is outlined in Chapter 6.

6. Conclusions and future work

Several conclusions were made about this research and defined in the preceding chapters. They are summarized in this chapter and followed by recommendations for future work.

6.1. Conclusions

This research involved studying the performance and control logic of a commercially available transcritical CO_2 HPWH. A numerical model of the HPWH was created and used in conjunction with experimental data to estimate the cycle pressures and compressor isentropic efficiency. Additionally, extensive performance data were measured and the control logic was deduced through observation of the experimental data and the numerical model.

The performance data for the HPWH was collated for the ambient air temperatures of 35°C, 25°C, 20°C, 10°C, 1.1°C, -10°C, -15°C, -20°C, and -29°C. The HPWH had the greatest COPs at the ambient air temperatures above 0°C and at the water inlet temperatures below 30°C. This is due to the compressor operating at reduced power for warmer ambient air temperatures and the gas cooler heat transfer rate being larger for cold water inlet temperatures. Additionally, while the COP was barely greater than 1 for many of the ambient air temperatures below zero, all the measured COPs were above 1.

The numerical model was utilized to estimate the cycle pressures and compressor isentropic efficiency as a function of ambient air temperature and water inlet temperature for the ambient temperatures of 25°C, 10°C, and -10°C. The model was calibrated with experimental data and verified through theoretical methods. A sensitivity analysis was performed on the model to determine the effect the measurement bias had on the estimated cycle pressures and isentropic

efficiency. The analysis showed that experimental data with less bias were required and that by measuring specific parameters the accuracy of the model could be greatly increased.

Through analysis of the experimental data, it was observed that the compressor motor speed and the compressor power varied primarily with the ambient air temperature. Furthermore, the water flow rate varied with the water inlet temperature. Therefore, it was concluded the compressor and evaporator are controlled by the ambient air temperature while the water pump is controlled by the water inlet temperature. Furthermore, it was hypothesized that the expansion valve controls the discharge pressure.

6.2. Future work

Further work is necessary to characterize the HPWHs state points and control logic in its air-source configuration before beginning the research on its water-source configuration. Future work should include a detailed understanding of the air-source control scheme and a developed control scheme for the water-source configuration. This can be achieved by increasing the model accuracy and by measuring the cycle state points with increased accuracy. The recommendations for increasing the model accuracy and for future work are described below.

One of the most vital recommendations includes experimentally measuring the cycle pressures. It is recommended to measure the cycle pressures because the bias associated with the model estimated pressures was found to be very large. For example, the measurement bias for the experimental data that was used to calibrate the model propagated into an estimated bias of 70% for the discharge pressure. Additionally, it was shown in Chapter 5 that the model is highly sensitive to the evaporator pressure. Coupled with the temperature discrepancy between the outlet and inlet of the evaporator, the evaporator pressure was a significant source of error in the model.

Measuring the pressures experimentally will result in more accurate results for the pressures and the compressor isentropic efficiency. Also, measuring the cycle pressures will allow for the model to be experimentally validated instead of theoretically verified. Another parameter that should be measured to increase the model accuracy is the mass flow rate of the refrigerant. Numerous assumptions were made to estimate the mass flow rate from the measured compressor motor speed and it was found that the model was very sensitive to these assumptions. Therefore, decreasing the uncertainty of the mass flow rate measurement will increase the accuracy of the model.

Another method to increase the model accuracy involves altering the approach in which the refrigerant temperatures were measured. The refrigerant temperatures were measured by placing the sensor on the outside surface of the refrigerant line. This resulted in significant measurement uncertainty for all refrigerant temperatures, but especially for the compressor discharge and gas cooler outlet temperature. The sensitivity analysis showed that both temperatures greatly influence the model. Thus, in future work the temperature measuring sensors should be immersed in the refrigerant.

Future work on the control logic of the system should include the study of the evaporator fan and the electronic expansion valve (EEV). The manufacturer states that the ambient air temperature controls the speed of the evaporator fan – it would be beneficial to confirm this and cultivate a deeper understanding of the evaporator in general. Especially considering the overarching goal driving this research is to operate this system as a water-source unit. At the time of this writing, the HPWH has been converted to a water-source unit, but the HPWH will not run unless the evaporator fan is running. Therefore, there is work to be done in regards to the control logic, which includes the evaporator fan. In addition, the control logic regarding the expansion valve should be studied, which can be achieved through the measurement of the cycle pressures.

Once a thorough understanding of the control logic is achieved for the unit in its air-source configuration, then a program can be developed to optimize performance for the unit it its water-source configuration.

There were many unknowns regarding the system that would have made the EES model more accurate, particularly the degree of superheat entering the compressor. It was found that the model is very sensitive to the compressor inlet state, therefore the degree of superheat of the compressor inlet state could be quantified in future work. Furthermore, it was assumed that the pressure drop in the gas cooler and evaporator were negligible. These pressure drops could be quantified and included in the EES model to increase the accuracy.

Future work can include these recommendations to develop a more accurate model and a control scheme for the HPWH in a water-source configuration. Once a control scheme is developed for the water-source configuration, performance data can be collated for this configuration. The performance data for the water-source configuration can be used to assess the seasonal performance of the system for providing domestic hot water and space heating for a multi-use residential building.

References

[1] G. of Canada, "Greenhouse gas sources and sinks: executive summary 2020." [Online]. Available: https://www.canada.ca/en/environment-climate-change/services/climate-change/greenhouse-gas-emissions/sources-sinks-executive-summary-2020.html. [Accessed: 01-Sep-2020].

[2] NRCan, "Energy and Greenhouse Gas Emissions (GHGs) | Natural Resources Canada." [Online]. Available: https://www.nrcan.gc.ca/science-data/data-analysis/energy-data-analysis/energy-facts/energy-and-greenhouse-gas-emissions-ghgs/20063#L5. [Accessed: 01-Sep-2020].

[3] "Households and the Environment: Energy Use: Analysis," 2015. [Online]. Available: https://www150.statcan.gc.ca/n1/pub/11-526-s/2013002/part-partie1-eng.htm. [Accessed: 14-Dec-2019].

[4] C. Francis, G. Maidment, and G. Davies, "An investigation of refrigerant leakage in commercial refrigeration Une étude des fuites de frigorigène en froid commercial," *Int. J. Refrig.*, vol. 74, pp. 12–21, 2017.

[5] Emerson, "Commercial CO2 Refrigeration Systems," *Emerson Climate Technologies*. p. 44, 2015.

[6] M. J. Moran, H. N. Shapiro, D. D. Boettner, and M. B. Bailey, *Fundamentals of Engineering Thermodynamics*, 9th ed. Hoboken, NJ: Don Fowley, 2018.

[7] J. A. Pyle, S. Solomon, D. Wuebbles, and S. Zvenigorodsky, "Ozone Depletion and Chlorine Loading Potentials," *Scientific Assessment of Ozone Depletion: 1991*, 1992. [Online]. Available: http://www.ciesin.org/docs/011-551/011-551.html. [Accessed: 31-

Mar-2020].

[8] United States Environmental Protection Agency, “Understanding Global Warming Potentials,” *Greenhouse Gas Emissions*. [Online]. Available: https://www.epa.gov/ghgemissions/understanding-global-warming-potentials. [Accessed: 31-Mar-2020].

[9] G. Lorentzen and J. Pettersen, “A new, efficient and environmentally benign system for car air-conditioning,” *Int. J. Refrig.*, vol. 16, no. 1, pp. 4–12, 1993.

[10] P. Murray, “PERFORMANCE ANALYSIS OF A TRANSCRITICAL , CO 2 HEAT PUMP WATER HEATER INCORPORATING A BRAZED-PLATE GAS-COOLER By,” 2014.

[11] “Engineering Recommendation: Heat Pump Water Heater,” 1997.

[12] M. H. Kim, J. Pettersen, and C. W. Bullard, “Fundamental process and system design issues in CO2 vapor compression systems,” *Progress in Energy and Combustion Science*, vol. 30, no. 2. Elsevier Ltd, pp. 119–174, 2004.

[13] F. Karlsson and P. Fahlén, “Capacity-controlled ground source heat pumps in hydronic heating systems,” *Int. J. Refrig.*, vol. 30, no. 2, pp. 221–229, Mar. 2007.

[14] M. Dongellini, M. Abbenante, and G. L. Morini, “A strategy for the optimal control logic of heat pump systems: impact on the energy consumptions of a residential building,” in *12th IEA Heat Pump Conference*, 2017.

[15] P. Fahlen, “REHVA Journal 05/2012 - Capacity control of heat pumps (Full version),” *REHVA J.*, 2012.

[16] C. Cuevas and J. Lebrun, “Testing and modelling of a variable speed scroll compressor,” *Appl. Therm. Eng.*, vol. 29, no. 2–3, pp. 469–478, Feb. 2009.

[17] Sanden International, *Sanden SANCO₂ Heat Pump Water Heater Technical Information*, no. October. 2017.

[18] A. Pearson, “Carbon dioxide - New uses for an old refrigerant,” *International Journal of Refrigeration*, vol. 28, no. 8. pp. 1140–1148, Dec-2005.

[19] M. Tammaro, C. Montagud, J. M. Corberán, A. W. Mauro, and R. Mastrullo, “Seasonal performance assessment of sanitary hot water production systems using propane and CO2 heat pumps,” *Int. J. Refrig.*, vol. 74, pp. 222–237, Feb. 2017.

[20] K. Nawaz, B. Shen, A. Elatar, V. Baxter, and O. Abdelaziz, “Performance optimization of CO2 heat pump water heater,” *Int. J. Refrig.*, vol. 85, pp. 213–228, 2018.

[21] P. Nekså, H. Rekstad, G. R. Zakeri, and P. A. Schiefloe, “CO2-heat pump water heater: Characteristics, system design and experimental results,” *Int. J. Refrig.*, vol. 21, no. 3, pp. 172–179, 1998.

[22] S. D. White, M. G. Yarrall, D. J. Cleland, and R. A. Hedley, “Modelling the performance of a transcritical CO2 heat pump for high temperature heating,” in *International Journal of Refrigeration*, 2002, vol. 25, no. 4, pp. 479–486.

[23] F. Kauf, “Determination of the optimum high pressure for transcritical CO2-refrigeration cycles,” *Int. J. Therm. Sci.*, vol. 38, no. 4, pp. 325–330, 1999.

[24] X. Liu, C. Liu, Z. Zhang, L. Chen, and Y. Hou, “Experimental study on the performance of water source trans-critical CO2 heat pump water heater,” *Energies*, vol. 10, no. 6, 2017.

[25] S. M. Liao, T. S. Zhao, and A. Jakobsen, “Correlation of optimal heat rejection pressures in transcritical carbon dioxide cycles,” *Appl. Therm. Eng.*, vol. 20, no. 9, pp. 831–841, 2000.

[26] J. Sarkar, S. Bhattacharyya, and M. R. Gopal, “Optimization of a transcritical CO2 heat pump cycle for simultaneous cooling and heating applications,” *Int. J. Refrig.*, vol. 27, 2004.

[27] P. Laipradit, J. Tiansuwan, T. Kiatsiriroat, and L. Aye, “Theoretical performance analysis of heat pump water heaters using carbon dioxide as refrigerant,” *Int. J. Energy Res.*, vol. 32, no. 4, pp. 356–366, Mar. 2008.

[28] L. Cecchinato, M. Corradi, E. Fornasieri, and L. Zamboni, “Carbon dioxide as refrigerant for tap water heat pumps: A comparison with the traditional solution,” *Int. J. Refrig.*, vol. 28, no. 8, pp. 1250–1258, Dec. 2005.

[29] N. Fernandez, Y. Hwang, and R. Radermacher, “Comparison of CO2 heat pump water heater performance with baseline cycle and two high COP cycles,” *Int. J. Refrig.*, vol. 33, no. 3, pp. 635–644, May 2010.

[30] B. M. Fronk and S. Garimella, “Water-coupled carbon dioxide microchannel gas cooler for heat pump water heaters: Part i - Experiments,” *Int. J. Refrig.*, vol. 34, no. 1, pp. 7–16, Jan. 2011.

[31] A. Cavallini, L. Cecchinato, M. Corradi, E. Fornasieri, and C. Zilio, “Two-stage transcritical carbon dioxide cycle optimisation: A theoretical and experimental analysis,” *Int. J. Refrig.*, vol. 28, no. 8, pp. 1274–1283, Dec. 2005.

[32] P. Byrne, J. Miriel, and Y. Lenat, “Design and simulation of a heat pump for simultaneous heating and cooling using HFC or CO2 as a working fluid,” *Int. J. Refrig.*, vol. 32, no. 7, pp. 1711–1723, Nov. 2009.

[33] A. Bastani, P. Eslami-Nejad, M. Badache, and A. T. A. Nguyen, “Experimental characterization of a transcritical CO2 direct expansion ground source heat pump for heating applications,” *Energy Build.*, vol. 212, p. 109828, Apr. 2020.

[34] A. Nguyen, P. Eslami-Nejad, M. Badache, and A. Bastani, “Influence of an internal heat exchanger on the operation of a CO2 direct expansion ground source heat pump,” *Energy Build.*, vol. 202, p. 109343, Nov. 2019.

[35] E. Atam and L. Helsen, “Ground-coupled heat pumps: Part 1 - Literature review and research challenges in modeling and optimal control,” *Renewable and Sustainable Energy Reviews*, vol. 54. Elsevier Ltd, pp. 1653–1667, 01-Feb-2016.

[36] M. Badache, P. Eslami-Nejad, A. Bastani, Z. Aidoun, and A. Nguyen, “Theoretical and experimental analysis of a vertical direct expansion geothermal evaporator using CO2 as refrigerant,” *Sci. Technol. Built Environ.*, vol. 25, no. 8, pp. 1081–1094, Sep. 2019.

[37] P. Eslami-Nejad, M. Badache, A. Bastani, and Z. Aidoun, “Detailed Theoretical Characterization of a Transcritical CO2 Direct Expansion Ground Source Heat Pump Water Heater,” *Energies*, 2018.

[38] B. T. Austin and K. Sumathy, “Transcritical carbon dioxide heat pump systems: A review,” *Renewable and Sustainable Energy Reviews*, vol. 15, no. 8. Pergamon, pp. 4013–4029, 01-Oct-2011.

[39] F. Cao, Y. Wang, and Z. Ye, “Theoretical analysis of internal heat exchanger in transcritical CO2 heat pump systems and its experimental verification,” *Int. J. Refrig.*, Oct. 2019.

[40] D. M. Robinson and E. A. Groll, “Efficiencies of transcritical CO2 cycles with and without an expansion turbine,” *Int. J. Refrig.*, vol. 21, no. 7, pp. 577–589, Nov. 1998.

[41] Y. Chen and J. Gu, “The optimum high pressure for CO2 transcritical refrigeration systems with internal heat exchangers,” *Int. J. Refrig.*, vol. 28, no. 8, pp. 1238–1249, Dec. 2005.

[42] P. C. Qi, Y. L. He, X. L. Wang, and X. Z. Meng, “Experimental investigation of the optimal heat rejection pressure for a transcritical CO2 heat pump water heater,” *Appl. Therm. Eng.*, vol. 56, no. 1–2, pp. 120–125, Jul. 2013.

[43] Y. G. Chen, “Optimal heat rejection pressure of CO2 heat pump water heaters based on pinch point analysis,” *Int. J. Refrig.*, Oct. 2019.

[44] Z. Ye, Y. Wang, and F. Cao, “Experimental study and optimal control strategy of a transcritical CO2 heat pump water heater ,” in *IOP Conf. Ser.: Mater. Sci. Eng.*, 2019.

[45] S. Minetto, “Theoretical and experimental analysis of a CO 2 heat pump for domestic hot water,” *Int. J. Refrig.*, vol. 34, no. 3, pp. 742–751, May 2011.

[46] S. A. Tassou, C. J. Marquand, and D. R. Wilson, “Comparison of the performance of capacity controlled and conventional on/off controlled heat pumps,” *Appl. Energy*, vol. 14, no. 4, pp. 241–256, 1983.

[47] J. R. Cole, “HEAT PUMP CONTROLS - PART ONE.”

[48] D. Rolando, H. Madani, G. Braida, R. Tomasetig, and Z. Mohammadi, “Heat pump system control: the potential improvement based on perfect prediction of weather forecast and user occupancy,” 2017.

[49] Y. Liu, Z. Zhuo, F. Zhang, and T. Bao, “CO2 heat pump water heater: System design and experimental study,” in *Proceedings of the 8th International Symposium on Heating, Ventilation and Air Conditioning*, 2014, vol. 262 LNEE, no. VOL. 2, pp. 131–142.

[50] F. Karlsson and P. Fahlén, “Capacity-controlled ground source heat pumps in hydronic heating systems,” *Int. J. Refrig.*, vol. 30, no. 2, pp. 221–229, Mar. 2007.

[51] C. Baek, J. Heo, J. Jung, H. Cho, and Y. Kim, “Optimal control of the gas-cooler pressure of a CO2 heat pump using EEV opening and outdoor fan speed in the cooling mode,” *Int. J. Refrig.*, vol. 36, no. 4, pp. 1276–1284, Jun. 2013.

[52] B. Y. Kimura de Carvalho, C. Melo, and R. H. Pereira, “An experimental study on the use of variable capacity two-stage compressors in transcritical carbon dioxide light commercial refrigerating systems,” *Int. J. Refrig.*, vol. 106, pp. 604–615, Oct. 2019.

[53] L. Cecchinato, M. Corradi, G. Cosi, S. Minetto, and M. Rampazzo, “A real-time algorithm for the determination of R744 systems optimal high pressure,” *Int. J. Refrig.*, vol. 35, no. 4, pp. 817–826, Jun. 2012.

[54] M. S. Kim, D. H. Kang, M. S. Kim, and M. Kim, “Investigation on the optimal control of gas cooler pressure for a CO2 refrigeration system with an internal heat exchanger,” *Int. J. Refrig.*, vol. 77, pp. 48–59, May 2017.

[55] B. Hu, Y. Li, R. Z. Wang, F. Cao, and Z. Xing, “Real-time minimization of power

consumption for air-source transcritical CO2 heat pump water heater system," *Int. J. Refrig.*, vol. 85, pp. 395–408, Jan. 2018.

[56] B. Larson and M. Logsdon, "Laboratory Assessment of Sanden GES-15QTA Heat Pump Water Heater," 2013.

[57] R. J. Moffat, "Describing the uncertainties in experimental results," *Exp. Therm. Fluid Sci.*, vol. 1, no. 1, pp. 3–17, 1988.

[58] Kamstrup, "MULTICAL 603 Data sheet." 2014.

[59] J. M. Gorman, E. M. Sparrow, and J. P. Abraham, "Differences between measured pipe wall surface temperatures and internal fluid temperatures," *Case Stud. Therm. Eng.*, vol. 1, no. 1, pp. 13–16, Oct. 2013.

[60] J. L. Yang, Y. T. Ma, M. X. Li, and J. Hua, "Modeling and simulating the transcritical CO2 heat pump system," *Energy*, vol. 35, no. 12, pp. 4812–4818, 2010.

[61] J. Sarkar, S. Bhattacharyya, and M. R. Gopal, "Optimization of a transcritical CO 2 heat pump cycle for simultaneous cooling and heating applications ` chaleur au Optimisation du cycle transcritique d ' une pompe a ´ e dans les applications de dioxyde de carbone utilise ´ s refroidissement et de chauf," vol. 27, pp. 830–838, 2004.

[62] A. T. Diaby, P. Byrne, and T. Maré, "Simulation of heat pumps for simultaneous heating and cooling using CO2," *Int. J. Refrig.*, Oct. 2019.

[63] Z. Wang, G. Li, F. Wang, Z. Liu, and M. Wang, "Performance analysis and operation optimization of air-to-water CO2 heat pump with phase change thermal storage," *Energy Build.*, vol. 209, 2019.

[64] Z. Wang *et al.*, “Experimental investigation on thermal characteristics of transcritical CO 2 heat pump unit combined with thermal energy storage for residential heating,” 2019.

[65] T. L. Bergman, A. S. Lavine, F. P. Incropera, and D. P. DeWitt, *Fundamentals of Heat and Mass Transfer*, 8th ed. New York: Wiley, 2017.

[66] L. Cecchinato, M. Corradi, and S. Minetto, “A simplified method to evaluate the energy performance of CO2 heat pump units,” *Int. J. Therm. Sci.*, vol. 50, no. 12, pp. 2483–2495, Dec. 2011.

[67] S. Sawalha, “Theoretical evaluation of trans-critical CO 2 systems in supermarket refrigeration. Part I: Modeling, simulation and optimization of two system solutions,” *Int. J. Re*, 2007.

[68] C. Subei and G. Schmitz, “Analysis of refrigerant pipe pressure drop of a CO2 air conditioning unit for vehicles,” *Int. J. Refrig.*, vol. 106, pp. 583–591, Oct. 2019.

[69] G. W. Zhang, P. Hu, L. X. Chen, and M. H. Liu, “Experimental and simulation investigation on heat transfer characteristics of in-tube supercritical CO2 cooling flow,” *Appl. Therm. Eng.*, vol. 143, pp. 1101–1113, Oct. 2018.

[70] S. Minetto, “Theoretical and experimental analysis of a CO 2 heat pump for domestic hot water,” *International Journal of Refrigeration*, vol. 34, no. 3. pp. 742–751, 2011.

[71] S. M. Liao and T. S. Zhao, “An experimental investigation of convection heat transfer to supercritical carbon dioxide in miniature tubes,” *Int. J. Heat Mass Transf.*, vol. 45, no. 25, pp. 5025–5034, Dec. 2002.

[72] L. Cecchinato *et al.*, “Thermodynamic analysis of different two-stage transcritical carbon

dioxide cycles," *Int. J. Refrig.*, vol. 32, no. 5, pp. 1058–1067, Aug. 2009.

[73] E. Brodal and S. Jackson, "A Comparative Study of CO2 Heat Pump Performance for Combined Space and Hot Water Heating," *Int. J. Refrig.*, Aug. 2019.

Appendix A: Uncertainty analysis for the water inlet to gas cooler temperature and refrigerant gas cooler outlet temperature

The locations of the RTDs were, at times, a significant distance from the point of interest (POI). The temperatures of these points of interest were estimated with the following calculations. Then, the temperature difference between the measured and estimated value was added to the bias. A bias of 0.01°C was added to the gas cooler outlet temperature and a bias of 0.1°C was added to the water outlet temperature. The details and assumptions regarding the calculation of the bias are covered in this appendix.

Gas cooler outlet temperature

The RTD was located 3 cm downstream from the outlet.

Table A - 1: Assumed values for refrigerant line specifications and surrounding conditions

Thermal conductivity, k_{copper}	401 W/mK
Convection coefficient, h	10 W/m^{2}K
Ambient temperature, T_{air}	-20°C
Pipe temperature at POI, T_R	45°C
Pipe length, L	3 cm
Pipe outer radius, r_o	4.8 mm

Using the above specifications and assumptions, the following thermal resistances were calculated. Furthermore, it was assumed that there was a constant surface heat flux over the pipe between the RTD and POI.

Table A - 2: Calculated refrigerant line resistances and heat transfer

Pipe interior convective resistance, $R_{conv,i}$	Assumed negligible
Conductive resistance, R_{cond}	0.005 K/W
Pipe exterior convective resistance, $R_{conv,e}$	110.5 K/W
Heat loss between RTD and POI, Q_{loss}	0.67 W

The following equation was used to estimate the enthalpy of the POI, which was then used with the pressure to determine the temperature of the POI.

$$Q_{\text{loss}} = \dot{m}(h_{\text{POI}} - h_{\text{RTD}})$$

The pressure was assumed to be the same between the RTD and the POI, however it was unknown. Therefore, the temperature was calculated over the expected range of pressures to ensure the resulting temperature was not overly sensitive to the pressure.

Table A - 3: How pressure affects final temperature difference between the RTD and POI

Pressure (kPa)	Temperature difference between RTD and POI (°C)
8000	0.01
8500	0.01
9000	0.00
9500	0.00
10000	0.01
10500	0.01
11000	0.01

11500	0.01
12000	0.01

Therefore, a bias of 0.01°C was added to the gas cooler outlet temperature.

Water inlet temperature

The RTD was located 64 cm upstream of the inlet to the gas cooler and insulated ½" type L copper pipe was used.

Table A - 4: Assumed values for water pipe specifications and surrounding conditions

Thermal conductivity, k_{copper}	401 W/mK
Convection coefficient, h	20 W/m^{2}K
Ambient temperature, T_{air}	-29°C
Pipe temperature at POI, T_R	40°C
Pipe length, L	106 cm
Pipe outer radius, r_o	1.6 cm
Pipe inner radius, r_i	1.4 cm
Insulation thickness	13 cm
Insulation conductivity	0.040 W/mK

Gnielinski's method for calculating the Nusselt number for $3000 \leq Re \leq 5 \times 10^6$ and $0.5 \leq Pr \leq 2000$ was used from [65]. The friction factor was calculated using Petukhov's equation for $3000 \leq Re \leq 5 \times 10^6$ from [65].

Table A - 5: Calculated dimensionless numbers to describe the water flow

Reynolds number, *Re*	4417
Prandtl number, *Pr*	4.35
Friction factor, *f*	0.040
Nusselt number, *Nu*	29.8

The following resistances and subsequent heat loss were calculated for the length of pipe in question. Using the heat loss and a water temperature of 45°C, the temperature of the POI is 44.9°C. A bias of 0.1°C was added to the water inlet temperatures. The conductive resistance for the insulation was assumed to be 3.7 K/W from tabulated values in ASHRAE 2017 for insulation.

Table A - 6: Calculated water pipe resistances and heat transfer

Pipe interior convective resistance, $R_{conv,i}$	0.00002 K/W
Pipe conductive resistance, $R_{cond,p}$	0.00008 K/W
Insulation conductive resistance, $R_{cond,i}$	3.7 K/W
Pipe exterior convective resistance, $R_{conv,e}$	0.86 K/W
Heat loss between RTD and POI, Q_{loss}	16 W

Appendix B: Gas cooler stray heat loss

The gas cooler is located directly below the evaporator fan. Although it is insulated, it is still expected that heat loss occurs from the gas cooler to the cooler air passing over it and to its surroundings. This appendix reviews the method that was used to estimate the heat loss from the gas cooler to the cooler surroundings. This heat loss term is added to the heat transfer rate from the refrigerant to the water in the gas cooler. Therefore it is used in the model and in the energy balance on the entire HPWH.

Convective heat loss

Several assumptions were made to estimate the heat loss from the gas cooler. First, while the pipe surface temperature of the gas cooler was known, the specifications of the insulation surrounding the gas cooler were not. Therefore, the outer surface temperature of the gas cooler was assumed to be a 50°C, which is at least 30°C less than the gas cooler outer pipe surface temperature. Furthermore, the surface was assumed to be isothermal. Heat losses from conduction were considered negligible compared to the radiative and convective heat losses. Newton's Law of Cooling is used to estimate the convective heat transfer rate, where T_∞ is the temperature of the ambient air, T_s is the insulation's outer surface temperature, $\bar{h}$ is the average convection coefficient, and A is the area of the insulation that is exposed to the airflow from the evaporator fan.

$$\dot{Q}_{\text{conv}} = \bar{h}A(T_\infty - T_s)$$

To find the average convection coefficient, $\bar{h}$, first the average Reynolds and Nusselt numbers were found. While the Prandtl number (Pr) is assumed to be independent of pressure, the same cannot be said for the kinematic viscosity (v). Since the pressure drop over the fan is

unknown, it was assumed that the pressure of the air is atmospheric. Additionally, these properties were evaluated at a film temperature of 300K.

$$Re_{\mathrm{L}} = \frac{u_\infty L}{\nu}$$

The flow was laminar for the entire length of the gas cooler, based upon the calculated Reynolds number of 19,824. The Nusselt number is found using the following equation [65], which is valid for $Pr \gtrsim 0.6$ and laminar flow over an isothermal plate.

$$\overline{Nu}_{\mathrm{L}} = 0.664 Re_{\mathrm{L}}^{1/2} Pr^{1/3}$$

Finally, the average convection coefficient can be found with the equation below. Limited information was given for the air flow rate of the evaporator fan, therefore the same airflow rate was used for each ambient temperature. Values for the convection coefficient ranged from 13.6 to 13.7 W/m^{2}K for ambient air temperatures of 35°C to -29°C. The resulting convective heat loss terms are found at the end of this appendix. Additionally, various parameters and properties used in these calculations are found in the table below.

$$\bar{h} = \frac{\overline{Nu}_L k}{L}$$

Table B - 1: Convective heat transfer parameters

Area exposed to air flow, A	0.084 m^2
Insulation outer surface temperature, T_s	50°C
Velocity of air, u_∞	2.1 m/s

Radiation heat loss

The heat loss due to radiation from the five exposed surfaces of the gas cooler was calculated while the conductive heat loss from the bottom surface was considered negligible. Enclosure analysis was used to estimate the heat loss through radiation heat transfer. Therefore, it was assumed the surfaces are diffuse (the emissivities, absorptivities, and reflectivities are independent of direction) and gray (independent of wavelength). Furthermore, it was assumed the surroundings of the gas cooler had a uniform temperature equal to the ambient air and the ratio of gas cooler surface area to the area of its surroundings was approximately equal to zero. Consequently, the following equation was taken from [65] and used to estimate the heat loss via radiation between the gas cooler and its surroundings.

$$\dot{Q}_{\text{rad}} = \sigma A_1 \varepsilon_1 (T_1^4 - T_2^4)$$

Similarly to the convective heat loss, it was assumed that surface temperature of the insulation was 50°C. The emissivity of the insulation was unknown, so the emissivity of gypsum was used for this calculation and was taken from Appendix A in [65]. Also, the presence of the HPWH cabinet was ignored.

Table B - 2: Radiative heat transfer parameters

Area exposed to radiative heat transfer, A_1	0.28 m^2
Stefan-Boltzmann constant, σ	5.67×10^{-8}
Insulation outer surface temperature, T_1	50°C
Emissivity, ε_1	0.9

Total stray heat loss

The convective and radiative heat losses were combined to form the total heat loss. This total heat loss is used in a first law energy balance on the HPWH and the value used for each ambient temperature can be found in the table below.

Table B - 3: Gas cooler passive heat loss results

Ambient temperature (°C)	Convective heat loss (kW)	Radiation heat loss (kW)	Total heat loss (kW)	Estimated error (kW)
35	0.017	0.027	0.04	
25	0.029	0.043	0.07	0.025
20	0.034	0.050	0.08	
10	0.046	0.064	0.11	0.029
1.1	0.056	0.075	0.13	
-10	0.069	0.087	0.16	0.034
-15	0.075	0.092	0.17	
-20	0.080	0.097	0.18	
-29	0.091	0.105	0.20	

Limitations

The error for the passive heat losses was estimated through a sensitivity analysis. Each assumption made during the calculation is varied and the change in the final heat loss value is recorded. Each “error” is combined in the root sum of squares method to provide the final error for the heat loss term. These are the values in the table above.

For the convective heat losses, the three assumptions that were varied were the velocity of the air stream, the surface area of the gas cooler, and the temperature of the surface of the gas cooler. The first two assumptions were varied by 15% and the final assumption was varied by 20%. Furthermore, the expressions used to solve for the convection coefficient can result in errors as large as 25% [65]. Therefore, the final convection coefficient was also varied by 25%.

Three assumptions were varied for the radiative heat loss: the emissivity, the gas cooler surface temperature, and the area. While the area and temperature were varied by the same percentages as they were for the convective heat loss, the emissivity was only varied by 6%.

Table B - 4: Error in convective heat loss estimates

Assumption	**Percent varied**	**Max difference in $\dot{Q}_{conv}$ (kW)**	**Ambient T (°C)**
Air velocity	15%	0.002	25
		0.003	10
		0.005	-10
Area	15%	0.004	25
		0.007	10
		0.01	-10
Convection coefficient	25%	0.007	25
		0.011	10
		0.017	-10
GC surface temperature	20%	0.011	25
		0.011	10

		0.011	-10

Table B - 5: Error in radiative heat loss estimates

Assumption	**Percent varied**	**Max difference in $\dot{Q}_{rad}$ (kW)**	**Ambient T (°C)**
Emissivity	5%	0.002	25
		0.003	10
		0.005	-10
Area	15%	0.020	25
		0.020	10
		0.020	-10
GC surface temperature	20%	0.011	25
		0.011	10
		0.011	-10

Appendix C: EES code

```
Procedure
compit(T[1],T[2],T[3],T[5],T[6],T[7],Q_out,W_comp,f,B_T_2,B_T_3,P[1],h[1]:dh3,dP,h_2L,P_2L,h_3L,P_3
L,h_3p,P[2],P[3],m_r,h[3],h[2],dh3_L)

rho[1]=density(CarbonDioxide,T=T[1],P=P[1])

N = (f*120)/6
m_r = (rho[1]*0.8*0.0000044*N)/60

"First iteration, determine how bad dh3 and dP are"
Call hpit(m_r,W_comp,Q_out,h[1],T[2],T[3]:h_2L,P_2L,h_3L,P_3L,h_3P,dh3,dP)

dh3_FI = dh3
P1[0] = P[1]


"Limit for dh3 is set at 3"
dh3_L = 3

"Calculate iteration limit for varying both T[2] and T[3]"
i_L = ((B_T_2*2)/0.5)+1
i_L_3 = ((B_T_3*2)/0.1)+1
i_L = round(i_L)
i_L_3 = round(i_L_3)

"First attempt to correct it. Change T[2] within its uncertainty"
If (dh3 > dh3_L) Then
    T[2] = T[2] + B_T_2 "Start T[2] at its upper limit"
    i = 0
    Repeat
    Call hpit(m_r,W_comp,Q_out,h[1],T[2],T[3]:h_2L,P_2L,h_3L,P_3L,h_3P,dh3,dP)
    dP_a = abs(dP)
    i = i + 1
    dh3[i] = dh3
    "Store each iteration's dh3 to determine the minimum and its corresponding T[2]"
    If (i = 1) Then
      T_2_min = T[2]
      dh3_min = dh3[i]
    Endif
    If (i > 1) Then
      If (dh3[i] < dh3_min) Then
        T_2_min = T[2]
        dh3_min = dh3[i]
      Endif
    Endif
    "Unless dh3 has achieved a reasonable value, continue decreasing T[2]"
    If ((dh3>3) or (dP_a > 100)) Then
      T[2] = T[2] - 0.5
    Endif
    Until ((dh3<dh3_L) or (i=i_L) or (dP_a<100))
Endif

"iteration limit calculated from T_2_min"
i_L_M = (1/0.1) +1
```

```
"Second attempt to correct. Change T[2] within its uncertainty, but for each iteration also vary T[3] within its uncertainty"
If (dh3 > dh3_L) Then
    T[2] = T_2_min + 0.5 "Start T[2] at the T_2_min which corresponds to the smallest dh3 found in the earlier repeat loop"
    i = 0
    Repeat
      Call hpit(m_r,W_comp,Q_out,h[1],T[2],T[3]:h_2L,P_2L,h_3L,P_3L,h_3P,dh3,dP)
      i = i + 1
      If (dh3>dh3_L) Then
        Call changet3(m_r,W_comp,Q_out,h[1],T[2],T[3],B_T_3,i_L_3,dh3_L:h_2L,P_2L,h_3L,P_3L,h_3P,dh3,dP,dh3_min_3,T_2_min_3,T_3_min)
      Endif
    If (dh3>dh3_L) Then
      T[2] = T[2] - 0.1
    Endif
    Until ((dh3<dh3_L) or (i=i_L_M))
Endif

"Sometimes dh3 will not converge to below its limit. Still want to use the minimum dh3 found and its corresponding pressures and temperatures"
    If (dh3 > dh3_L) Then
      T[2] = T_2_min_3
      T[3] = T_3_min
      Call hpit(m_r,W_comp,Q_out,h[1],T[2],T[3]:h_2L,P_2L,h_3L,P_3L,h_3P,dh3,dP)
    Endif



"Set P[2], P[3] and h[3] for rest of model"
P[2] = P_2L
P[3] = P[2]
h[3] = h_3L
h[2] = h_2L

End


Procedure HPit(m_r,W_comp,Q_out,h[1],T[2],T[3]:h_2L,P_2L,h_3L,P_3L,h_3P,dh3,dP)
h_2L = (W_comp/m_r) + h[1]
P_2L=pressure(CarbonDioxide,T=T[2],h=h_2L)

h_3L = h_2L - (Q_out/m_r)

P_3L=pressure(CarbonDioxide,T=T[3],h=h_3L)
h_3P=enthalpy(CarbonDioxide,T=T[3],P=P_2L)

dh3 = abs(h_3L - h_3P)
dP = P_2L - P_3L
End
```

```
Procedure
changet3(m_r,W_comp,Q_out,h[1],T[2],T[3],B_T_3,i_L_3,dh3_L:h_2L,P_2L,h_3L,P_3L,h_3P,dh3,dP,dh3
_min_3,T_2_min_3,T_3_min)
T[3] = T[3] + B_T_3
i_3 = 0
Repeat
Call hpit(m_r,W_comp,Q_out,h[1],T[2],T[3]:h_2L,P_2L,h_3L,P_3L,h_3P,dh3,dP)
i_3 = i_3 + 1
dh3[i_3] = dh3

"Store each iteration's dh3 to determine the minimum and its corresponding T[3]"
    If (i_3 = 1) Then
      T_2_min = T[2]
      T_3_min = T[3]
      dh3_min = dh3[i_3]
    Endif
    If (i_3 > 1) Then
      If (dh3[i_3] < dh3_min) Then
        T_2_min = T[2]
        T_3_min = T[3]
        dh3_min = dh3[i_3]
      Endif
    Endif

If (dh3>dh3_L) Then
T[3] = T[3] - 0.1
Endif
Until ((dh3<dh3_L) or (i_3=i_L_3))

dh3_min_3 = dh3_min
T_2_min_3 = T_2_min

End


Procedure ihxs(P_2L,P_3L,T[4],dh3:P[4],h[4]) "IHX, high pressure side"
    If (dh3 > 75) Then
      P[4] = P_3L
    Else
      P[4] = P_2L
    Endif

    h[4]=enthalpy(CarbonDioxide,T=T[4],P=P[4])
End

Procedure expand1(P[1],h[4]:h[5],P[5],x[5])
P[5] = P[1]
h[5] = h[4]
x[5]=quality(CarbonDioxide,P=P[5],h=h[5])

End

Procedure evap(T[5],T[6],P[5],h[5],m_r:h[6],Q_in_r,P[6])
    P[6] = P[5]
If (T[6] < T[5]) Then
    x[6] = 1
```

```
    h[6]=enthalpy(CarbonDioxide,x=x[6],P=P[6])
Else
    h[6]=enthalpy(CarbonDioxide,T=T[6],P=P[6])
Endif

Q_in_r = m_r * (h[6] - h[5])

End

Procedure ihx(h[3],h[4],m_r,h[6],h[1]:Q_IHX_L,Q_IHX_H)
    Q_IHX_L = m_r*(h[1] - h[6])
    Q_IHX_H = m_r*(h[3] - h[4])
End

Procedure
run(T[1],T[2],T[3],T[4],T[5],T[6],T[7],Q_out,W_comp,f,B_T_2,B_T_3:dh3,dP,n_s,P[1],P[2],P[3],P[4],P[5],P[
6],h[1],h[2],h[3],h[4],h[5],h[6],m_r,dQ,n_s_3L,s_1,s_2,P_2L,P_3L,h_2L,h_3L,N,Q_in,Q_in_r)

"determine P[1] for first iteration"
If (T[1] > T[5]) Then
    P[1]=p_sat(CarbonDioxide,T=T[5])
    h[1]=enthalpy(CarbonDioxide,T=T[1],P=P[1])
Else
    P[1]=p_sat(CarbonDioxide,T=T[6])
    h[1]=enthalpy(CarbonDioxide,T=T[1],P=P[1])
Endif

rho[1]=density(CarbonDioxide,T=T[1],P=P[1])

N = (f*120)/6
m_r = (rho[1]*0.8*0.0000044*N)/60

    "First iteration, determine how bad dh3 and dP are"
    Call hpit(m_r,W_comp,Q_out,h[1],T[2],T[3]:h_2L,P_2L,h_3L,P_3L,h_3P,dh3,dP)
    P[2] = P_2L
    P[3] = P[2]
    h[2] = h_2L
    h[3] = h_3L

    Call ihxs(P_2L,P_3L,T[4],dh3:P[4],h[4])
    Call expand1(P[1],h[4]:h[5],P[5],x[5])
    Call evap(T[5],T[6],P[5],h[5],m_r:h[6],Q_in_r,P[6])
    Call ihx(h[3],h[4],m_r,h[6],h[1]:Q_IHX_L,Q_IHX_H)

    Q_in = Q_out - W_comp
    dQ = Q_in_r - Q_in

    "switch 1 turns on when state1 is called. if state 1 isn't called, then x[6] needs to be defined"
    s_1 = 0
"Iterate to find best state 1 if either dh3 or dQ are large"
    If ((dh3>100) or (dQ > 1.5)) Then
      Call state1(P[1],h[4],m_r,W_comp,Q_out,T[2],T[3],T[4],T[5],T[6]:x[6],h[1],h_3e)
      s_1 = 1
    Endif
```

```
    Call
compit(T[1],T[2],T[3],T[5],T[6],T[7],Q_out,W_comp,f,B_T_2,B_T_3,P[1],h[1]:dh3,dP,h_2L,P_2L,h_3L,P_3
L,h_3p,P[2],P[3],m_r,h[3],h[2],dh3_L)

    "After finding best T[2] and T[3], recalculate rest of state points"
    Call ihxs(P_2L,P_3L,T[4],dh3:P[4],h[4])
    h[5] = h[4]
    If (s_1 = 0) Then
      x[6] = 1
    Endif
    h[6]=enthalpy(CarbonDioxide,x=x[6],P=P[1])
    Call ihx(h[3],h[4],m_r,h[6],h[1]:Q_IHX_L,Q_IHX_H)

    Q_in_r = m_r * (h[6] - h[5])
    Q_in = Q_out - W_comp
    dQ = Q_in_r - Q_in

    "Calculate isentropic efficiency"
    s[1]=entropy(CarbonDioxide,T=T[1],P=P[1])
    h_2s=enthalpy(CarbonDioxide,s=s[1],P=P[2])
    n_s = (h_2s - h[1])/(h_2L - h[1])
    s_2 = 0

    "if dh3 is outrageously large and P_2L is super low, then use P_3L to calculate n_s"
    If ((dh3 > 5) and (P_2L < P_3L)) Then
      h_2s_2=enthalpy(CarbonDioxide,s=s[1],P=P_3L)
      n_s_3L = (h_2s_2 - h[1])/(h_2L - h[1])
      s_2 = 1
    Endif

    If (s_2 = 0) Then
      n_s_3L = n_s
    Endif

End


Procedure state1(P[1],h[4],m_r,W_comp,Q_out,T[2],T[3],T[4],T[5],T[6]:x[6],h[1],h_3e)
 "This procedure changes the quality of state 6 in order to shift the state point of 1"
    i = 0
    x[6] = 0.9
    i_L = (0.95-0.9)/0.01
    Repeat
    i = i + 1
    h_3e=enthalpy(CarbonDioxide,T=T[3],P=P[1])
    h[6]=enthalpy(CarbonDioxide,x=x[6],P=P[1])
    h[1] = h[6] + (0.2*(h_3e - h[6]))
    x[1]=quality(CarbonDioxide,P=P[1],h=h[1])
    Call hpit(m_r,W_comp,Q_out,h[1],T[2],T[3]:h_2L,P_2L,h_3L,P_3L,h_3P,dh3,dP)
    Call ihxs(P_2L,P_3L,T[4],dh3:P[4],h[4])
    h[5] = h[4]

    Q_in_r = m_r * (h[6] - h[5])
    Q_in = Q_out - W_comp
    dQ = Q_in_r - Q_in
```

```
    dQ[i] = dQ
    If (i = 1) Then
      x_6_min = x[6]
      dQ_min = dQ[i]
      h_1_min = h[1]
    Endif
    If (i > 1) Then
      If (dQ[i] < dQ_min) Then
        x_6_min = x[6]
        dQ_min = dQ[i]
        h_1_min = h[1]
      Endif
    Endif

    If (dQ > 0.5) Then
      x[6] = x[6] + 0.01
    Endif
    Until ((i = i_L) or (dQ <= 0.5))

h[1] = h_1_min
x[6] = x_6_min

End


"Main Program"
"inputs"

"ambient air = 25 deg C"
"T[7] = 18.5
Q_out = 3.97
W_comp = 0.87
T[1] = 14
T[2] = 82.2
T[5] = 5.9
T[3] = 18.4
T[4] = 13.87
T[6] = 5.2
f = 123
B_T_2 = 5
B_T_3 = 0.7
T[9] = 25"

 "procedures"
Call
run(T[1],T[2],T[3],T[4],T[5],T[6],T[7],Q_out,W_comp,f,B_T_2,B_T_3:dh3,dP,n_s,P[1],P[2],P[3],P[4],P[5],P[
6],h[1],h[2],h[3],h[4],h[5],h[6],m_r,dQ,n_s_3L,s_1,s_2,P_2L,P_3L,h_2L,h_3L,N,Q_in,Q_in_r)
```